1972

Effect of electrotransport on the solidification of some tin-bismuth and tin-lead alloys

Jairus Charles Warner
Iowa State University

INFORMATION TO USERS

This dissertation was produced from a microfilm copy of the original document. While the most advanced technological means to photograph and reproduce this document have been used, the quality is heavily dependent upon the quality of the original submitted.

The following explanation of techniques is provided to help you understand markings or patterns which may appear on this reproduction.

1. The sign or "target" for pages apparently lacking from the document photographed is "Missing Page(s)". If it was possible to obtain the missing page(s) or section, they are spliced into the film along with adjacent pages. This may have necessitated cutting thru an image and duplicating adjacent pages to insure you complete continuity.

2. When an image on the film is obliterated with a large round black mark, it is an indication that the photographer suspected that the copy may have moved during exposure and thus cause a blurred image. You will find a good image of the page in the adjacent frame.

3. When a map, drawing or chart, etc., was part of the material being photographed the photographer followed a definite method in "sectioning" the material. It is customary to begin photoing at the upper left hand corner of a large sheet and to continue photoing from left to right in equal sections with a small overlap. If necessary, sectioning is continued again — beginning below the first row and continuing on until complete.

4. The majority of users indicate that the textual content is of greatest value, however, a somewhat higher quality reproduction could be made from "photographs" if essential to the understanding of the dissertation. Silver prints of "photographs" may be ordered at additional charge by writing the Order Department, giving the catalog number, title, author and specific pages you wish reproduced.

University Microfilms

300 North Zeeb Road
Ann Arbor, Michigan 48106

A Xerox Education Company

Effect of electrotransport on the solidification of some tin-bismuth and tin-lead alloys

by

Jairus Charles Warner

A Dissertation Submitted to the
Graduate Faculty in Partial Fulfillment of
The Requirements for the Degree of
DOCTOR OF PHILOSOPHY

Major: Metallurgy

Approved:

Signature was redacted for privacy.

In Charge of Major Work

Signature was redacted for privacy.

For the Major Department

Signature was redacted for privacy.

For the Graduate College

Iowa State University
Ames, Iowa

1972

TABLE OF CONTENTS

INTRODUCTION

Until the early 1950's there was very little theoretical basis with which to explain the causes of the interface morphology which occurs when metallic alloys pass from the liquid to the solid state, even though virtually all metal products under go this process at one time or another. While the theory presented by Tiller, Jackson, Rutter, and Chalmers (62) was severely limited (and included some restrictions which have since been found unnecessary) the principles developed in it have been used in a number of applications to different types of solidification problems since then (5, 43, 39). Due in large part to the Tiller et al. theory (62) and subsequent experimental work, some commercial work today in the heavy metals industry is making use of controlled solidification techniques (74).

At present the experimental variables in directional solidification include composition, temperature gradient, solidification rate, and the amount of convection, all to a limited extent. Additional forces and phenomena such as electric and magnetic fields and thermotransport effects (in restricted cases), offer possible ways of increasing the variability and control of the solidification process.

Consider an alloy system with the equilibrium distribution coefficient $k_o = C_s/C_\ell\big|_i$ different than 1 where

C_s, C_ℓ are the concentrations in the solid and liquid, respectively at the interface. As the alloy solidifies with a plane interface, the solute concentration at the interface increases or decreases depending on whether $k_o \lesseqgtr 1$; the concentration in the solid alters to remain in equilibrium with the interface liquid; and the temperature of the interface drops to the solidification point of the liquid at the interface, which is lower than the freezing temperature of the bulk liquid. Thus it should be possible for portions of the liquid to be below the local equilibrium freezing point even in a positive temperature gradient. This phenomenon of constitutional supercooling was first put on a quantitative basis by Tiller et al. (62). They were able to show that for a flat interface to be stable

$$G \geq \frac{R}{D} C_o \, (-m_\ell) \, \frac{(1-k_o)}{k_o} \qquad [1]$$

where G is the temperature gradient in the liquid, R, is the solidification rate, C_o is the original liquid composition, and m_ℓ is the liquidus slope. To obtain this result they assumed i) steady-state, ii) no fluid mixing, iii) no diffusion in the solid. In addition, surface energy, volume change on freezing, and orientation effects were ignored.

Experiments designed to test Eq. [1] have been performed a number of times. Davies (18) treated a large portion of

the data available to him in 1968. He concluded that for the low concentrations and usually fast rates used in most of the studies the Tiller-Chalmers theory has been well supported.

Mullins and Sekerka (43) and Sekerka (56) studied the problem of interface stability by first considering a flat interface with a sinusoidal perturbation of indefinite wavelength, and then determining under what conditions the wave perturbation would grow or decay. If the amplitude decayed for all wavelengths, then the interface would be stable for those growth conditions.

The differences between the Tiller-Chalmers and Mullins-Sekerka theories are not great for most experimental conditions. The only serious effort to compare the two (23), makes the tentative conclusion that the capillarity terms, which make up a large portion of the Mullins-Sekerka theory, under certain conditions may not be as significant as predicted.

One of the questions to be determined by this research project was whether an electric current, concentrating along low resistance paths, would melt back small perturbations, thus making the flat interface more resistant to breakdown. Suppose a small sinusoidal wave is superimposed on a planar surface. Some distance from the interface where the wave does not disturb linearity the electric potential is constant on a transverse plane. The various possible paths

by which current travels from one side of the interface to the other can be considered as parallel circuits, each having the same potential drop. The joule heat generated in any given volume is given by

$$W/V = E^2/\rho \qquad [2]$$

where W is watts, V is volume, E is electric field, and ρ is the specific resistivity. A circuit which passes through the tip of a sinusoidal perturbation on the interface will have lower resistivity and greater heating in the region of the perturbation than a parallel circuit which passes through the trough of the perturbation. Thus there would be local heating at the tips of small perturbations, which would tend to prevent their growth.

Some other effects were expected as well. The joule heat generated within the sample should raise the gradient well above that obtainable by heating with a resistance furnace. Electrotransport of solute at the interface will alter the critical gradient for stability (Eq. [1]). Two effects, being functions of the field direction, could adversely influence the remaining results: a field at the interface might alter the kinetics of solidification, thus changing the melting point of even pure metal, and Peltier heat generated or absorbed at the interface could be significant.

The intent of the portion of this thesis dealing with solidification of Sn-Bi alloys was to test whether any "melt-back" effect could be detected, taking into account electrotransport and the enhanced temperature gradient. Effects on the kinetics of solidification and Peltier heat were also considered.

Eutectic alloys hold out great potential in a number of commercial applications, particularly where stresses are approximately unidirectional. A directionally solidified eutectic structure is in essence an aligned composite material in which the components are compatible and well bonded, obtained without the necessity of fabricating masses of tiny fibers.

Unfortunately, the theory for eutectic growth is not as well developed in some aspects as that for single phase growth. Within a year after the first complete derivation was presented (33), Mollard and Flemings (40) showed experimentally that direct application of single phase growth concepts to the eutectic-dendrite transition of off-eutectic alloys was only qualitatively valid. Verhoeven and Gibson (69) have just presented evidence which indicates that all previous work on the eutectic to dendrite transition is in serious question. Clearly much work remains to be done before the experimental conditions for even the eutectic-dendritic transition can be predicted

with a degree of confidence.

The theoretical derivation performed for this thesis indicated that with a proper selection of variables one could control the solid composition profile to a large degree. When mixing alone is present in an off-eutectic alloy, the solid always approaches C_E (72). Mixing will always be present if the alloy is such that the liquid at the eutectic composition is less dense than the bulk liquid, as on the lead side of the Sn-Pb eutectic. In this situation an electric field can add a force which tends to make the solid composition more uniform.

The research on the effect of an electric field on eutectic solidification was exploratory in that, while a derivation was made to account for electro-transport and to predict the critical conditions for the eutectic-dendritic transition, the basis for the latter was known to be in error, and some of the assumptions required for a tractable mathematical treatment were suspect. The tentative conclusions which can be drawn, however, have some interesting implications, and the work does show promise.

THEORETICAL CONSIDERATIONS - SINGLE PHASE GROWTH

In normal solidification of an alloy with a distribution coefficient less than 1, as a flat interface moves forward a solute build-up occurs, as shown in Fig. 1. We take R, the measured solidification rate, as the mass average velocity in the solid at the interface, defined positive when solidification is toward the right. This is correct when the solid does not move with respect to the container wall, and diffusion and electrotransport in the solid are very small. Then $v_m = R\frac{\rho_s}{\rho_\ell}$ is the mass average velocity in the liquid near the interface. Here ρ_s, ρ_ℓ are the densities of the solid and liquid, respectively. The flux of component 1 in the liquid with respect to any reference velocity v_R is thus

$$J_1 = -C_1\rho_\ell\, v_R + C_1\, \rho_\ell\, (v_1 - v_R) \qquad [3]$$

where v_1 is the average velocity and C_1 is the weight percentage of component 1. It is reasonable at this point to choose $v_R = v_m$. In a binary alloy

$$v_m = C_1 v_1 + C_2 v_2 \qquad [4]$$

Combining the above two equations, the flux of component 1 near the interface is

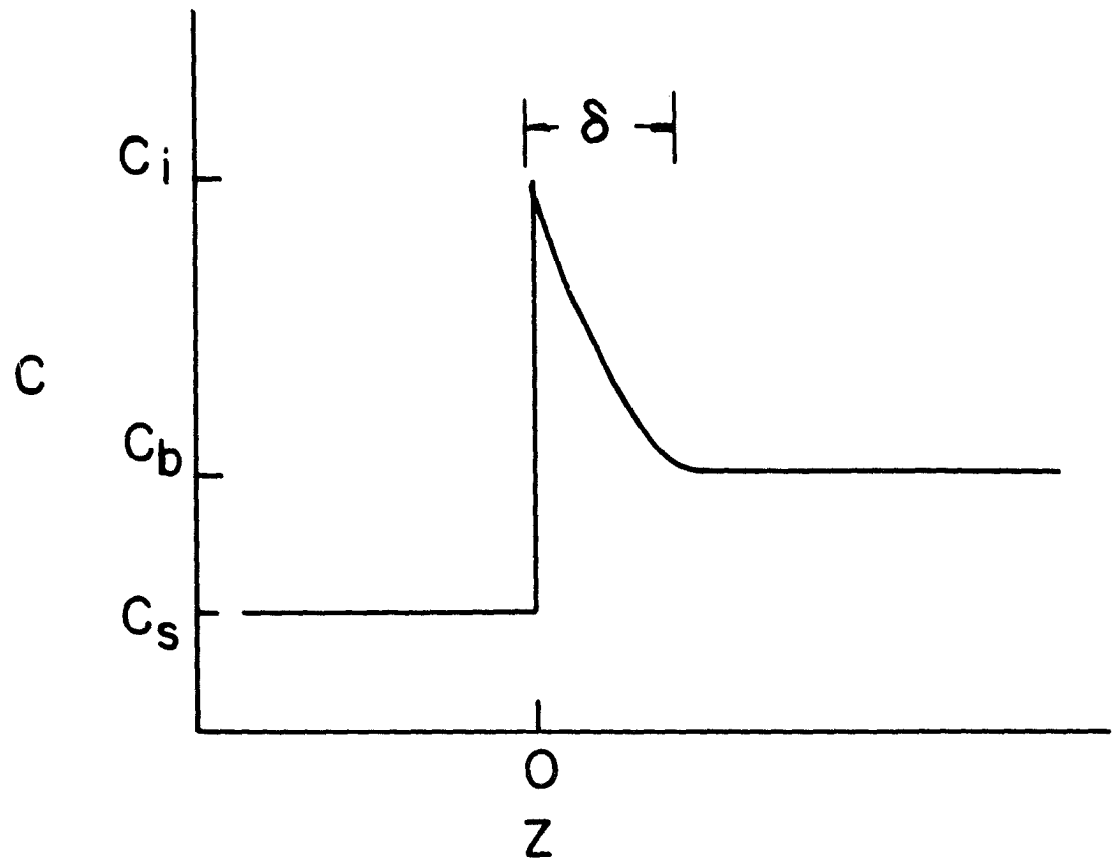

Fig. 1 -- Solute profile of an alloy solidifying toward the right, with $k_o < 1$. The interface is at $z = 0$. When δ is not infinite mixing is present

$$J_1 = -C_1\rho_\ell v_m + C_1C_2\rho_\ell[v_1-v_2] \qquad [5]$$

The differential velocity (v_1-v_2) is due to two sources, for this case, chemical diffusion and electrotransport,

$$J_1 = -C_1\rho_\ell v_m + C_1C_2\rho_\ell[(v_1-v_2)_D + (v_1-v_2)_E] \qquad [6]$$

It has been shown (4) that the interdiffusion coefficient is given by

$$(v_1-v_2)_D = -\frac{D_{12}}{C_1C_2}\frac{dC}{dZ} \qquad [7]$$

where the gradient of C is only in the Z direction. The definition of U_{12}, the differential electric mobility, is

$$(v_1-v_2)_E = U_{12}E \qquad [8]$$

The flux in the solid is $J = C_1^s\rho_s R$, so a flux balance at the interface is

$$-C_1^s\rho_s R = -C_1\rho_\ell v_m - \rho_\ell D_{12}\frac{dC}{dZ} + U_{12}C_1C_2E\rho_\ell \qquad [9]$$

Dividing by ρ_ℓ, and manipulating, we get

$$-D_{12}\frac{dC}{dz} = C_1\frac{\rho_s}{\rho_\ell}R(1-k_o) - U_{12}C_1C_2E \qquad [10]$$

The equilibrium temperature at the interface is $T_i = T_{mp} + m_\ell C_i$. In order for the interface to remain stable, the real temperature at any point must be equal to or greater than the equilibrium temperature. Since the two are equal at the interface, this means that

$$G \equiv \frac{dT}{dz} \geq \frac{dT_{eq}}{dz} = m_\ell \frac{dC_1}{dz} \qquad [11]$$

Inserting into Eq. [10] the result is

$$G = \frac{(-m)(1-k_o)}{k_o D} RC_1^s \frac{\rho_s}{\rho_\ell} - \frac{(-m)U_{12}C_1^s EC_2}{k_o D} \qquad [12]$$

where $C_1 = C_1^s/k_o$ has been applied. For tin the difference between solid and liquid density is about 2.7 pct and will be neglected here. The electric mobility which is actually measured is U_{12}. Throughout this work, where U appears the correspondence with the measured mobility will be $U = U_{12}C_2$.

As will be discussed in more detail later, when convection is present in the liquid the model shown in Fig. 1 can be used. It is assumed that the liquid is stagnant between the interface and δ, and the effective distribution

coefficient, k_e, is defined as C_s/C_B, where C_s is the concentration of the solute in the solid in weight percent, and C_B is the concentration of the liquid at distances greater than δ. Using k_e, Eq. [12] can be written

$$G/C_B = \frac{(-m_\ell)k_e(1-k_o)R}{k_o D} - \frac{(-m_\ell)k_e UE}{k_o D} \qquad [13]$$

Figure 2 is a plot of Eq. [13] for both E positive and E negative, using parameters approximating the Sn-Bi system.

Equation [13] has a number of drawbacks for use in experimentally testing of solidification theory. First, k_e is a function of R as well as the mixing length and the direction of the field. The derivation of k_e also assumes that the liquid concentration is constant beyond δ in front of the interface, as will be shown later. This assumption may not be the case when a differential body force is present. To avoid these complications Eq. [12] can be used, if C_s near the interface can be determined.

In most of the work of this sort G/R is used as the measure of stability. However in this case, use of G/R does not separate the variables, since the UE term then contains R. Instead of G/R the equivalent formulation

Fig. 2 -- Stable-unstable transition curves predicted from Eq. [13], using parameters approximating the Sn-Bi system. Experimental conditions above the appropriate line should produce stable interfaces; below the line instability is expected

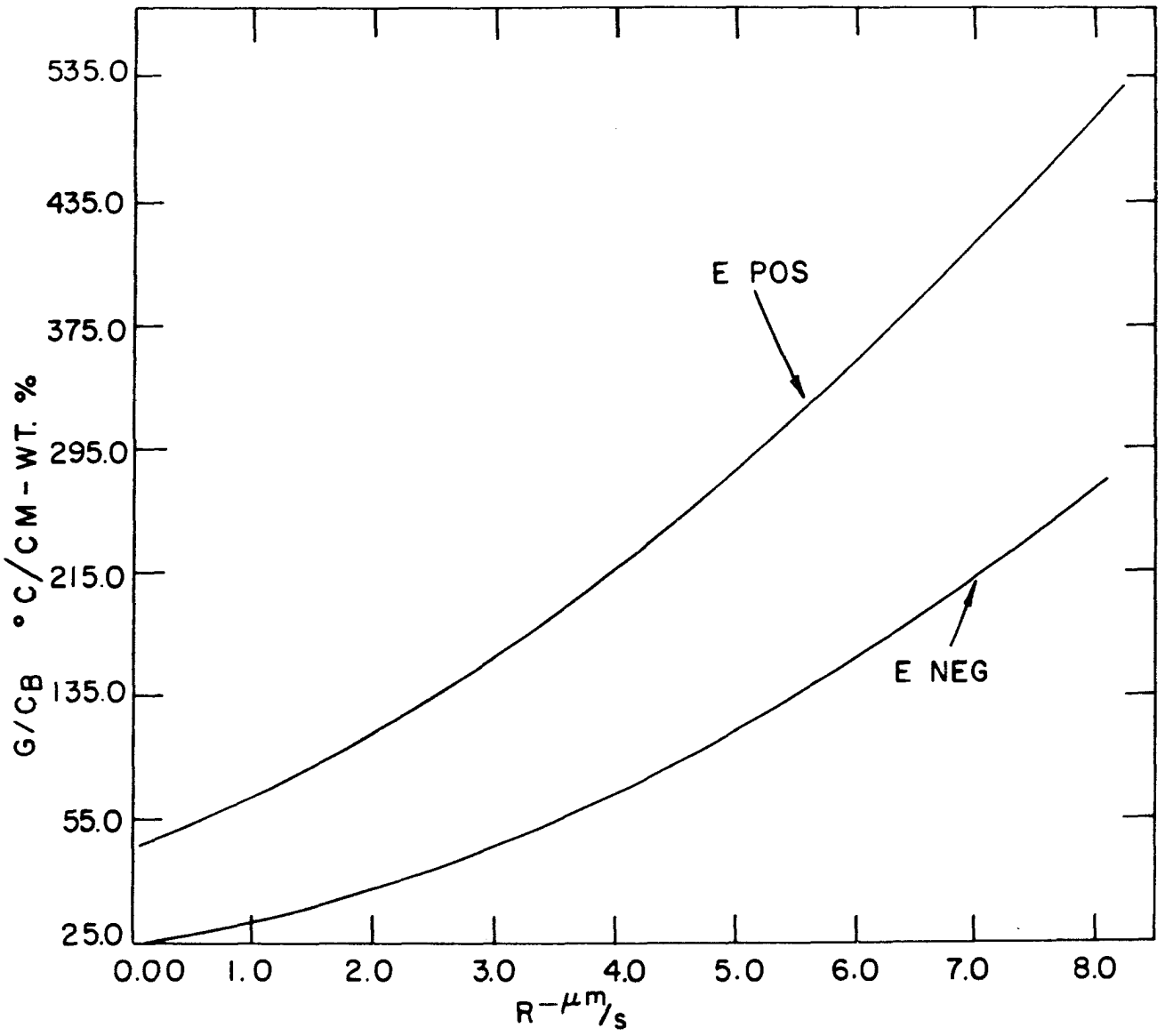
535.0
435.0
375.0
295.0
215.0
135.0
55.0
25.0
G/C_B °C/CM-WT. %
E POS
E NEG
0.00
1.0
2.0
3.0
4.0
5.0
6.0
7.0
8.0
R-μm/s

$$G/C_s = \frac{(-m_\ell)(1-k_o)R}{k_o D} - \frac{(-m_\ell)UE}{k_o D} \qquad [14]$$

will be used. If the parameters of the system were constants independent of temperature or composition, then a plot of the critical values of G/C_s against R would be two straight lines with R = 0 intercepts of equal magnitude and opposite sign. For a given direction of electric field, concentration, and rate, the points (R, G/C_s) which fell above the transition line for that field direction would be stable, with flat interfaces, and those which fell below the the transition line would be unstable, with broken interfaces. When k_o, m_ℓ, D, E, and U are made functions of temperature and composition, Eq. [14] is no longer single valued. However, if only one gradient is used, the ordinate is equivalent to $1/C_s$. It is worth noting that the present derivation avoids the least realizable assumptions required of the earlier derivation. In particular, since the equation is evaluated at the interface, all the parameters may be determined for a specific composition and temperature.

Tiller (61) has developed a theory which includes the possibility that deep grooves may be stable on an otherwise planar interface. The model he used is shown in Fig. 3. He hypothesizes the presence of stable grooves and determines the consequences of this hypothesis. Three

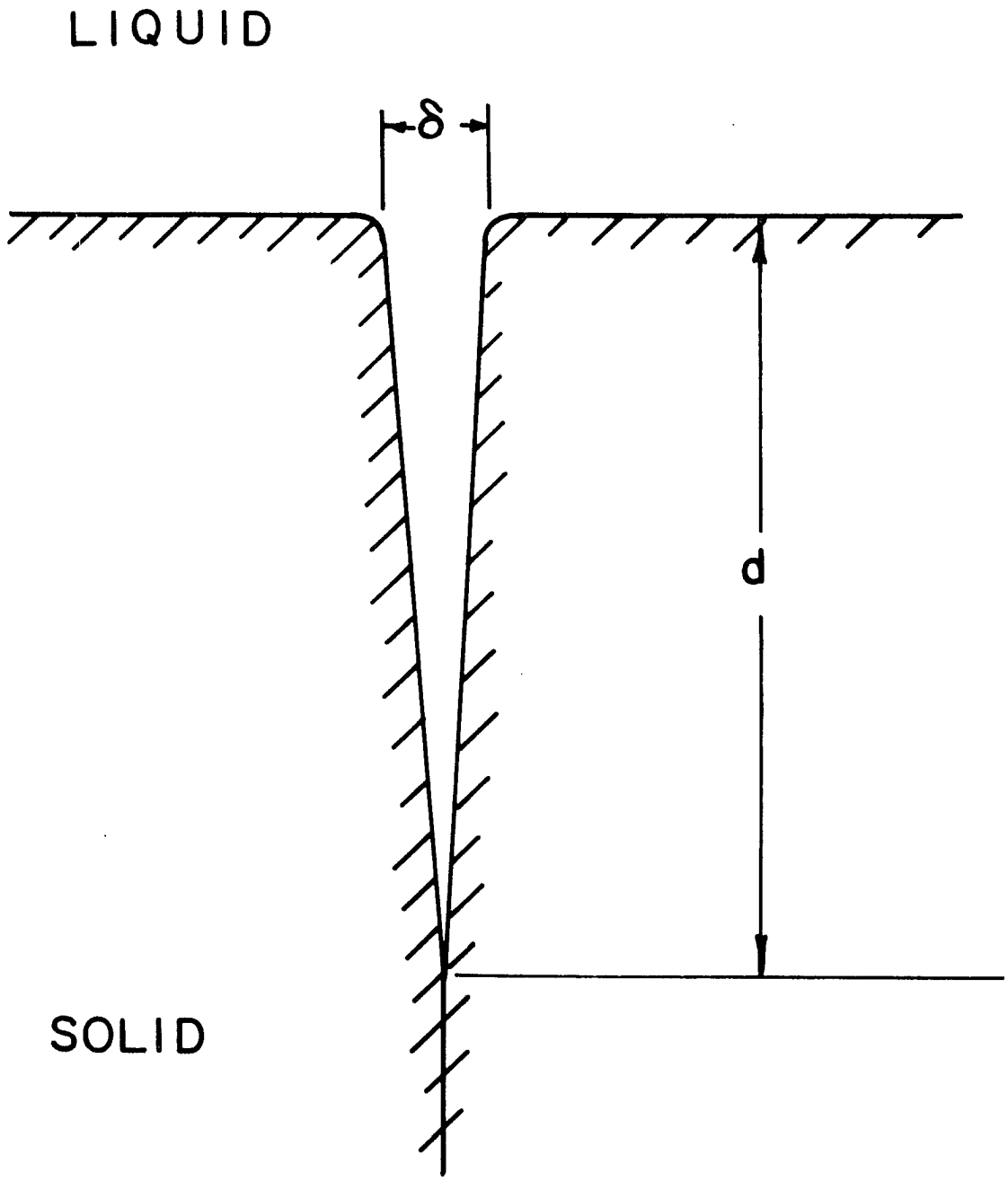

Fig. 3 -- The groove shape used in the theory of groove stability

specific assumptions are made. First, the concentration in the plane of the interface, $z = 0$, is C_i for all points in the plane. Second, he assumes equilibrium at the groove wall between the solid and liquid and that the solid temperature gradient is equal to the critical gradient in the z direction everywhere within the groove. Lastly, he assumes that, because of the small width of the groove, there is no lateral diffusion.

Tiller hypothesizes grooves with straight, stable walls in the solid and determines the necessary conditions for their existence. Let L_g be the length of groove per unit area of interface. Let ΔC be the amount of solute solidified in the groove in excess of that over an equal area of planar interface. At the straight wall we assume $G_s = m \frac{dC}{dz}$, which is to say local equilibrium prevails. The net flux into the solid behind the grooves is

$$\delta L_g (k_o C_i + \langle \Delta C_i \rangle_{av}) R = \delta L_g C_i R - \frac{DG_s}{(-m)} \delta L_g \qquad [15]$$

Solving for $\langle C \rangle_{av}$

$$\langle \Delta C \rangle_{av} = C_i (1-k_o) - \frac{DG_s}{(-m)R} \qquad [16]$$

$$= C_i (1-k_o) \left[1 - \frac{DG_s}{(-m)RC_i(1-k_o)} \right] \qquad [17]$$

Now at the interface in a planar region a similar flux balance yields

$$G_c = \frac{(-m)C_i(1-k_o)R}{D} \qquad [18]$$

Inserting this value of the critical gradient into Eq. [17] one obtains

$$\langle \Delta C \rangle = C_i(1-k_o)\left[1 - \frac{G_s}{G_c}\right] \qquad [19]$$

Because ΔC must be greater than zero for the grooves to exist and be stable, the term inside brackets must be greater than zero. Since for stability of the planar interface G_c must be less than G_ℓ , we then have

$$\frac{G_s}{G_c} < 1 < \frac{G_\ell}{G_c} \qquad [20]$$

When the first inequality holds there can be stable straight walled grooves, and when the second holds the interface will be planar.

Morris and Winegard (42) used this derivation to explain some of their experimental results. They found that the ratio of the critical rate for the stable presence of deep grooves at a grain boundary to the critical rate for stability of a planar interface was about 0.8, which they

felt was in good agreement with predictions from Tiller's theory.

Now let us consider the same situation with an electric field. The flux balance of Eq. [15] now is

$$\delta L_g(k_o C_i + \langle \Delta C \rangle)R = \delta L_g C_i R - \frac{DG_s \delta L_g}{(-m)} - UEC_i \delta L_g \qquad [21]$$

where UE positive indicates solute flux away from the interface. Solving for ΔC, we obtain

$$\langle \Delta C \rangle_{av} = C_i(1-k_o)\left[1 - \frac{DG_s}{(-m)(1-k_o)RC_i} - \frac{UE}{R(1-k_o)}\right] \qquad [22]$$

From Eq. [12], the flux balance at the planar interface gave

$$G_{CE} = \frac{(-m)C_i(1-k_o)R}{D} - \frac{(-m)UEC_i}{D} \qquad [23]$$

where G_{CE} is the critical gradient in the presence of an electric field. Inserting the term G_c as before from Eq. [18], Eq. [22] becomes

$$\langle \Delta C \rangle = C_i(1-k_o)\left[1 - \frac{UE}{R(1-k_o)} - \frac{G_s}{G_c}\right] \qquad [24]$$

Again, we require that the term in brackets be greater than zero, for the same reasons. Thus

$$\frac{G_s}{G_c} < 1 - \frac{UE}{R(1-k_o)} \qquad [25]$$

For planar stability G_ℓ must be greater than G_{CE} , which dividing by G_c results in

$$\frac{G_\ell}{G_c} > 1 - \frac{UE}{R(1-k_o)} \qquad [26]$$

Hence, in a manner similar to Eq. [20]

$$\frac{G_s}{G_c} < 1 - \frac{UE}{R(1-k_o)} < \frac{G_\ell}{G_c} \qquad [27]$$

Again, if the left inequality is true, grooves will be stable, and if the the right inequality holds the planar interface will be stable. For UE greater than zero, (flux away from the interface), the system is less likely to have stable grooves and more likely to have a planar interface than for UE = 0. The latter result was expected, since the right inequality is simply Eq. [14] in slightly different form. The more questionable assumptions Tiller makes are that the walls are straight and that the concentration at the mouth is $C_i = C\big|_{z=0}$. As long as the latter assumption

is used, electrotransport will have no effect because at that point the flux due to electrotransport will be the same at all points on the interfacial plane, UEC_i. Relaxing that latter assumption would require a solution in all three directions, since $\partial C/\partial x$ and $\partial C/\partial y$ would not be zero near the mouth of a groove.

If the walls were slightly curved, either convex or concave, little change would result because the radius of curvature would be large. The etching technique used in this work limited the possibility of measuring the specific shape of the grooves, but it does seem evident that grooves are shaped more with parallel walls tapered slightly down to approximately hemispherical caps at the bottom. Photographs will be shown later in Fig. [18-20]. Until the width of the grooves reached very small values, little effect on the above derivation should be expected.

Tiller makes one other assumption which he does not specify clearly. When he assumes the concentration gradient in the liquid is at the critical value, he writes $\frac{dC}{dz} = G_s/m_\ell$ and applies this to the groove material, including that exactly at $z = 0$. This is equivalent to assuming $G = G_\ell$ for z greater than zero and $G = G_s$ for z less than zero. More likely the temperature gradient, at least in the region of the groove, undergoes a more gradual transition. Again, relaxation of the simple model would require a three-di-

mensional solution of the heat flux equations.

One result of this derivation is that under certain conditions narrow grooves may be stable, and thus present, even while the remainder of the interface is flat. This would suggest that the methodological problem of specifying a flat and non-flat interface is even more difficult than had been thought. This particular problem will be covered in more detail in the discussion of sources of error in the Sn-Bi work.

THEORETICAL CONSIDERATIONS - EUTECTIC GROWTH

Jackson and Hunt (33) assuming no mixing, a perfectly planar interface, and some other restrictions, derived a series of related equations for the liquid concentration, $C(x,z)$, and the lamellar spacing, $\lambda(R,C_o)$, for various eutectic structures. Following the analysis of Jackson and Hunt, Verhoeven and Homer (72), retaining the planar interface approximation, derived the equations to account for mixing in the liquid. An interesting result is that, in a closed system with mixing, an off-eutectic melt will never freeze with constant composition, $\overline{C}_s$.

The present derivation will allow for the presence of an electric field. In this work the solvent will be the element which is the major component of the alpha phase, and the solute will be the element which is the major constituent of the beta phase. Since, with proper care for signs, the equations can be applied equally to the system with solute in the place of solvent, there is no loss of generality.

We start with an eutectic alloy growing into its melt, as shown in Fig. [4]. The equation of concentration in the liquid is

$$D \frac{\partial^2 C}{\partial z^2} + D \frac{\partial^2 C}{\partial y^2} + R \frac{\partial C}{\partial z} + UE \frac{\partial C}{\partial z} = \frac{\partial C}{\partial t} \qquad [28]$$

since $J\Big|_z = -D\nabla C - RC - UEC$ and $\nabla \cdot J = -\frac{\partial C}{\partial t}$

Here, z is taken as the direction normal to the plane of the freezing interface, positive sense into the liquid; y is normal to z and the eutectic plates. To be rigorously correct the electrotransport term would have to be $U_{12}E\ X_1X_2$ in the flux equation. However, since this would complicate the mathematics, U will be taken as $U_{12}X_2$. Considering that, like U, the diffusion coefficient is a function of temperature and composition, and that both have to be assumed constant in order to make the analysis, simplifying U in this manner is not as great an imposition on the facts as one might fear. Unlike the analysis for single phase growth, the analysis here must be taken over the entire liquid region out to δ, and the errors introduced in this way may be significant. R is taken as the mass average velocity of the liquid just in front of the interface, with respect to the interface. We will consider only those conditions where near steady-state exists.

The boundary conditions are

(bc-1) $$C(z,y) = C(z,y+w) \qquad [29]$$

(bc-2) $$\frac{\partial C}{\partial y}(z,0) = \frac{\partial C}{\partial y}(z, \frac{w}{2}) = 0 \qquad [30]$$

(bc-3) $$C(\delta,y) = C_B \qquad [31]$$

(bc-4) $$\frac{\partial C}{\partial z}(0,y) = a \quad ; \quad 0 \leq y \leq \frac{W_\alpha}{2}$$

$$b \quad ; \quad \frac{W_\alpha}{2} \leq y \leq \frac{W}{2} \qquad [32]$$

Figure 4 defines W_α and W. Boundary conditions (bc-1) and (bc-2) are statements of periodicity in the system in the y direction. Condition (bc-3) indicates that some degree of mixing is present. When δ goes to infinity one obtains the solution for no mixing. Condition (bc-4) requires that the concentration gradient in front of each plate be independent of position on the plate. Actually the plates are curved slightly, and dC/dz across each plate is not precisely constant, but the assumption appears to be close. A standard separation of variables technique performed on Eq. [28], given in detail in Appendix D, provides an equation for the composition in the liquid as a function of z and y,

$$C(z,y) = C_B - \frac{[af_\alpha+bf_\beta][e^{-\rho' Z} - e^{-\rho'\delta}]}{\rho'}$$

$$+ \sum_1^\infty D_n e^{\frac{-\rho' Z}{2}} \cos\left(\frac{2n\pi y}{W}\right) \sinh \gamma_n(\delta - Z) \qquad [D-46]$$

where

$$D_n = \frac{-2(a-b)\ \sin n\pi f_\alpha}{\pi[\gamma_n \cosh \gamma_n\delta + \frac{\rho'}{2} \sinh \gamma_n\delta]} \qquad [D\text{-}47]$$

To get the values of a and b, one must make a mass balance at the interface. This is usually done with the assumption that the solid and liquid densities are equal, so that the volume velocity is constant at all points. In point of fact the measured velocity is usually the velocity of the solid with respect to the interface at a point just behind that interface. Since diffusion in the solid can be neglected, this is also the mass average velocity at that point. The mass average velocity in the liquid, R, is related to that in the solid, R^S, by

$$R^S = R\,\frac{\rho_\ell}{\rho_s} \qquad [33]$$

where ρ_s and ρ_ℓ are the densities of the solid and liquid, respectively.

The temperature at the interface is slightly undercooled, which provides the kinetic driving force and a concentration gradient for diffusion. Consequently, the concentrations of the components are not precisely those of the equilibrium phase diagram. Referring to Fig. 5,

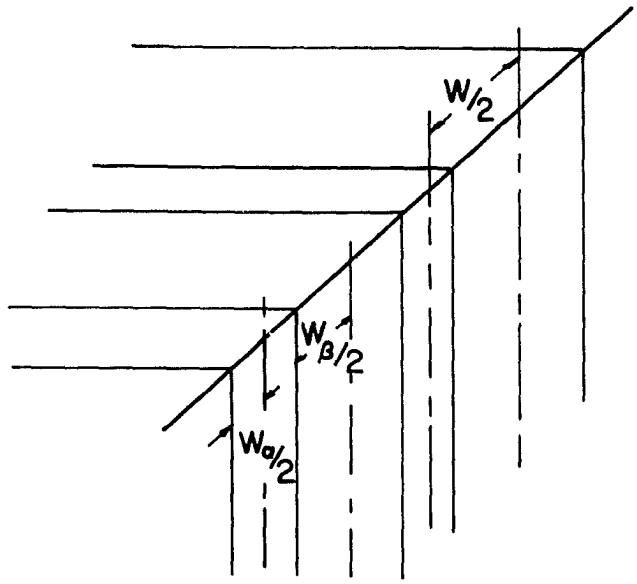

Fig. 4 -- The model of eutectic growth used in the derivation of equations for eutectic solidification. The front is plane, and the plates are uniform and parallel

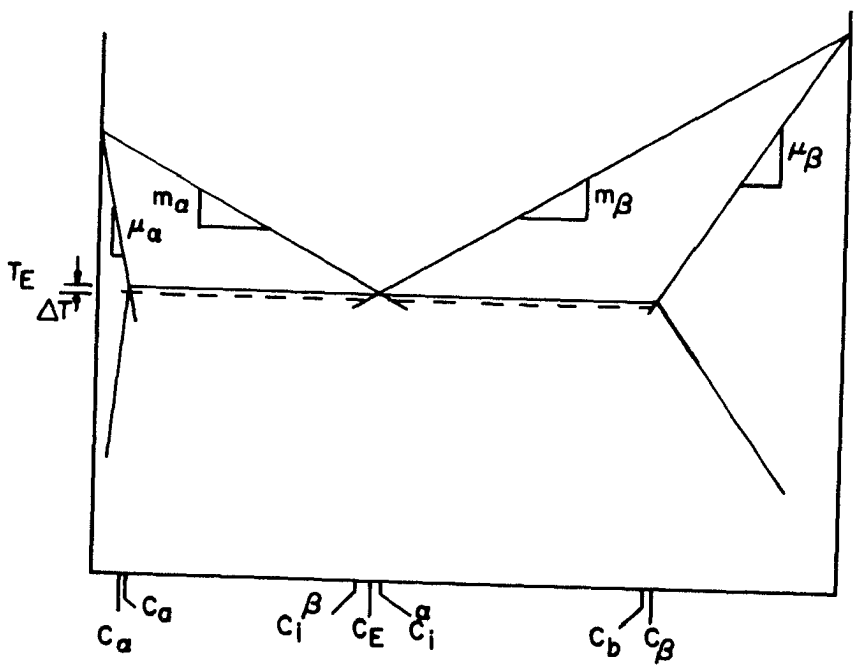

Fig. 5 -- Schematized phase diagram, showing eutectic compositions when a slight undercooling is present

$$
\begin{aligned}
C_a &= C_\alpha + \mu_\alpha \Delta T \\
C_b &= C_\beta - \mu_\beta \Delta T \\
C_i^\alpha &= C_E + m_\alpha \Delta T \\
C_i^\beta &= C_E - m_\beta \Delta T
\end{aligned}
\qquad [34]
$$

where $m_{\alpha,\beta}$ are the liquidus slopes and $\mu_{\alpha,\beta}$ are the solidus slopes of the alpha and beta phases, all defined positive, and ΔT is the amount of undercooling at the interface below the eutectic temperature.

Accounting for the difference in densities and for the undercooling, a mass balance at the interface in front of an alpha plate gives

$$
\begin{aligned}
RC_i^\alpha &= R^S C_a - D \left.\frac{\partial C}{\partial Z}\right|_i - UEC_i^\alpha \\
\left.\frac{\partial C}{\partial Z}\right|_i &= \frac{R^S C_a}{D} - \frac{(R-UE)}{D} C_i^\alpha
\end{aligned}
\qquad [35]
$$

Let $\rho^S = \frac{R^S}{D}$, $\rho = \frac{R}{D}$ and $\rho' = \frac{R-UE}{D}$ Then

$$
\left.\frac{\partial C}{\partial Z}\right|_c^\alpha = \rho^S C_\alpha - \rho' C_i^\alpha \equiv a \qquad [36]
$$

and

$$\left.\frac{\partial C}{\partial Z}\right|_i^{\beta} = \rho^s C_\beta - \rho' C_i^\beta \equiv b \qquad [37]$$

for the corresponding derivation in front of a beta plate. Substituting the definitions of Eqs. [34] into [36] and [37], we get

$$af_\alpha + bf_\beta = \rho^s [C_a f_\alpha + C_b f_\beta] - \rho' [C_E + \Delta T(f_\alpha m_\alpha - f_\beta m_\beta)] \qquad [38]$$

Here, $C_a f_\alpha + C_b f_\beta$ is just the solid concentration, C_s. If one assumes the liquidus and solidus slopes constant, as in Fig. 5, then for an alloy near the eutectic, f_α will be small when m_α is large, and vice-versa. Hence the coefficient of ΔT will be near 0. Taking this combined with the fact that ΔT is itself quite small, we can write Eq. [38] as

$$af_\alpha + bf_\beta = \rho^s C_s - \rho' C_E = \rho C_s \frac{\rho_\ell}{\rho_s} - \rho' C_E \qquad [39]$$

and so

$$D_o = \frac{\rho' C_E - \rho C_s \frac{\rho_s}{\rho_\ell}}{\rho'} \qquad [40]$$

from Eq. [D-46]. Again, from Eq. [36] and [37], using Eq. [34], the difference a-b is

$$a-b = \rho(C_\alpha - C_\beta)\frac{\rho_s}{\rho_\ell} + [(\mu_\alpha+\mu_\beta) - (1-\alpha)\frac{\rho_s}{\rho_\ell}(m_\alpha+m_\beta)]$$

$$\rho\Delta T \frac{\rho_\ell}{\rho_s} \qquad [41]$$

where $\alpha = UE/R$. Here, μ is greater than m for both sides of the eutectic. Since ΔT is again small the second term is dropped. In a faceting material with $\alpha>0$, however, that term could be significant. Neglecting ΔT, D_n then becomes

$$D_n = \frac{2\rho^s(C_\beta - C_\alpha)\ \sin n\pi f_\alpha}{[\gamma_n \cosh \gamma_n\delta + \frac{\rho'}{2} \sinh \gamma_n\delta]} \qquad [42]$$

Thus we arrive at the concentration in the liquid in front of the interface

$$C(z,y) = C_B + \frac{(\rho' C_E - \rho C_s \frac{\rho_s}{\rho_\ell})}{\rho'}[e^{-\rho' Z} - e^{-\rho'\delta}]$$

$$+ e^{-\rho' Z_2} \sum_1^\infty D_n \cos(\frac{2n\pi y}{W}) \sinh \gamma_n(\delta - Z) \qquad [43]$$

Careful analysis shows that UE has only the smallest effect on the summation term.

This result has parallels with the case of single phase growth, which are best seen by eliminating variations in y. Averaging over W, the summation term drops out,

resulting in

$$\bar{C}(z) = C_B + \frac{(\rho' C_E - \rho^s C_s)}{\rho'} [e^{-\rho' z} - e^{-\rho' \delta}] \qquad [44]$$

At the interface, $z = 0$, $\bar{C}(z) = \bar{C}_i$

$$\bar{C}_i = C_B + \frac{(\rho' C_E - \rho^s C_s)}{\rho'} [1 - e^{-\rho' \delta}]$$

Solving for the exponential term,

$$e^{\rho' \delta} = \frac{\rho^s C_s - \rho' C_E}{(\rho' \bar{C}_i - \rho' C_B + \rho^s C_s - \rho' C_E)} \qquad [45]$$

$\bar{C}_i$, the average liquid concentration at the interface, is a weighted average of the concentrations in front of the plates.

$$\bar{C}_i = f_\alpha C_i^\alpha + f_\beta C_i^\beta = C_E + \Delta T[f_\alpha m_\alpha - f_\beta m_\beta] \qquad [46]$$

Again, the term in brackets is small, expecially since in this case the concentration at the interface is close to C_E , so the average concentration in the liquid at the interface can be taken as C_E. Substituting into Eq. [45], we get

$$e^{\rho' \delta} = \frac{\rho^s C_s - \rho' C_E}{\rho^s C_s - \rho' C_B} \qquad [47]$$

At E = 0 this becomes Eq. [14] of Ref. (72), which is the same as that of Burton, Prim, and Slichter's derivation (7).

In an experiment, one must determine C_B and C_s for the closed system. Solving Eq. [47] for C_s, we get

$$C_s = \frac{\rho'(C_B e^{\rho'\delta} - C_E)}{\rho^s(e^{\rho'\delta} - 1)} \qquad [48]$$

Let $C_s = A + BC_B$;

$$C_s = \frac{\rho'}{\rho^s}\frac{C_E}{(1-e^{\rho'\delta})} - \frac{\rho'}{\rho^s}\frac{e^{\rho'\delta}}{1 - e^{\rho'\delta}} C_B \qquad [49]$$

Consider a system at quasi-steady state, with a composition profile as in Fig. 1. Assume that the liquid concentration beyond the solute build-up near the interface is independent of position. When a small section is so liquified, one can make a mass balance at the interface, as in Pfann (48),

$$C_B dz = C_s dz + dC_B[L - (z+dz)] \qquad [50]$$

and

$$\frac{dz}{L - z} = \frac{dC_B}{C_B - C_s} \qquad [51]$$

where the terms have their usual meanings. The build-up

at the interface is small compared to the total length, so one can use $C_\ell = C_B$. Recalling that $C_s = A + BC_B$, substituting into Eq. [51] and integrating,

$$\frac{1}{1-B}\int_{C_B^o}^{C_B}\frac{1}{C_B(1-B)-A}(1-B)\,dC_B$$

$$= -\int_{o}^{Z}\frac{-dZ}{L-Z} \qquad [52]$$

$$\ln\left[\frac{(1-B)C_B-A}{(1-B)C_B^o-A}\right] = \ln\left(1-\frac{Z}{L}\right)^{B-1} \qquad [53]$$

and finally,

$$\frac{(1-B)C_B-A}{(1-B)C_B^o-A} = (1-g)^{B-1} \qquad [54]$$

where $g = Z/L$, the fraction solidified. Recalling Eq. [49] for B,

$$1-B = \frac{1+(\frac{\rho'}{\rho_s}-1)e^{\rho'\delta}}{1-e^{\rho'\delta}} = \frac{1+(\sigma-\alpha)\frac{\rho_s}{\rho_\ell}e^{\rho'\delta}}{1-e^{\rho'\delta}} \qquad [55]$$

where $\sigma = \dfrac{\rho_s - \rho_\ell}{\rho_s}$

Also from Eq. [49],

$$A = (1 + \alpha)\,\frac{\rho_s}{\rho_\ell}\,\frac{C_E}{1 - e^{\rho'\delta}} \qquad [56]$$

so that

$$(1-B)C_B - A = \frac{[1 + (\sigma-\alpha)\,\frac{\rho_s}{\rho_\ell}\,e^{\rho'\delta}]C_B - (1-\alpha)\,\frac{\rho_s}{\rho_\ell}\,C_E}{1 - e^{\rho'\delta}} \qquad [57]$$

Putting this into Eq. [54]

$$\frac{[1+(\sigma-\alpha)\,\frac{\rho_s}{\rho_\ell}\,e^{\rho'\delta}]\,C_B - (1-\alpha)\,\frac{\rho_s}{\rho_\ell}\,C_E}{[1+(\sigma-\alpha)\,\frac{\rho_s}{\rho_\ell}\,e^{\rho'\delta}]\,C_B^o - (1-\alpha)\,\frac{\rho_s}{\rho_\ell}\,C_E} = (1-g)^{B-1} \qquad [58]$$

If the length of the initial transient is much less than L, then at the end of the transient $C_B^o = C_o$, since the extra solute rejected into the liquid is about equal to the extra solute contained in the liquid build-up.

Taking the bulk concentration at the end of the transient as C_o , Eq. [58] can then be solved for C_B , to get

$$C_B = \frac{\{[1+(\sigma-\alpha)\frac{\rho_s}{\rho_\ell} e^{\rho'\delta}]C_o-(1-\alpha)\frac{\rho_s}{\rho_\ell} C_E\}(1-g)^{B-1}+(1-\alpha)\frac{\rho_s}{\rho_\ell} C_E}{[1 + (\sigma-\alpha) \frac{\rho_s}{\rho_\ell} e^{\rho'\delta}]} \quad [59]$$

Then from Eq. [48]

$$C_s = (1 - \alpha) \frac{\rho_s}{\rho_\ell} \frac{(C_B e^{\rho'\delta} - C_E)}{e^{\rho'\delta} - 1} \quad [60]$$

and recalling Eq. [55],

$$B - 1 = \frac{1 + (\sigma-\alpha)\frac{\rho_s}{\rho_\ell} e^{\rho'\delta}}{e^{\rho'\delta} - 1} \quad [61]$$

At E = 0, σ = 0 these equations reduce to those of Verhoeven and Homer (72), as expected. If one can assume that the liquid and solid densities are the same, i.e. σ = 0, then Eqs. [59] - [61] reduce to

$$C_B = \frac{\{[1-\alpha e^{\rho'\delta}] C_o - (1-\alpha) C_E\}(1-g)^{B-1} + (1-\alpha) C_E}{[1 - \alpha e^{\rho'\delta}]} \quad [62]$$

$$C_s = (1 -\alpha)\frac{(C_B e^{\rho'\delta} - C_E)}{e^{\rho'\delta} - 1} \quad [63]$$

and

$$B\text{-}1 = \frac{1 - \alpha e^{\rho'\delta}}{e^{\rho'\delta} - 1} \qquad [64]$$

If the assumptions used here are valid, these three equations should predict the composition along the solidified section of an eutectic rod.

One of the interesting results of Verhoeven and Homer's report (72) is that at sufficiently small values of δ one could freeze out single phase solid from near-eutectic liquid. Since the eutectic growth equations apply only when the solid has an eutectic structure, they derived the equation

$$e^{\rho\delta} \geq \frac{C_E - C_\alpha}{C_o - C_\alpha} \qquad [65]$$

which specifies the limiting values of C_o , R, and δ for eutectic growth. For the derivation with an electric field it is necessary to have two such limits, one separating the conditions for eutectic growth from single phase growth of alpha phase, and the second dividing the conditions between eutectic growth and single phase beta growth. With just mixing, the composition of the solid will always be on the same side of eutectic as the original composition, C_o. With an electric field, however, the solid in principle

can be anything. The limiting equation tells when the first solid will be within the extremes of C_α and C_β and when it will not be. The derivation of the correct limiting equation begins from

$$e^{\rho'\delta} = \frac{\rho'C_E - \rho^S C_S}{\rho'C_o - \rho^S C_S} \qquad [47]$$

which is always true.

It is easier to work in terms of $\alpha = UE/R$. Note that for the derivation it matters not whether UE is more generally given as $F\mu$, so long as F and μ are defined such that when α is positive the beta phase, or solute, is transported away from the interface.

Equation [47] in terms of α is

$$e^{(1-\alpha)R\delta/D} = \frac{(1-\alpha)C_E - C_S}{(1-\alpha)C_B - C_S} \qquad [66]$$

At the end of the transient $C_B = C_o$. In point of fact the test for eutectic growth can be made at any point simply by inserting the current value of C_B , but usually the greatest extreme is reached at the beginning of the solidification. We shall require that $C_\alpha < C_S < C_\beta$, as otherwise eutectic growth is not obtained. Taking the derivation in detail,

$$[1-\alpha)C_o - C_s]e^{\rho'\delta} = (1-\alpha)C_E - C_s \quad ;$$

$$C_s(1-e^{\rho'\delta}) = (1-\alpha)[C_E - C_o e^{\rho'\delta}] \qquad [67]$$

$$C_s = \frac{(1-\alpha)[C_E - C_o e^{\rho'\delta}]}{1-e^{\rho'\delta}} \qquad [68]$$

Now $C_\alpha < C_s$, so

$$C_\alpha < \frac{(1-\alpha)[C_E - C_o e^{\rho'\delta}]}{[1-e^{\rho'\delta}]} \qquad [69]$$

First take the case where $1 - e^{\rho'\delta} < 0 \Rightarrow \rho'\delta > 0 \Rightarrow \alpha > -1$

$$C_\alpha(1-e^{\rho'\delta}) > (1-\alpha)[C_E - C_o e]$$

$$\frac{C_\alpha(1-e^{\rho'\delta})}{1-\alpha} > C_E - C_o e^{\rho'\delta} \Rightarrow C_o e^{\rho'\delta} > C_E - \frac{C_\alpha(1-e^{\rho'\delta})}{1-\alpha}$$

$$C_o > \frac{C_E}{e^{\rho'\delta}} - \frac{C_\alpha(1-e^{\rho'\delta})}{e^{\rho'\delta}(1-\alpha)}$$

Hence

$$C_o > C_E e^{-\rho'\delta} + \frac{C_\alpha(1-e^{-\rho'\delta})}{1-\alpha} \qquad [70]$$

Taking $1 - \alpha < 0$ merely switches the sign of the inequality twice between Eq. [69] and [70], so the final result is identical. For the case of $\alpha \to +1$, that is $1 - \alpha \to 0$, one applies L'Hopital's Rule to Eq. [70] to get

$$C_o > C_E + \frac{R\delta}{D} C_\alpha \qquad [71]$$

The derivation for the upper limit, with $C_s < C_\beta$, is quite similar. Replacing C_s in Eq. [68] with C_β instead of C_α, one gets

$$C_\beta > \frac{(1-\alpha)[C_o e^{\rho'\delta} - C_E]}{e^{\rho'\delta} - 1} \qquad [72]$$

which in the same manner as Eqs. [69] - [71] becomes

$$C_o < C_E e^{-\rho'\delta} + \frac{(1-e^{-\rho'\delta})C_\beta}{1-\alpha} \qquad [73]$$

for all values of α.

The extremes of $\rho'\delta \to 0$ and $\rho'\delta \to \infty$ are of interest. As $\rho'\delta \to 0$, one gets $C_o > C_E$ and $C_o < C_E$, hence $C_o = C_E$. As $\rho'\delta \to \infty$ Eqs. [70] and [72] reduce to

$$\frac{C_\alpha}{1-\alpha} < C_o < \frac{C_\beta}{1-\alpha} \qquad [74]$$

These limits represent the cases of complete mixing and no mixing, respectively. As the amount of mixing increases, the range of allowable compositions of C_o tends to be located near C_E, regardless of α. As the amount of mixing decreases to nothing the region of allowed values of C_o and α increases toward the extreme ends of the range of eutectic compositions. Note that with no mixing and no body force the allowed C_o is between C_α and C_β, as one would expect. Figure 6 is a graph of Eqs. [70] and [73], with Eq. [74] also included to indicate the outer limits of acceptable C_o, α combinations.

In the eutectic equations derived above the normal freezing equation, Eq. [47], is used as a boundary condition. The normal freeze equation assumes the liquid concentration is uniform beyond δ from the interface, while in the presence of differential body forces such as electric fields there may be a concentration gradient in the liquid. Although exact mathematical solutions are not available, one would like some estimate of how much error is introduced by ignoring this effect.

Taking g as the dimensionless position of the interface, z/L, and f as a general position in the liquid, z/L, where $f \geq g$, suppose that C_ℓ is given by

$$C_\ell = mf + b \qquad [75]$$

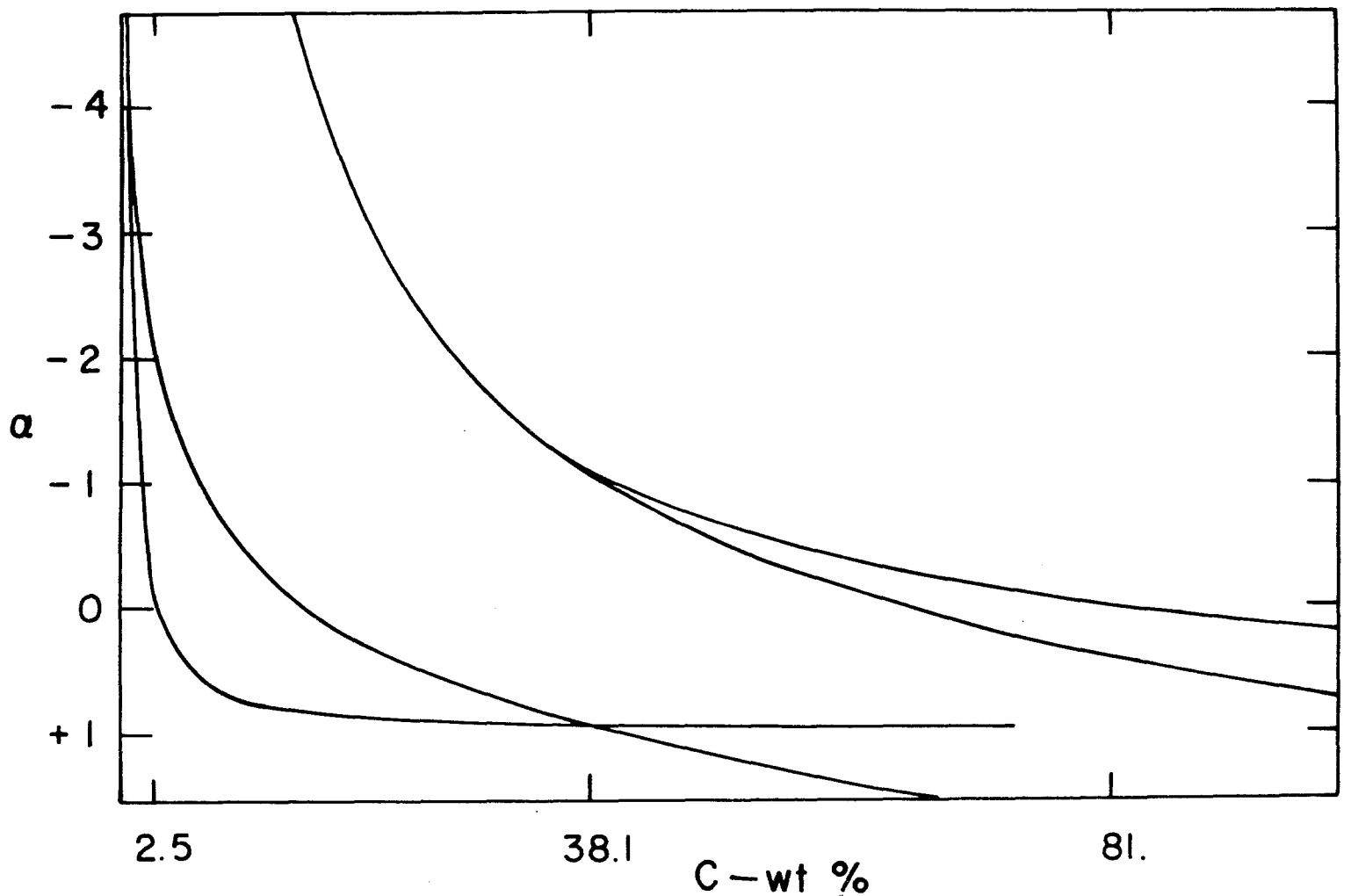

Fig. 6 -- The limits of composition and α which can result in two phase eutectic structure upon solidification, as calculated for the Sn-Pb system. Experimental conditions inside the limits will be two phase. The inner limits are for $R\delta/D = 1.$, the outer limits for $R\delta/D = \infty$

where m is constant, and b = b(g). C_B is now the average concentration at any point in the run

$$\frac{1}{1-g}\int_g^1 C_\ell df = C_B$$

from which one obtains the expression for b

$$b = C_B - \frac{m}{2}(1+g) \qquad [76]$$

Again performing a mass balance at the interface, g, one gets

$$dC_\ell(1-g) = (C_\ell - C_s)\Big|_g dg = (1-k_e)\, C\Big|_g dg \qquad [77]$$

which, with insertion for C_ℓ and b becomes

$$[mdf + dC_B - \frac{m}{2}dg](1-g) = (1-k_e)[C_B - \frac{m}{2}(1-g)]dg \qquad [78]$$

Here the use of dC_ℓ instead of $dC_\ell\Big|_g$ on the left side of Eq. [77] results in the presence of three differentials. If we can take f = g and df = dg, then Eq. [78] can be rearranged into

$$dC_B - \frac{(1-k_e)}{(1-g)} C_B dg = - \frac{(2-k_e)}{2} m\ (1-g)dg \qquad [79]$$

This equation may be made exact by the use of an integrating factor, $v = (1-g)^{(1-k)}$. Then it is a simple matter to integrate and solve for C_B, and hence for C_ℓ and C_s

$$C_s = k_e[F(1-g)^{(k_e-1)} + \frac{m}{2} \frac{(2-k_e)}{(3-k_e)} (1-g)^2 - \frac{m}{2}(1-g)] \qquad [80]$$

where F is constant.

By conservation of mass

$$\lim_{a \to 1} \int_0^a C_s dg = C_o \qquad [81]$$

which leads to

$$F = C_o + \frac{m}{4} - \frac{m}{6} \cdot \frac{(2-k_e)}{(3-k_e)} \qquad [82]$$

and hence the final solution

$$C_s = k_e \left(C_o + \frac{m}{4} - \frac{m}{6} \cdot \frac{(2-k_e)}{(3-k_e)} \right) \cdot (1-g)^{k_e-1} + \frac{m}{2} \cdot \frac{(2-k_e)}{(3-k_e)} \cdot (1-g)^2 - \frac{m}{2}(1-g)] \qquad [83]$$

At m = 0 Eq. [83] reduces to the normal freeze equation (78),

$$C_s = kC_o(1-g)^{k-1} \qquad [84]$$

A computer program has been written to compare Eqs. [83] and [84]. The calculations were taken over the range $0 \leq g \leq 0.9$ in increments of 0.01. The concentration C_s of each incremental section was calculated by taking the average of the concentration at each side of the increment. Table I gives a summary of the comparisons. Examination of Eq. [83] will show that if m is taken as a linear function of C_o, then C_s/C_o and DIF/C_o in Table I will be constant.

A similar derivation can be made for the case of

$$C_\ell = m(1-f)^2 + b \qquad [85]$$

In this case, following the above derivation exactly,

$$b = C_b - \frac{m}{3}(1-g)^2 \qquad [86]$$

$$C_b = F(1-g)^{k_e-1} - \frac{3-k_e}{4-k_e} \cdot \frac{2m}{3} \cdot (1-g)^3 \qquad [87]$$

so that finally

Table I. Comparison of normal solidification for non-uniform solute profile with normal solidification for uniform solute profile. $C_o = 1$ for all calculations

k_e	m	g	C_s	C_s Eq.[84]	$(C_s^f - C_s^n)/C_s^n$ DIF, pct	Diff. in mass balance, pct
			C_s by Eq. [83]			
0.3	-0.1	0.	0.301	0.300	0.401	
		0.34	0.401	0.401	-0.009	
		0.90	1.483	1.504	-1.357	-1.026
0.1	-0.1	0.	0.100	0.100	0.316	
		0.28	0.134	0.134	0.007	
		0.90	0.784	0.794	-1.349	-1.273
			C_s by Eq. [88]			
0.3	0.1	0.	0.305	0.300	1.500	
		0.65	0.626	0.626	-0.010	
		0.90	1.499	1.504	-0.289	0.881
0.0656	0.1	0.	0.067	0.066	1.63	
		0.78	0.270	0.270	0.001	
		0.90	0.564	0.564	-0.057	1.263

$$C_s = k_e \left(C_o + \left(\frac{3-k_e}{4-k_e}\right) \cdot \frac{m}{6} - \frac{2m}{9} \right) \cdot (1-g)^{k_e-1}$$

$$+ \frac{2m}{3}(1-g)^2 - \frac{(3-k_e)}{(4-k_e)} \cdot \frac{2m}{3} \cdot (1-g)^3] \quad [88]$$

This equation for C_s was also compared with Eq. [34] as shown in Table I.

An attempt to solve the problem for the case of

$$C_\ell = be^{mf} \quad [89]$$

was not successful.

What is a reasonable m? At steady state for a closed system, where a force per unit potential, F, and potential, μ, exist, the steady-state flux balance is

$$-D \frac{\partial C}{\partial Z} + \mu F C = 0 \quad [90]$$

Integrating and applying the condition that the total mass of solute is C_B , one gets

$$C_\ell = \frac{\phi C_B e^{\phi f}}{[e^{\phi} - 1]} \quad [91]$$

where $\phi = F\mu L/D$. For thermal diffusion $\phi = D'GL/D$. The ratio D'/D for Pb in Sn is about 2×10^{-3} (73), the gradient

used in this work was about 300°C per cm with just furnace heating, and the sample length was about 10 cm when ϕ was about 6. For electrotransport, using typical values of U, E, and D, ϕ was about 90.

Two things help reduce ϕ. The derivation for the steady state uses D for the case of no mixing, while with the electric field significant mixing is expected, while would raise D_{eff} by a large factor. Secondly the derivation of Eq. [91] assumes that steady state in fact exists. The time to reach steady state for a sample length of 10 cm, given in Table II, can be long. It is evident that significant time could be required. Thus, as an approximation, it should be safe to take ϕ, and hence any errors, as less than the values for steady state. If one approximates Eq. [91] with Eq. [85], the value of m turns out to be quite close to ϕ.

To summarize this chapter, a solution for the directional solidification of off-eutectic alloys has been derived to include electrotransport (Eq. [62-64]), assuming constant parameters D, U, and E. The effects of kinetic undercooling at the interface and volume change on freezing have been shown to be small. Equations specifying the experimental conditions under which eutectic growth occurs have been developed (Eq. [71, 73]). Finally, the assumption of uniform composition in the bulk liquid, required for a

Table II. Time required for a closed system with differential body force to reach 99 pct of steady state, adapted from Ref. 66. $D = 1 \times 10^{-5}$ cm^2 per s, sample length = 10 cm

$F\mu/D$	t_∞ in days
11.5	$1 < t < 5$
7.0	$5 < t < 10$
6.0	$5 < t < 10$
1.55	$10 < t$
0.95	$10 < t$

solution of the equations, has been discussed in detail. The analysis suggests that this assumption will be reasonably well satisfied by the experimental conditions used in this work.

EXPERIMENTAL METHOD

The starting materials for the alloys were all high purity: from Vulcan Materials Corp., the tin was 99.999 pct, the bismuth 99.998 pct, and the Cominco American lead 99.999 pct pure. A total of 50 or 100 g of the starting metals was weighed out to within 0.02 pct of nominal composition.

The charge was then placed in a Pyrex crucible about 5 cm I.D. and put into a vacuum chamber. This chamber was evacuated and backfilled twice with helium before final evacuation. The pressure maintained while melting was less than 5 μm Hg. After the furnace had reached 400°C, the alloy melted in less than 15 min, but it was always left for at least 1/2 hr before casting. Shortly before the alloy was cast, a rod with a small bladed paddle on the end was lowered into the alloy and rotated to ensure complete mixing. Then the Pyrex crucible was raised to within about 15 cm of the top of the furnace and a 5-mm I.D. Pyrex tube, 60 cm in length and sealed on one end, was lowered until the open end rested near the bottom of the crucible. The vacuum system was then backfilled quickly with helium so the alloy would be driven up into the tube. The alloy in the portion of the tube outside the vacuum system froze almost instantly, on the order of a few seconds, while the portion near the vacuum seals required a somewhat longer

time but less than a minute. Sections from both the top and bottom were removed and analyzed to be absolutely sure that no macrosegregation had occurred.

For the following description of the equipment reference is made to Figs. 7 and 8. In making a run, 3.5 and 4.0 g of cast alloy were cut from the master alloy. The sample tube was quartz and had a bottom section 2 mm I.D. and 3 mm O.D., which had been fused to a top section 6 mm I.D. and 8 mm O.D. The lower section was 15 cm long and the top section was about 20 cm in length, while the over-all length was closely controlled to 35.6 cm. The ends were ground square and were not firepolished.

A copper insert, covered with a thin coat of graphite just fitted 5 cm up inside the lower tube and rested on the top of a 2.5 cm diam copper support rod. "O"-rings and clamping plates were used to seal the tube vacuum tight at the bottom. The upper support for the quartz tube was a brass tube with a connection on one side to the vacuum system and a standardized "O"-ring seal to the quartz on the bottom. Electrical and water connections were at the top. A nylon plug threaded outside with the center cut out was placed on top of the tube so that the tube could not move vertically. When the preparations reached this state, the alloy material was cleaned with acetone and alcohol and placed in the tube where it dropped down to the top of

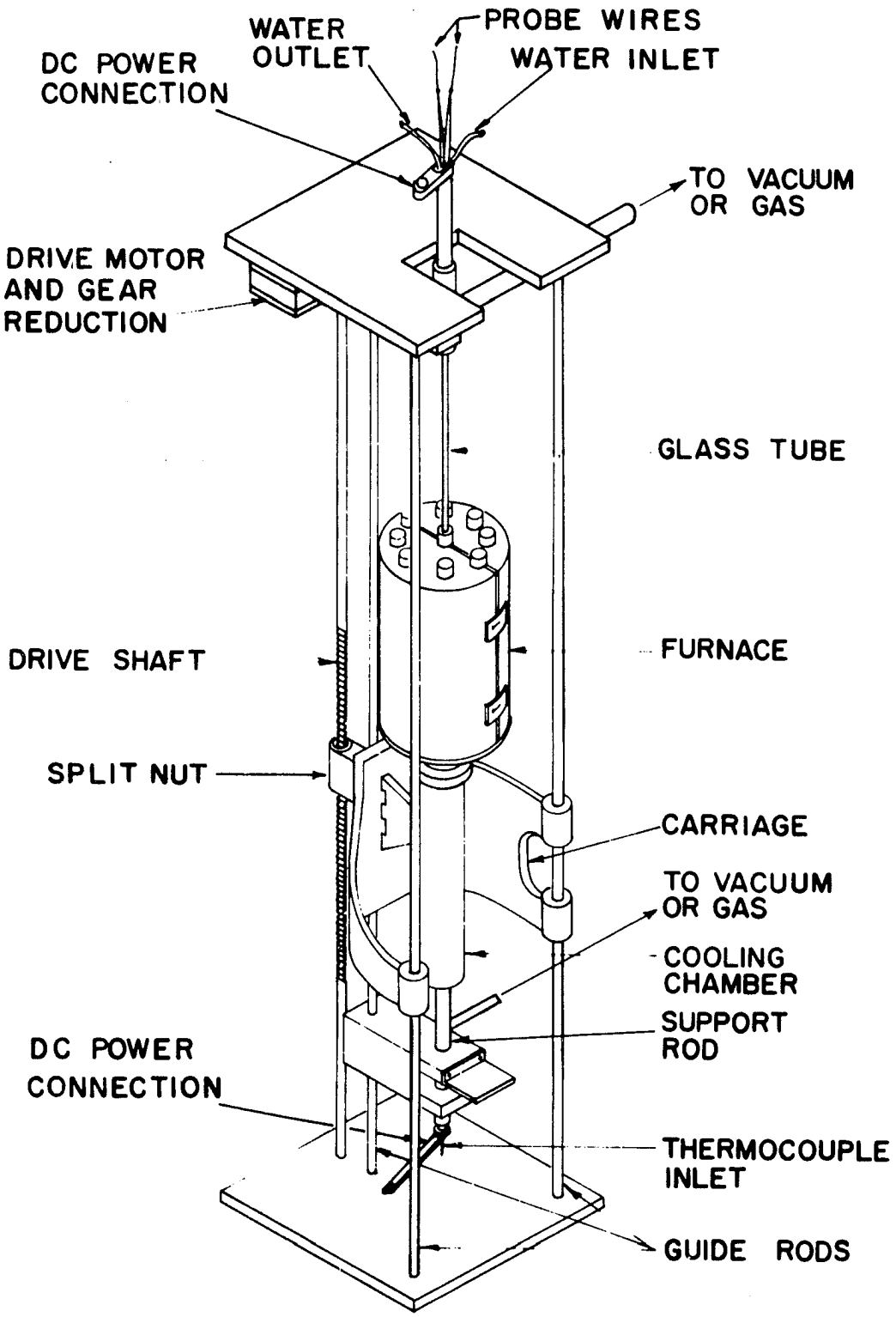

Fig. 7 -- Experimental apparatus for controlled solidification of alloys in an electric field

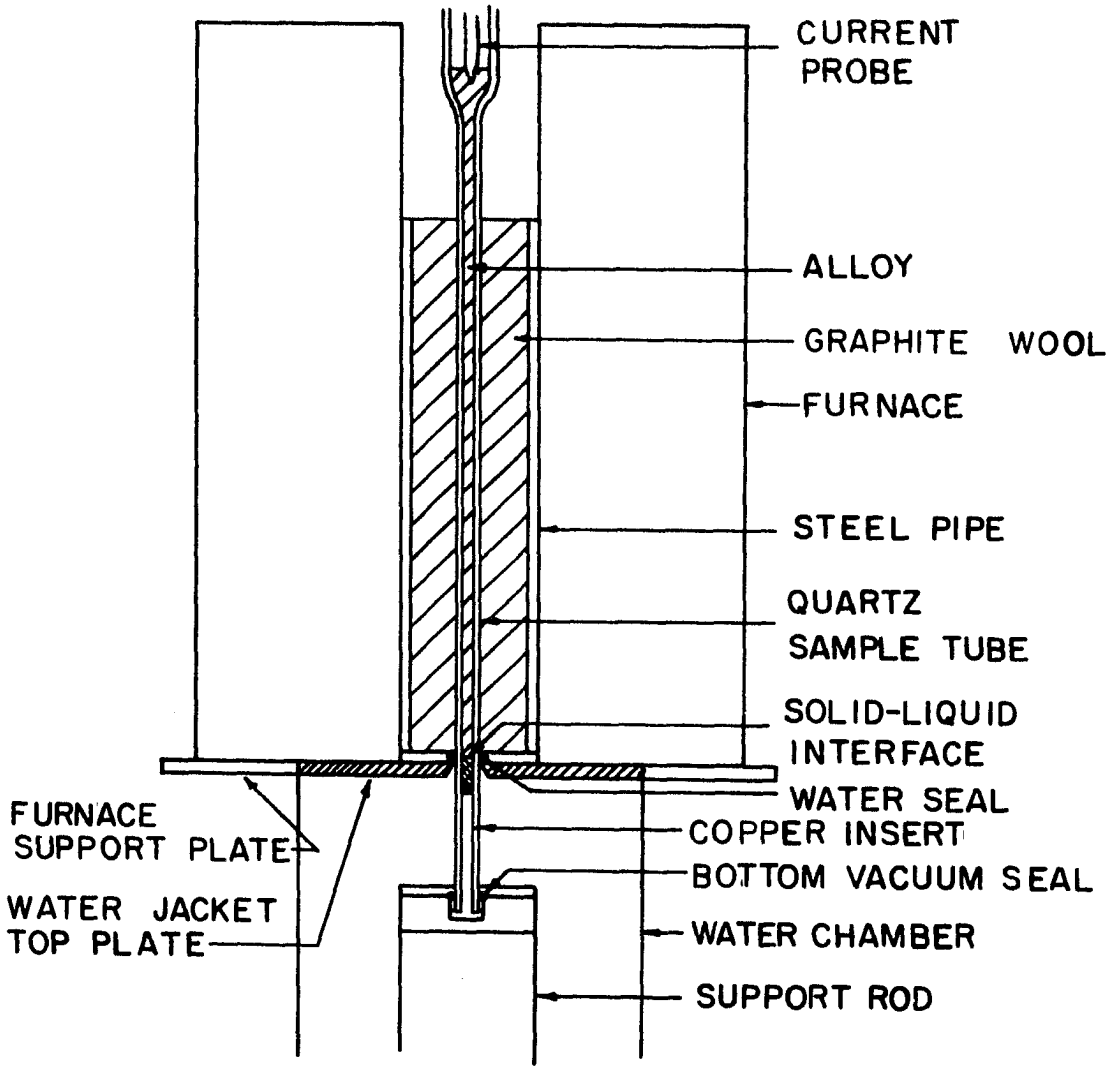

Fig. 8 -- Sectional view through the sample and surroundings

the quartz tube.

Then the top plate of the water chamber was threaded on. The former had a hole in the center for the sample tube. The water chamber, or jacket, was symmetrical with the sample tube and copper shaft and slid up and down along the center-line axis. An "O"-ring and clamping plate were put in place on the top plate of the water jacket to seal the water in. This ring had to be well lubricated since it was the only source of longitudinal stress on the sample tube. Next a stainless steel tube was threaded onto the top clamping plate. It was 2.5 cm O.D., 2.1 cm I.D., 15 cm long, and filled with small bits of graphite wool. The steel tube and wool served to eliminate any possibility of free convection of air inside the pipe.

Then the furnace support plate was brought up and attached to the flange on the top plate of the water chamber, a graphite wool pad put on, and the split half furnace put in position around the steel pipe. The furnace was 20 cm high and consisted of four half sections of grooved ceramic with coiled Nichrome wire in the slots. The ends of the commercially supplied heating sections were shortened to maximize the heating zone. A graphite wool and glass wool pad was wrapped around the tube at the top of the furnace to reduce air flow and heat loss.

Finally the probe system was installed at the top of

the upper holder, see Fig. 7. This consisted of three probes, one a tantalum shaft, 1.42 mm in diam, which could fit all the way down to the copper insert at the bottom; a small 0.457 mm tungsten wire which could also reach the bottom; and a copper shaft 3.80 mm in diam, threaded on the lower end. A tungsten probe tip, 3.28 mm in diam, was press fitted into a copper support piece which in turn was threaded into the long copper shaft. The tungsten was about 4 cm long and slightly pointed on the end. The three probes were held in the upper holder, 2.5 cm in diam, which was sealed at each end. Water passed from the lower water chamber into and out of the holder at the top side, while the tantalum shaft and tungsten wire slid through in vacuum sealed tubes separated from the water. The copper probe was threaded into the bottom of the tube, and a connection was made to the current supply at the top of the holder on the side. This completed the assembly of the sample apparatus preparatory to making a run.

The apparatus was constructed so that the water chamber and the bottom copper shaft were electrically grounded, while the upper tube support and all attached to it were electrically floating. The water was pumped from a constant level reservoir by an impeller pump through the lower water chamber, then through the upper brass tube chamber and into a drain.

To make a run the chamber was first evacuated to less than 5 μm pressure. Then the furnace was turned on and raised to about 600°C in less than 4 hr. A thermocouple buried in the graphite wool monitored the furnace temperature. During this period the system was backfilled with about 1/3 atmosphere of methane to remove oxide from the surface of the sample and to keep the current probe clean. After the furnace reached a temperature near 650°C, the tantalum rod was placed all the way down to the bottom. Thus, most of the alloy was pushed up into the upper part of the tube where the temperature was higher. The system was evacuated while the furnace continued to heat up to 725°C. After the rod had been in place for 1/2 hr while the furnace was at 725°C, it was removed and the tungsten wire was put all the way down to the bottom. When the rod was removed, the alloy ran down into the small section and some bubbles formed. The wire was raised slowly while being rotated to remove these. A continuity meter was connected between the probes and the bottom of the copper shaft below so that it was possible to tell when bubbles were present. The alloy extended about 6 mm into the large section of the sample tube. After all the bubbles had been removed, the alloy was allowed to sit under vacuum at maximum temperature for at least 1/2 hr more, during which time more bubbles usually formed.

After the last bubbles had been removed, the system was backfilled with 1/3 atmosphere methane, 2/3 atmosphere helium to a positive pressure of 1 lb. gauge. The furnace and water jacket were raised for 2.5 cm to the same position for each run at a rate between 80 and 130 μm per s. Care was taken to be sure continuity was maintained. Simultaneously the furnace temperature was lowered to 600°C. When the furnace and jacket were in proper position, the drive was shifted to the setting selected for the run and started at a rate between 2 and 10 μm per s. Hopefully the furnace temperature had dropped to 600°C at this point; if not the drive was halted until it did. The furnace setting was made manually because there was no point in the furnace which could be expected to maintain constant temperature throughout a run.

Immediately when the current was cut in, the interface position in the sample dropped down as the joule heating began in the sample. The temperature in the graphite wool rose quickly, usually to about 625°C. Then it slowly dropped for the duration of the run because the furnace had not reached its equilibrium condition and because the thermocouple tip was near to the probe-alloy contact at the start.

The current passing through the sample was determined by measuring the voltage drop across a 1 ohm resistance

with a K-3 potentiameter. The current supply was very steady, but there was a warm-up period which could not be avoided. The result was that the current started at 40.05 amp, rose to around 40.30 amp in 15 min, then dropped back a few hundredths of an amp over the duration of the run. It would have been possible to adjust the current to maintain more constant output, but it was found that when an adjustment was made, a band usually formed across the eutectic pattern of a Sn-Pb alloy, indicating a short transient in the rate of interface motion.

A dial gauge marked to 0.001 in., mounted near the axis of the sample below the water jacket, and a timer reading to 0.01 s were used to measure the actual furnace rate of the run. The gauge extended as the furnace and water jacket moved up. The current and furnace temperature were monitored throughout.

Two types of runs were made, "short runs" and "long runs." The former were Sn-Bi alloys. For these the furnace was raised 2.5 cm at a slow rate after the current was turned on and then the alloy was quenched to preserve the interface morphology. At the conclusion the furnace was turned off and within 10 s the water jacket and furnace were raised by hand quickly at least 2 cm to quench in the interface structure. Frequently the "O"-ring failed during the quench and water from below ran up into the graphite

wool in the pipe. Raising the water jacket in this manner was found to produce a finer structure in the quenched liquid than simply disconnecting the current. The long runs were Sn-Pb near-eutectic alloys. These were run over as much of the length of small tube as design permitted. At the end of a long run the current was disconnected and the furnace turned off and opened. After disassembly, the sample was broken out of the quartz tube by gently hammering it and was then given an electropolish as detailed below to reveal the interfaces. There was a small ring on the surface near the bottom of each sample which indicated the position of the interface at the start of the run. On the short runs there was another line indicating the quench line 2.5 cm above the current start line. On the long runs there was a line slightly below the top of the neck of the sample. The interface line in each case was marked with a razor to facilitate location.

Next the sample was sectioned for analysis and milled in a lathe using a 0.040 in. (1 mm) wide tool bit. For the short runs sections were taken from six points on the sample, the top, a point 2 in. above the interface, one in. above the interface, just below the quench interface, just below the previous cut, and the very bottom as shown in Fig. 9. All the cuts but the top one were 2 mm wide in order to increase the weight of the sections to facilitate

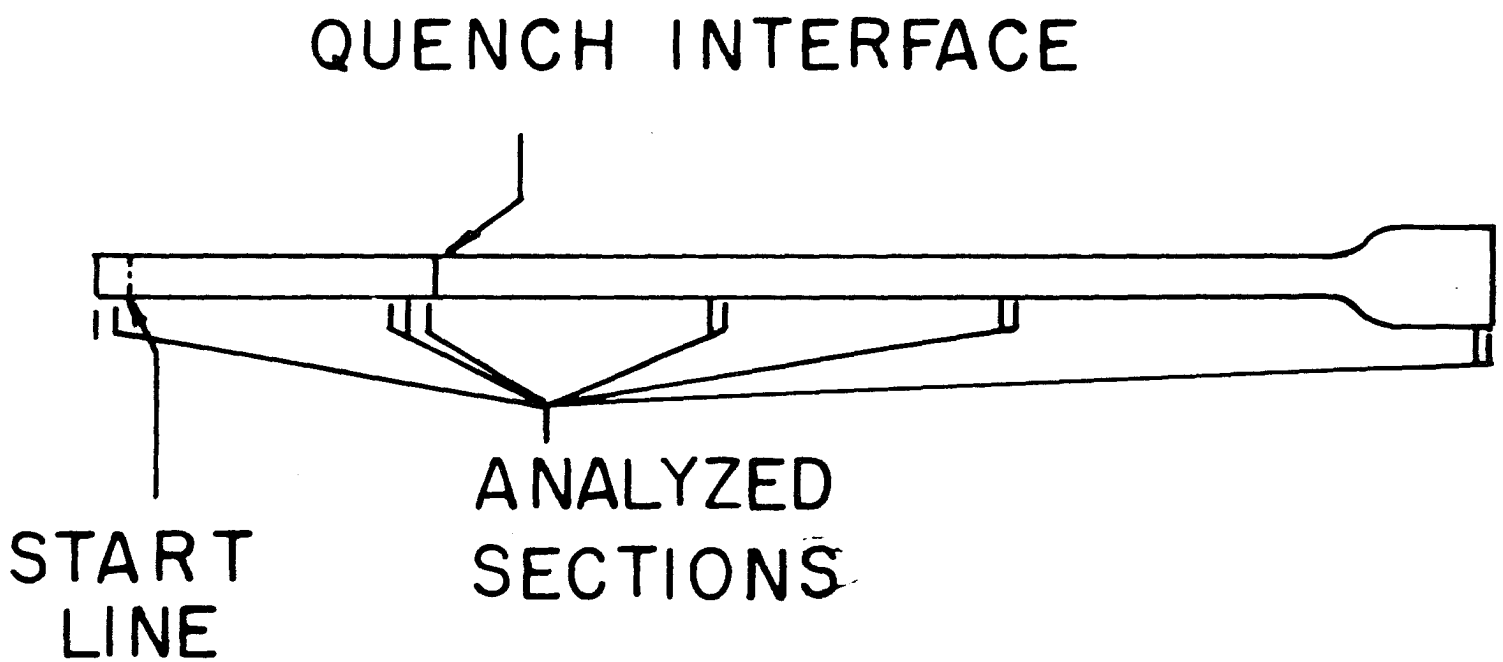

Fig. 9 -- The positions of the various interfaces and analyzed sections on the Sn-Bi sample

better chemical analysis. The sections containing the quenched interface were mounted and polished as described below for metallographic examination. Photographs were taken of every quenched interface.

For the long runs sections were cut from the very top and then just below the large section, but still in the liquid region. A section was taken off the very bottom, below the electric field start line, then a distance of 0.200 in. (5.08 mm) was carefully measured from the cut end, so that exactly 0.200 in. was cut off. Since the tool bit was 0.040 in. wide, this left a 0.0160 in. length unmilled. Both were placed in their respective sample bottles and the process repeated until the whole sample was sectioned in this manner. Each milled section of 1 mm weighed about 22 mg.

For the long runs the 4 mm sections were first weighed to the nearest 0.01 mg, then mounted in Quik-Mount to which copper powder had been added to make it conductive. The samples were ground down first on #320 grit, then #600 grit silicon carbide paper. A polishing paste, Extra-Prima, was used to wipe away all the carbide grit on the surface and was then itself removed by washing the samples in soap and water and an alcohol rinse. After the copper part of the mount had been masked with Macro-Stop lacquer, the samples were electropolished in a 6 pct perchloric acid in methanol solution and kept in a bath of dry ice-acetone which

maintained the solution below -50°C all the time. Electropolishing was done at about 40 v for 1/2 to 1 min.

Without further treatment it was immediately obvious under a microscope at 50X whether a particular transverse section contained dendrites or not. The eutectic structure was very fine, with Sn appearing bright and Pb looking darker. Tin or Pb dendrites, with diameters many times larger than the lamellar spacing, showed up very clearly at a glance.

If there were no dendrites in any section of the sample, then the milled sections from the very top and the very bottom, and every second milled section over the length, were submitted for chemical analysis. If dendrites appeared, the top and bottom sections were submitted, along with a few sections from the dendritic region, and milled sections from the eutectic region present.

The technique used for the analysis of Bi was the spectrophotometric method. Two different modifications were used in the course of the work. At first the sample was dissolved in aqua-regia and bromic acid was added. Then the tin tetrabromide was fumed off by heating. A metal complex color indicator, Xylenol Orange, was added. Finally the color density of the solution was determined by measuring the absorption of light at the 519 mμ wavelength.

The second modification was somewhat simpler and

faster. The sample was dissolved in HCl containing a small amount of HNO_3. After further additions of the two acids the solution contained a bismuth chloride complex with a known amount of nitric acid. The percent absorption of the solution at the 326 mμ wavelength was then determined spectrophotometrically.

The spectrophotometric method is sensitive to the presence of most metals, specifically iron, while the $HCl-HNO_3$ modification is rather less sensitive to most common metallic contaminants. A completely different technique was used for the lead analysis. The sample was dissolved in HNO_3 containing some NaF. A buffer and NH_3 were used to adjust the pH to 5.0 and Xylenol Orange was added. Then the solution was titrated with EDTA (Ethylene-diamemetetra-acetic acid), the end point being determined by the change in color from pink or red to yellow.

For the measurement of G, and the determination of the mixing length the system was very like that described in detail above. The only difference was that a thermo-couple was inserted from below to record the temperature profile during solidification as shown in Fig. 7. The working end of the thermocouple consisted of two 0.075 mm thermocouple wires of Chromel and Constantin. After being coated with Pyrex, they were broken out at the end and welded together. This end was coated with a slurry of

boron nitride, then dried and baked. The completed section was put into a tantalum tube, 0.5 mm O.D., 0.35 mm I.D. which was in turn fitted at the bottom end to a small brass adaptor. Two 0.30 mm thermocouple wires contained in a stainless steel tube, 3 mm O.D., were welded to the small wires and the adaptor was soldered to the stainless steel.

This resulted in a very small thermocouple tip, less than 0.5 mm across, electrically insulated from the melt but thermally quite sensitive to sudden changes in temperature. The bottom of the sample tube rested on the flanges of the small copper insert, which for this part of the work contained a hole just large enough to allow the tantalum tube portion of the thermocouple to pass. The thermocouple was pushed up into the melt after outgassing and stirring.

Preparation for making a run was also like that described above. When the chamber had been backfilled and the furnace raised, the current was turned on, either up or down, and the furnace and water jacket were raised slowly while the output from the thermocouple was recorded on a strip chart as a function of time. The gradients were straight lines on the chart. A ruler was used to draw a line along each straight segment and thus obtain the gradient. The change in temperature as the thermocouple passed from the liquid to solid was quite easily observed. The inter-

section of the two ruler lines was taken as the interface temperature. At the end of travel up, the furnace and water jacket were returned to the start position.

DETERMINATION OF MIXING LENGTH

The mixing length, δ, enters into the equation for k_e. Since the relationship, including the effect of electric field, has been derived (2, 50), it will only be outlined here.

Consider the situation where an alloy is solidifying with convection in the liquid as shown in Fig. 1. We specify no mixing between the interface and δ and complete mixing further from the interface. At the interface itself, there is equilibrium between the solid and liquid. Thus the liquid at that point, C_i, is C_s/k_o. C_b is held uniform, i.e., independent of z at all distances beyond δ from the interface.

This model of mixing is admittedly not an accurate representation of the facts. In the case of turbulent mixing there is a buffer region between the turbulent region and the "stagnant" region near the wall in which diffusion and convection both contribute to mass transport. However, the model has been shown to predict behavior quite well (78).

Making a flux balance in the liquid in front of the solidifying interface and using the two boundary equations, $C_\ell = C_i$ at $z = 0$, and $C = C_b$ at $z = b$, one can obtain

$$C_\ell = C_b + \frac{C_i C_b}{1-e^{\rho'\delta}} \left[e^{-\rho' z} - e^{-\rho'\delta}\right] \; ; \; \rho' = \frac{R-UE}{D} \qquad [92]$$

the equation of the liquid composition between the interface and δ. To obtain this result it is necessary to assume that quasi-steady state conditions exist, that the bulk liquid composition is uniform with distance beyond δ, and that D, U, and E are constant within the stagnant layer.

Taking a flux balance at the interface and using the definitions of k_o and k_e, one can derive

$$k_e = \frac{k_o(1 - \frac{UE}{R})}{k_o + (1 - \frac{UE}{R} - k_o)e^{-(1 - \frac{UE}{R})\frac{R\delta}{D}}} \qquad [93]$$

It is clear that to use equations involving k_e it will be necessary either to make measurements at all experimental rates for both current directions or to determine δ, the course taken here.

The composition at the interface depends in part on the direction of the electric field. Using the superscripts $^+$ or $^-$ to indicate field direction, the difference in composition between E^+ and E^- can be given as

$$\Delta C_i = C_i^+ - C_i^- = \frac{C_s^+}{k_o} - \frac{C_s^-}{k_o} = C_b(k_e^+ - k_e^-)/k_o \qquad [94]$$

which, using the equation for the liquidus curve, becomes

$$\Delta T_i = T_i^+ - T_i^- = m_\ell \Delta C_i \qquad [95]$$

Given experimental measurements of ΔT_i , δ can be determined. The experimental method has been described in the chapter, Experimental Method. Eleven runs with E positive and six with E negative were made successfully on an alloy of 2 pct Bi at a rate such that the interface was expected to be quite stable. The difference $k_e^+ - k_e^-$, calculated from Eq. [93], is zero when δ is zero. As δ is increased the difference goes through a maximum (at δ = 0.045 cm in this work) which is only slightly greater than 2UE/R. The maximum calculated from the experimental conditions corresponds to a temperature difference of 2.08°C. The measured difference in interface temperature was 3.64°c, significant at the 99.9 pct confidence level. Thus, no value of delta could be found to satisfy Eqs. [93-95]. With the method used here one must assume δ is independent of the direction of the electric field. If most of the mixing is caused by the current the assumption may be valid, but if mixing is largely the result of density inversions it will obviously be false. The results of the eutectic solidification work, to be discussed later, support the latter possibility.

In making measurements of ΔT_i the temperature gradients in the liquid and solid were also obtained. Measurements were made at various rates, current directions, and furnace travel directions. No discernable difference in the

gradients could be found among any of the different conditions. For 64 measurements made during solidification, the best estimate of the gradient in the liquid was 648 ± 4.°C per cm at the 66 pct confidence interval, the value used throughout this thesis.

Central to this work was the assumption that the electric field had no effect on the kinetics of solidification. Jackson and Chalmers (32) developed a theory of solidification kinetics based on an activation model. According to their theory, when an electric field is imposed on the interface in order to move atoms toward the liquid, the effect is to make the atoms more likely to pass into the liquid than they would usually at the same temperature. Using likely values of mobility and electric field and estimates of the activation energy (32), the difference in equilibrium temperature for Sn is on the order of one part in 10^6, or 0.005°C at the melting point.

Cahn (8) developed a "diffuse interface" theory, in which atoms settle down from a liquid to a solid state, passing through a region in which they are neither wholly liquid nor solid. This theory suggests that the activation energies could be much lower than those deduced by Jackson. If this is true, then the electric field might produce a real difference in the interface temperature of a pure metal. Twenty-two measurements of the melting point with

the field positive and twenty-three measurements with the field negative resulted in melting points of 230.17 ± 1.27°C and 231.37 ± 0.46°C, respectively, at the 90 pct confidence level. The temperatures could be low because of errors in calibration, but this would not effect the difference in melting points. Thus, a current density of 1285 amp per cm^2 does not produce a significant difference in the melting point of pure tin.

Also during this work, it became relevant to ask whether the thermocouple significantly altered the temperature profile and whether the temperature gradients were "real." These questions were prompted by the fact that the ratio of liquid gradient to solid gradient, which should be in the ratio of k_s/k_ℓ for the large gradients used here, was on the order of 2.1, and that at higher current densities it was 2.6, as opposed to the expected value of 1.8.

The thermocouple occupied about 6 pct of the total cross-section of the sample tube. To see if this change in cross-section had any noticeable effect on the measurements, a computer simulation of the experimental system was made.

The model consisted of a tube of a metal sample with a thermocouple inserted part way into it along the center line from the bottom as shown in Fig. 10. The tube was cooled

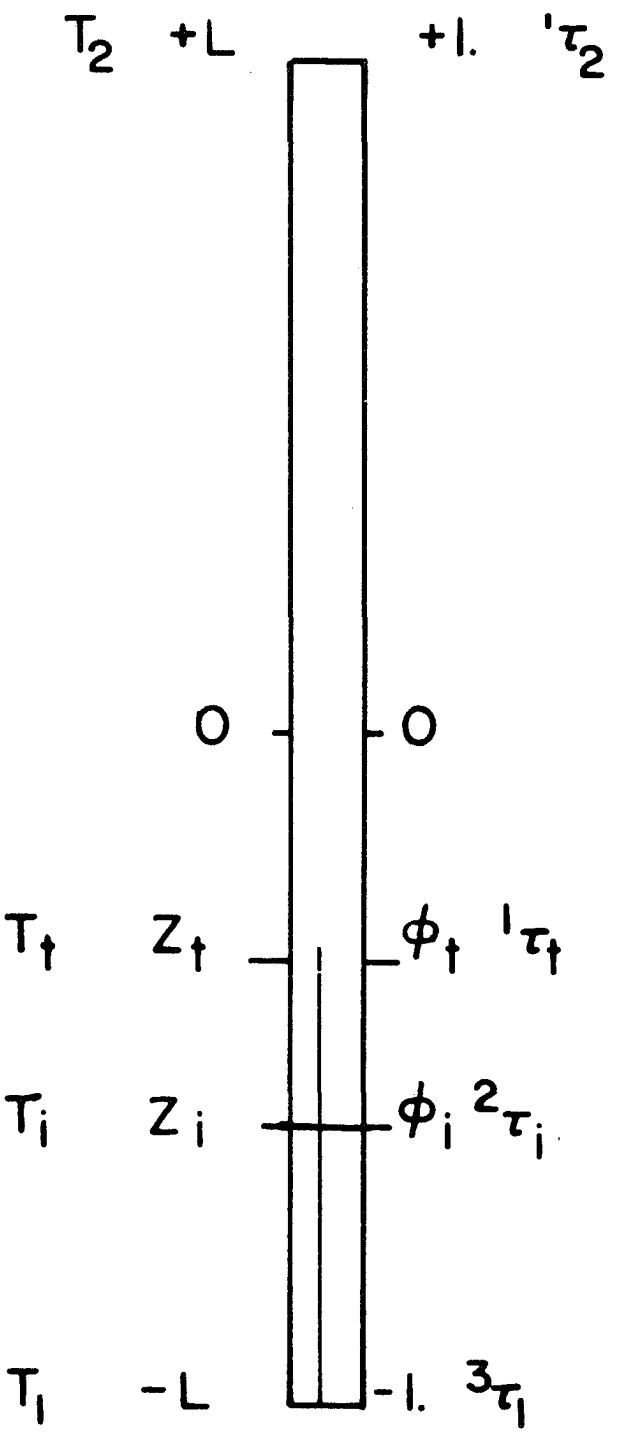

Fig. 10 -- The model used to simulate the temperature profile in the experimental system

at the bottom and a current was passed through. Secondary effects were ignored, as were temperature variations in thermal conductivity and the temperature dependence of specific resistivity, ρ, beyond the first order.

The joule heat generated internally was given by

$$Q = J^2\rho = J^2(a' + b'T) \qquad [96]$$

Hence, at steady state, the heat flux equation was

$$k\frac{d^2T}{dz^2} + \frac{k}{r}\frac{d}{dr}\left(r\frac{dT}{dr}\right) + J^2a' + J^2b'T = 0 \qquad [97]$$

Since the radius of the tube was much smaller than the length, dT/dr was set to 0. Also, z/L was set equal to ϕ, where L was the characteristic length, here one-half the over-all length. Setting

$$\frac{L^2J^2b'}{k} \equiv b^2 \quad ; \quad \frac{L^2J^2a'}{k} \equiv a^2 \qquad [98,99]$$

and defining

$$T = \frac{T + \frac{a^2}{b^2}}{T_A} \qquad [100]$$

where T_A is an arbitrary constant temperature, Eq. [97] was put into its simplest form,

$$\frac{d^2T}{d\phi^2} + b^2T = 0 \qquad [101]$$

for which the solution is sinusoidal so long as b^2 is greater than 0.

When the simulated thermocouple tip was in the liquid, three such equations had to be used, one each for the liquid section, the liquid section with thermocouple, and the solid section, the only difference being the value of b^2 and the ratio a^2/b^2. The six constants of integration were determined by use of the six boundary conditions at the ends of the three regions. The temperature at the thermocouple and the position of the interface were found from the conditions of constant heat flux across the thermocouple position and the interface.

The procedure was to determine the various constants from the given system parameters and then determine the interface position by iteration. From these the constants of integration, the desired temperatures and the gradients were calculated.

To simulate the rising of the furnace, the bottom temperature was specified at E, which was increased from -1 by small increments. The top temperature likewise was specified to be D = 2. + E.

Figure 11 is a plot of a typical temperature profile for a thermocouple occupying 6 pct of the cross section. Certain interesting results are immediately apparent. The maximum temperature in Fig. 10 is not at the top of the system but somewhat below it. This was bothersome until it was observed than when a sample was outgassing while being heated by a current, bubbles always formed at a point rather below the top of the small tube, demonstrating that indeed the maximum temperature was at that point. The numerical computations indicated that the interface moved slightly faster than the dial gauge. The current density was greater below the tip than it would have been if the thermocouple had been removed. Hence, as the bottom was raised, the length of the thermocouple above the position of the lower fixed temperature decreased, slightly less heat was generated, and the interface moved up with respect to the bottom of the system. This difference was quite small for a thermocouple of this size in the liquid.

In sum, for a thermocouple occupying 6 pct of the cross section, the error in solidification rate and in gradient measurement was determined to be well within experimental error. For large thermocouples this generalization does not necessarily hold.

The largest single assumption made in preparing this problem was that dT/dr equalled 0, which is to say, no heat

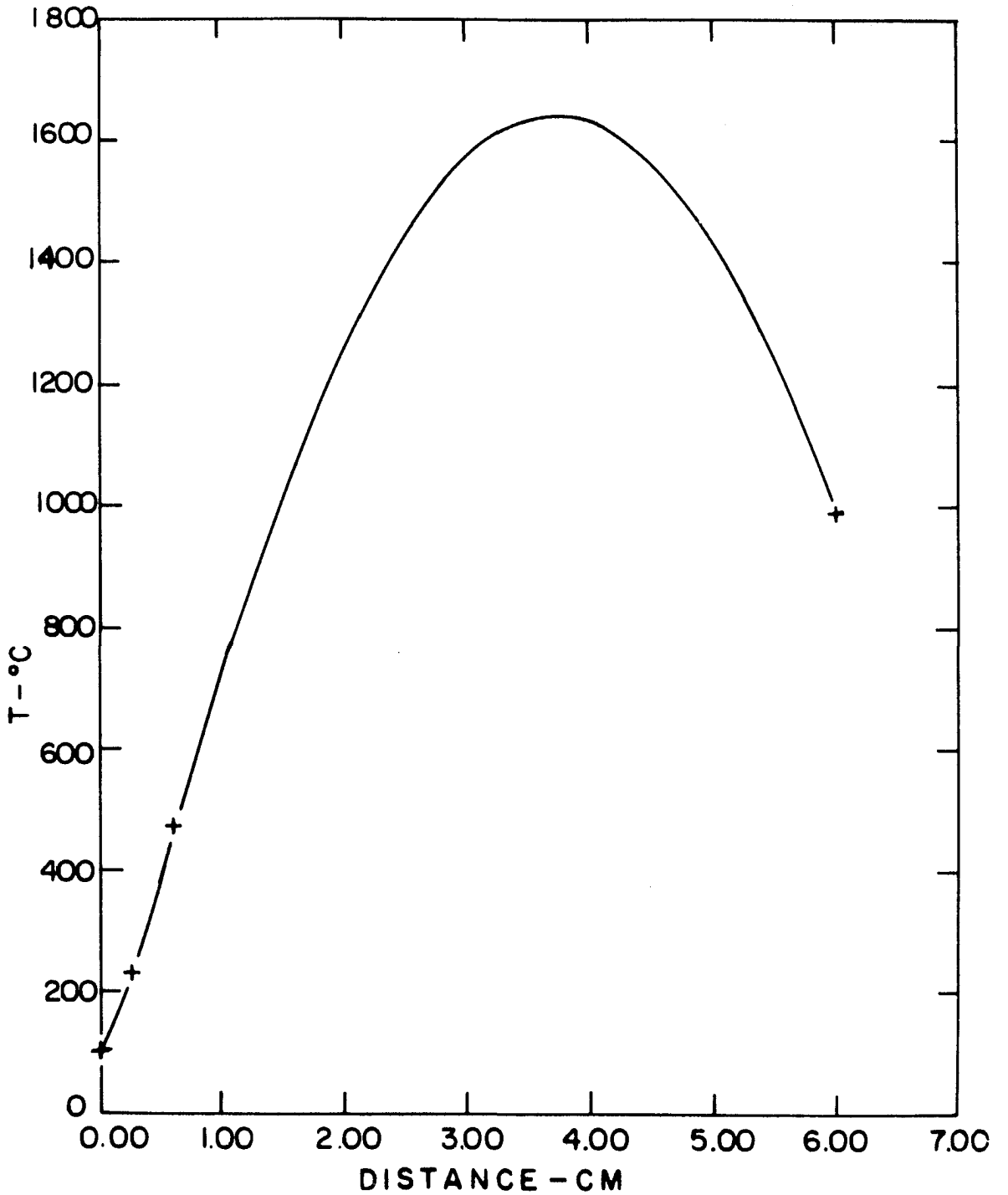

Fig. 11 -- Temperature profile for the model shown in Fig. 10. From the lower left, crosses represent; bottom of the sample, interface, thermocouple tip, and top of the sample

was lost out the side wall. It was assumed that the liquid gradient of 1000°C/cm at the interface, observed when $J = 1700$ amp per cm^2, was real. Then by integration over the liquid it was found that a current density of about $1000A/cm^2$ would produce this gradient.

If heat loss through the wall was allowed, it served only to reduce the maximum temperature and the gradients overall. Specifically, in the liquid above the water jacket, increasing lateral heat loss raised a^2 slightly and reduced b^2. Below the water jacket a^2 was raised only a little but b^2 became negative, making the solution in this region exponential instead of sinusoidal. The net result was that if heat loss through the wall were taken into account, the errors in the measurement of R and G, would be lessened or at least not increased.

RESULTS AND DISCUSSION - SINGLE PHASE SOLIDIFICATION

Aside from the run number, data for each run included the measured rate, the observed concentration at the interface, the direction of the electric field, and the observed structure of the interface. The constants of the alloy system, D, k_o, m_ℓ, specific resistivity ρ, and U were determined from other research so as to be functions of T_i and C_s. For the diffusion coefficient, a best fit of the Arrhenius equation was made between the two points, D = 1. x 10^{-5} cm^2 per s at 232°C and the value reported by Niwa, Shimoji, Kado, Watanabe, and Yokokawa (44) at their lowest temperature to obtain D = 0.0006998 exp (4263/RT). The justification for this selection is given in Appendix A. As detailed in Appendix B, k_o and m_ℓ were obtained from Verhoeven and Gibson (71), and Davidson (17). Resistivity was found by putting the data given by Verhoeven (67) into the form

$$\rho = AR + BR \cdot T_i + CR \cdot C + DR \cdot T_i \cdot C \quad [102]$$

where AR, BR, CR, and DR are constants. Verhoeven also made 88 determinations of U between 5 and 20 at. pct at temperatures from 250 to 520°C. Of seven different multiple regression fits of this data the best was that which included T, T^2, C, and C^2.

In comparing the theory with the observations, the general pattern was to try to adjust the parameters so that a theoretical transition line on the G/C_s vs R plot would fall in such a way that all the runs with flat interfaces would be on the "flat" or stable side of the line, and the unstable runs would be on the unstable side. Usually a best straight line through this type of data is placed by eye. Standard least-squares analysis is inapplicable because the points actually bracket the line and are not expected to fall on it. Given a run which has a flat interface and a specific G/C_s and R, all one can say is that the transition line should have a lower critical gradient at that rate. This may seem an obvious matter, but it has not apparently been made well enough before. Davies (18) for example, made numerical fits on just this sort of data, complete with error estimates, although he failed to specify how he did it. His only reference to statistical methods (19) does not mention any means of obtaining that sort of result.

To make a comparison between the data and a pair of theoretical transition curves, the interface temperature was first calculated from the equation for the solidus and C_s. Then k_o, m, D, U, and E were found from the functions of T_i and C_s. With these and the measured rate, the critical G/C was computed and compared with the observed

value. If the calculated critical G/C was greater than the observed, then the expected interface structure was broken; if less, then it was expected to be flat. The observed and expected interface structures were next compared. If both were the same, then the run was "OK". If the observation was flat while the prediction was broken, then the run was "MORE" stable; if the observed interface was broken while the prediction was for flat, the run was "LESS" stabe. Table III shows this relationship. The runs with E positive and negative were considered separately.

Table III. The relationship between the theoretically predicted and the observed interface structure, and hence between the stability of the observations and the predicted stability

		Predicted morphology	
		F	B
Observed Morphology	F	OK	MORE
	B	LESS	OK

Making this comparison for all the data, one obtains the information contained in Tables IV and V. The number of "MORE" and "LESS" runs for E positive and E negative were used to form an M/L matric, shown in Table VI. The

Table IV. Calculations on the Sn-Bi data with the electric field positive. G/C_s crit is the critical G/C_s calculated from R, m_ℓ, k_o, D, U_{12}, and E, with the interface temperature derived from the solidus slope and the observed C_s. The parameters used in the calculations were those determined from other research

Run #	Rate μ/s	C_s wt.pct	T_i	m_ℓ	k_o	D
2#26	3.856	6.19	204.9	-1.579	.32	.78565E-05
2#52	3.679	4.37	212.8	-1.468	.30	.84538E-05
2#68	3.012	4.47	212.4	-1.473	.30	.84236E-05
3#03	3.386	3.82	215.2	-1.438	.30	.86412E-05
3#15	2.482	6.42	203.9	-1.594	.32	.77826E-05
3#28	1.993	5.26	208.9	-1.520	.31	.81596E-05
3#32	3.650	4.14	213.8	-1.455	.30	.85329E-05
3#35	3.722	3.28	217.6	-1.409	.30	.88258E-05
3#39	3.784	2.88	219.3	-1.388	.29	.89655E-05
3#56	2.011	2.13	222.6	-1.352	.29	.92258E-05
3#69	2.344	8.00	196.9	-1.707	.33	.72834E-05
4#08	3.748	2.95	219.0	-1.392	.29	.89378E-05
4#09	3.825	3.22	217.8	-1.406	.30	.88464E-05
4#10	3.629	4.08	214.1	-1.452	.30	.85525E-05

Averages: k_o = 0.303; m_ℓ = -1.474; T_i = 212.8; E = 0.0681; U_{12} = 1.426; D = 0.846E-05. Total no. is 14; no. more: 5; no. less: 1.

U_{12}	E	Sign of E	G/C_s Obs.	G/C_s Crit.	Int. Obs.	Int. Exp.	Stability
1.404	.072	POS	104.5	219.9	F	B	MORE
1.438	.069	POS	147.9	195.1	B	B	ok
1.437	.069	POS	144.9	169.2	F	B	MORE
1.442	.068	POS	169.4	178.9	F	B	MORE
1.398	.073	POS	100.8	161.7	B	B	ok
1.426	.071	POS	123.0	133.1	B	B	ok
1.440	.069	POS	156.3	191.9	F	B	MORE
1.442	.067	POS	197.3	187.6	F	F	ok
1.440	.067	POS	225.0	186.9	B	F	LESS
1.432	.065	POS	303.8	117.5	F	F	ok
1.339	.075	POS	80.8	167.3	F	B	MORE
1.441	.067	POS	219.0	186.2	F	F	ok
1.442	.067	POS	200.9	191.0	F	F	ok
1.441	.069	POS	158.5	198.4	B	B	ok

Table V. Calculations on the Sn-Bi data with the electric field negative. Again, the parameters were the best fit values from other research.

Run #	Rate μ/s	C_s wt pct	T_i	m_ℓ	k_o	D
2#20	3.891	1.78	224.1	-1.335	.28	.93494E-05
2#24	1.531	3.40	217.1	-1.415	.30	.87846E-05
2#25	3.878	5.27	208.9	-1.521	.31	.81563E-05
2#26	7.713	1.87	223.7	-1.339	.28	.93175E-05
2#60	6.957	2.37	221.5	-1.364	.29	.91397E-05
2#61	4.485	5.87	206.2	-1.558	.31	.79585E-05
2#62	3.564	8.56	194.5	-1.750	.33	.71130E-05
2#69	2.996	5.13	209.5	-1.513	.31	.82008E-05
2#71	5.532	5.17	209.3	-1.515	.31	.81892E-05
2#72	8.267	2.20	222.3	-1.355	.29	.92011E-05
3#04	5.108	3.26	217.7	-1.408	.30	.88326E-05
3#05	8.347	1.37	225.9	-1.316	.28	.94954E-05
3#12	5.003	2.48	221.1	-1.369	.29	.91030E-05
3#14	3.328	2.69	220.2	-1.379	.29	.90298E-05
3#27	6.077	4.04	214.3	-1.450	.30	.85667E-05
3#30	8.165	3.52	216.5	-1.422	.30	.87435E-05
3#33	8.234	.93	227.9	-1.297	.27	.96541E-05
3#34	8.269	2.24	222.1	-1.357	.29	.91871E-05
3#42	5.991	2.81	219.6	-1.385	.29	.89881E-05
3#43	5.808	3.54	216.4	-1.423	.30	.87349E-05
3#45	5.712	2.76	219.9	-1.383	.29	.90054E-05
3#47	5.659	2.33	221.7	-1.362	.29	.91538E-05
3#48	5.525	2.49	221.0	-1.369	.29	.90978E-05
3#49	5.355	2.51	220.9	-1.370	.29	.90908E-05
3#50	5.254	3.26	217.7	-1.408	.30	.88326E-05
3#57	5.375	5.79	206.6	-1.553	.31	.79854E-05
3#58	3.522	10.90	184.3	-1.960	.35	.64196E-05
3#59	5.077	6.29	204.4	-1.585	.32	.78227E-05
3#60	4.929	6.84	202.0	-1.622	.32	.76485E-05
3#61	3.010	8.52	194.7	-1.747	.33	.71237E-05
3#62	3.193	5.84	206.4	-1.556	.31	.79698E-05

U_{12}	E	Sign of E	G/C_S Obs.	G/C_S Crit.	Int. Obs.	Int. Exp.	Stability
1.426	.065	NEG	303.5	97.3	F	F	ok
1.442	.067	NEG	190.3	11.6	F	F	ok
1.426	.071	NEG	122.8	110.8	F	F	ok
1.428	.065	NEG	346.0	235.9	F	F	ok
1.436	.066	NEG	272.4	210.7	F	F	ok
1.413	.072	NEG	110.1	140.7	F	B	MORE
1.313	.076	NEG	75.6	121.9	B	B	ok
1.428	.070	NEG	126.0	73.5	F	F	ok
1.428	.071	NEG	125.1	178.5	B	B	ok
1.433	.065	NEG	294.1	257.6	F	F	ok
1.442	.067	NEG	198.5	147.1	F	F	ok
1.418	.064	NEG	472.3	258.6	F	F	ok
1.437	.066	NEG	200.9	139.4	F	F	ok
1.439	.066	NEG	240.5	78.1	F	F	ok
1.441	.069	NEG	160.1	190.1	B	B	ok
1.442	.068	NEG	183.8	265.7	B	B	ok
1.406	.063	NEG	697.2	259.1	F	F	ok
1.434	.065	NEG	288.8	257.9	F	F	ok
1.440	.066	NEG	230.2	177.6	B	F	LESS
1.442	.068	NEG	182.5	175.7	F	F	ok
1.439	.066	NEG	234.4	166.9	F	F	ok
1.435	.066	NEG	277.1	162.9	F	F	ok
1.437	.066	NEG	259.3	158.7	F	F	ok
1.437	.066	NEG	257.3	152.5	F	F	ok
1.442	.067	NEG	198.5	152.6	F	F	ok
1.415	.072	NEG	111.7	178.0	B	B	ok
1.177	.080	NEG	59.4	145.3	B	B	ok
1.402	.072	NEG	102.8	170.2	B	B	ok
1.364	.073	NEG	94.6	169.3	B	B	ok
1.315	.076	NEG	75.9	94.2	B	B	ok
1.414	.072	NEG	110.8	85.2	B	F	LESS

Table V. (continued)

Run #	Rate μ/s	C_s wt pct	T_i	m_ℓ	k_o	D
3#70	2.599	5.87	206.3	-1.558	.31	.79617E-05
3#71	4.490	4.53	212.1	-1.477	.30	.84018E-05
3#72	8.384	2.65	220.4	-1.377	.29	.90454E-05
3#73	8.282	1.21	226.6	-1.309	.27	.95527E-05
3#74	8.158	2.11	222.7	-1.351	.29	.92310E-05
4#02	8.430	1.90	223.6	-1.341	.28	.93069E-05
4#03	8.496	1.50	225.4	-1.322	.28	.94490E-05
4#11	4.697	4.26	213.3	-1.462	.30	.84941E-05
4#14	4.518	4.31	213.1	-1.465	.30	.84756E-05
4#15	4.504	3.85	215.1	-1.439	.30	.86310E-05
4#16	4.488	6.28	204.5	-1.584	.32	.78275E-05
4#20	4.677	3.96	214.6	-1.445	.30	.85937E-05
4#21	4.623	4.37	212.8	-1.468	.30	.84538E-05
4#22	4.540	4.65	211.6	-1.484	.31	.83634E-05
4#23	4.496	4.43	212.5	-1.472	.30	.84337E-05
4#24	4.460	3.48	216.7	-1.420	.30	.87555E-05

Averages: k_o = .300, m_ℓ = -1.454, T_i = 214.7, E = .0684, U = 1.419, D = .861E-05. Total no. is 47, no. more: 1, no. less: 8.

Averages for both E positive and E negative: k_o = .301, m_ℓ = -1.459, T_i = 214.2, E = .0685, U = 1.421, D = .858E-05. Total no. is 61.

U_{12}	E	Sign of E	G/C_s Obs.	G/C_s Crit.	Int. Obs.	Int. Exp.	Stability
1.413	.072	NEG	110.3	59.9	F	F	ok
1.437	.069	NEG	142.8	131.0	B	F	LESS
1.438	.066	NEG	244.6	265.2	B	B	ok
1.414	.064	NEG	534.7	257.1	F	F	ok
1.432	.065	NEG	305.9	253.1	B	F	LESS
1.429	.065	NEG	340.5	262.0	F	F	ok
1.421	.064	NEG	431.3	263.7	F	F	ok
1.439	.069	NEG	152.1	137.4	F	F	ok
1.439	.069	NEG	150.1	130.7	B	F	LESS
1.442	.068	NEG	168.1	127.4	B	F	LESS
1.402	.072	NEG	103.0	144.3	B	B	ok
1.441	.068	NEG	163.4	134.7	F	F	ok
1.438	.069	NEG	147.9	135.3	F	F	ok
1.435	.070	NEG	139.3	133.7	B	F	LESS
1.438	.069	NEG	145.9	130.6	B	F	LESS
1.442	.068	NEG	185.7	123.7	F	F	ok

Table VI. The M/L matric which results when all the constants are set at the best determined values from other work. $D = 0.85797 \times 10^{-5}$ cm^2 per s, $E = 0.0685$ v per cm, and $U_{12} = -0.001421$ cm^2 per v-s

	E pos	E neg
M	5	1
L	1	8

The problem now is to convert this matrix into some form which gives a measure of the extent of agreement between prediction and observation. One is faced here with a non-parametric type of data resulting in a problem common to social science research (47, 57). To obtain a statistical measure of the quality of each selected fit, a modification of the binomial, or sign test, was chosen. In the sign test (79) no assumptions were made about the population from which the sample was drawn, in particular assumptions of normal distribution and constant variance.

The sign test is computed from a binomial distribution (79)

$$P_i[i \leq k] = \sum_{i=0}^{k} b(i,n) < \frac{\alpha}{2} \qquad [103]$$

where α is the significance level and b(i,n) is given by

$$b(i,n) = \frac{n!}{i!(n-i)!} \left(\frac{1}{2}\right)^n \qquad [104]$$

where the observed M/L distribution is k/(n-k), n is the total number, P_i is the probability of obtaining a given M/L pair (as 5/1 for E pos from Table VI), or a more extreme distribution.

By using $\left(\frac{1}{2}\right)^n$ in Eq. [104] one is actually assuming that the probability, p, of a run being MORE stable, or a run being LESS stable, is one half. If the probability of a particular distribution is sufficiently small, then some non-random factor is probably involved. Usually the result is given in terms of a confidence interval, C.I. = (1-2x) x 100 pct. Essentially then, P is the probability that the observed distribution, or a more extreme one, could occur by chance alone, assuming $p = \frac{1}{2}$. The probability of two such distributions occurring simultaneously, in either order, is

$$P_t = 2P_1 \times P_2 \qquad [105]$$

The overall confidence interval, C.I., is calculated, using P_t in Eq. [104]. In applying this to the work at hand, if the theoretical line deviates from the "true" transition line, then there will be a preponderance of

either M's or L's. If the difference is large enough, then one can reject the fit on statistical grounds alone. Conversely, the fit with the lowest C.I. is most likely to be close to the "true" transition line.

Consider again Eq. [14]. Written in the form

$$\frac{1}{C_s} = \frac{(-m_\ell)}{GD}\left[\frac{(1-k_o)R}{k_o} - \frac{UE}{k_o}\right] \qquad [106]$$

one can better visualize the effects of altering the terms in the M/L matrix. When $|UE|$ is less than predicted, then the system will be more stable when E is positive and less stable when E is negative than theoretically expected. In this situation the G/C_s vs R plot will appear as in Fig. 12a, and the diagonal terms will be largest as in Table VI. Conversely, if $|UE|$ is larger than predicted the G/C_s vs R plot will appear as in Fig. 12b, and the off-diagonal terms will be largest. If $(-m_\ell)/GD$ is larger (smaller) than predicted, then the situation shown in Fig. 12c (12d) holds and the M elements are largest (smallest). Incorrect predictions of k_o can have any of the above results, depending on the value of k_o. Setting all the constants to their best determined values resulted in the matrix in Table VI, which indicated that Fig. 12a described the situation. The actual data are presented in Fig. 13 for E positive and Fig. 14 for E negative. Figure 15 presents

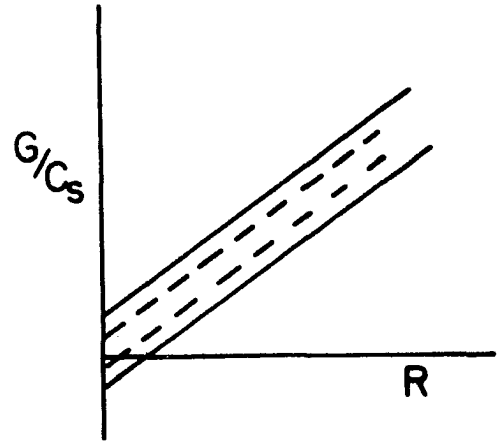

Fig. 12a -- Diagonal elements of the M/L matrix largest

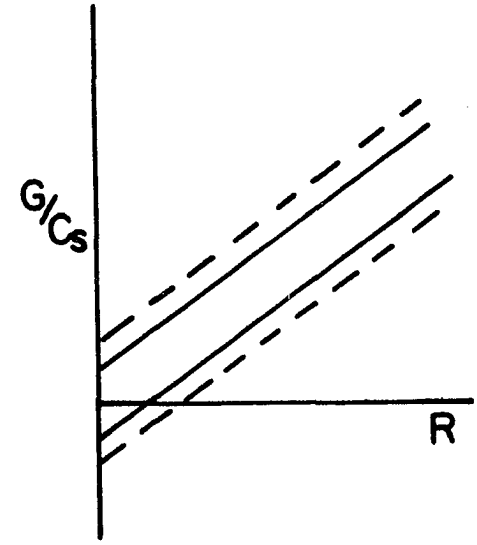

Fig. 12b -- Off-diagonal elements largest

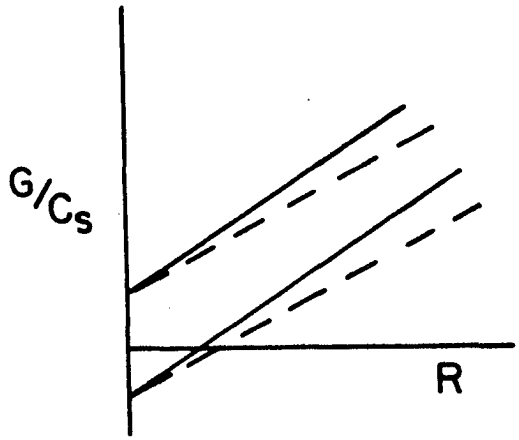

Fig. 12c -- M components largest

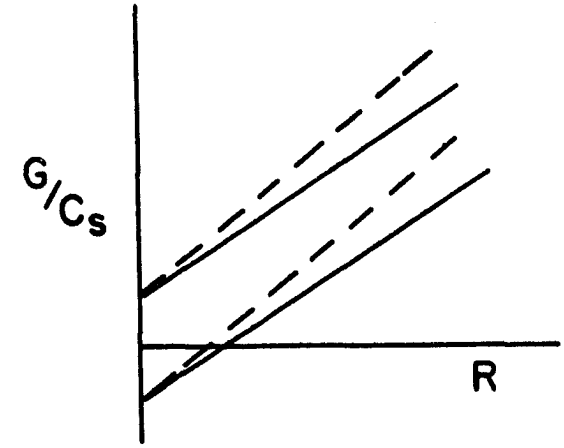

Fig. 12d -- L components largest

Fig. 12 -- Possible relationships between the predicted stable-unstable transition (solid lines) and the observed transition (dotted lines). Above a transition line an interface should be stable, below it, unstable. In each case the upper pair of lines is for E positive, the lower pair for E negative

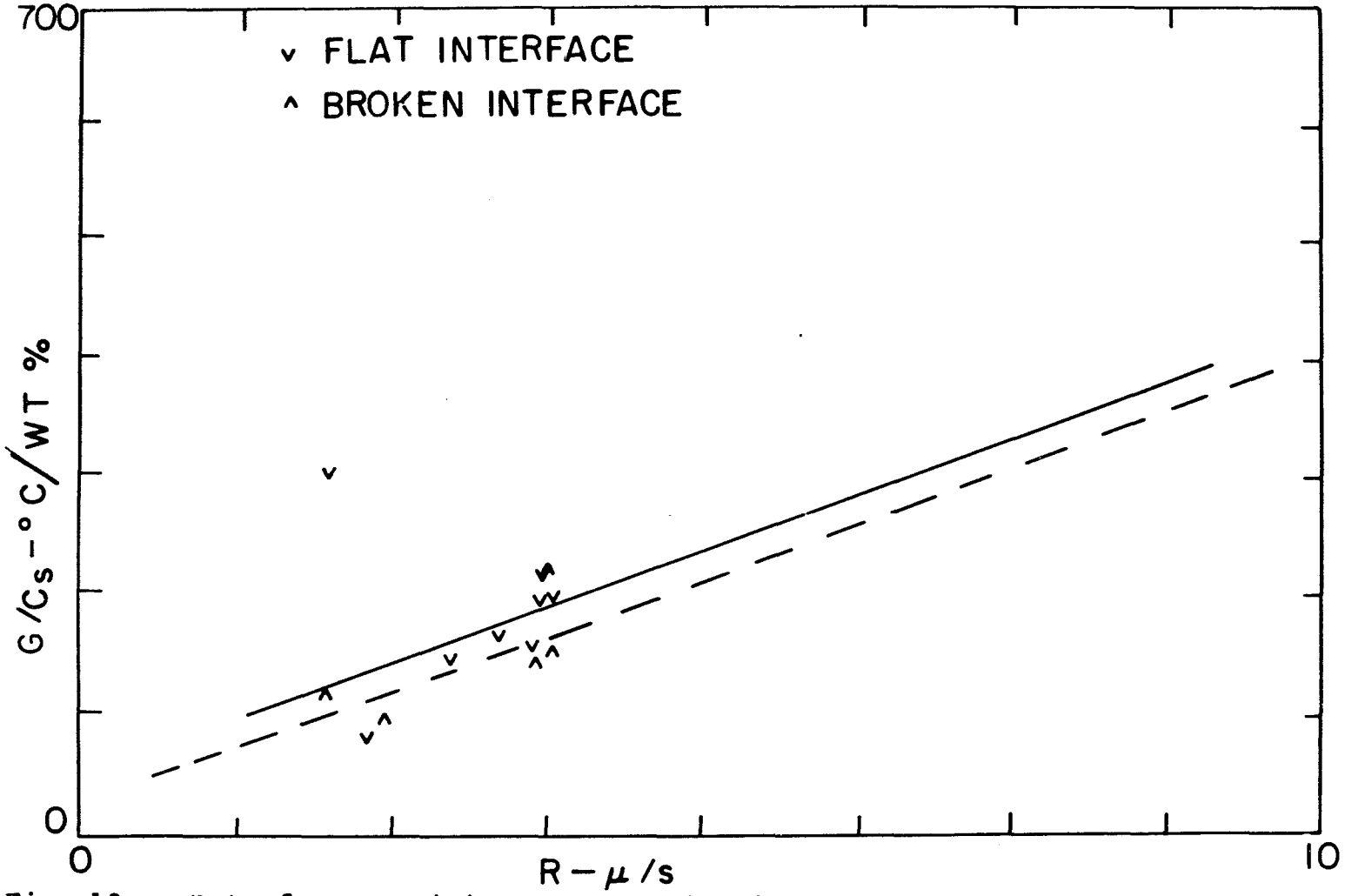

Fig. 13 -- Data for E positive. The solid line is the predicted stable unstable transition curve. The dotted curve is the best fit of the observations. The observations are expected to be stable above the line, unstable below it

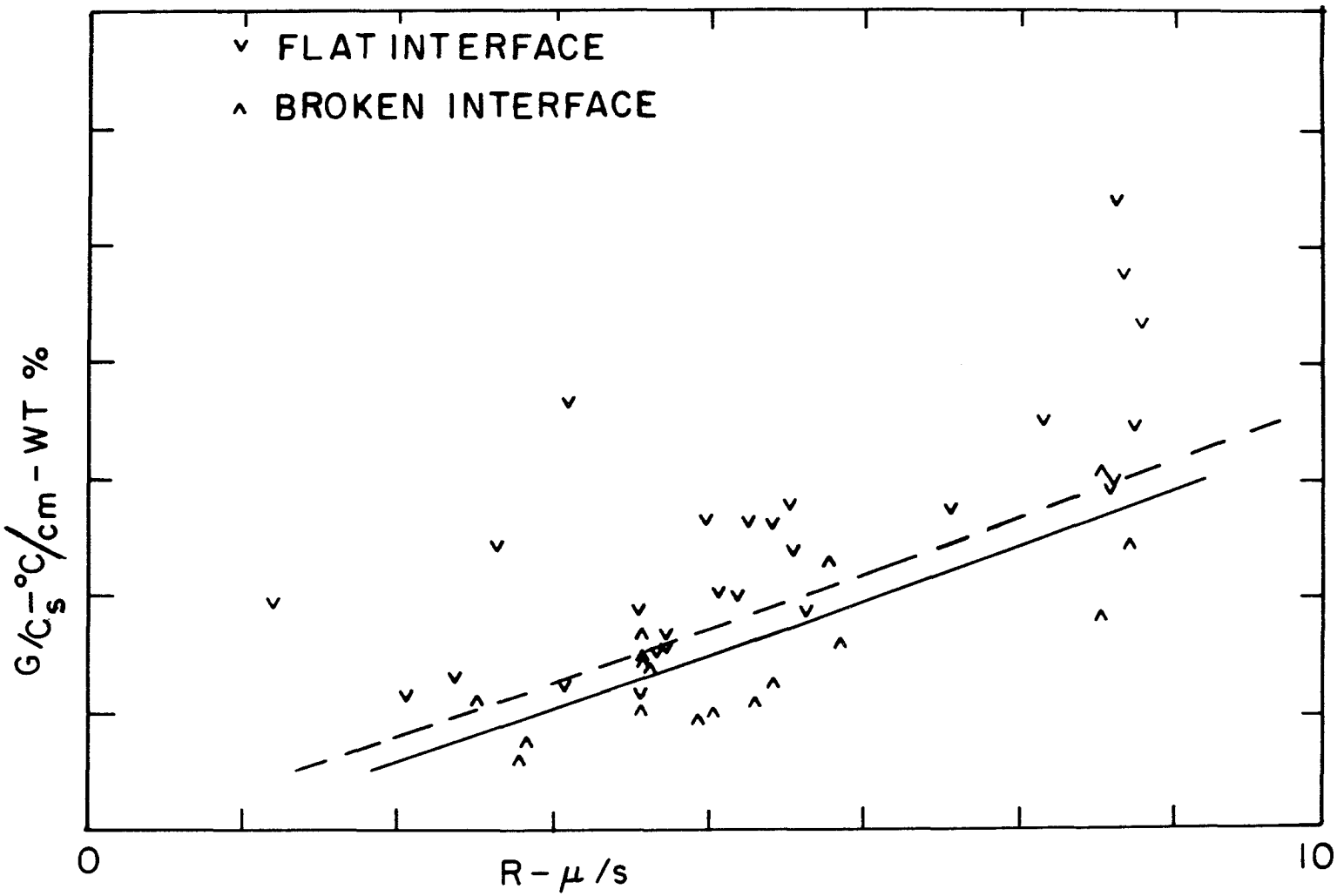

Fig. 14 -- Data for E negative. The solid line is the predicted stable unstable transition curve. The dotted line is from the best fit of the observations

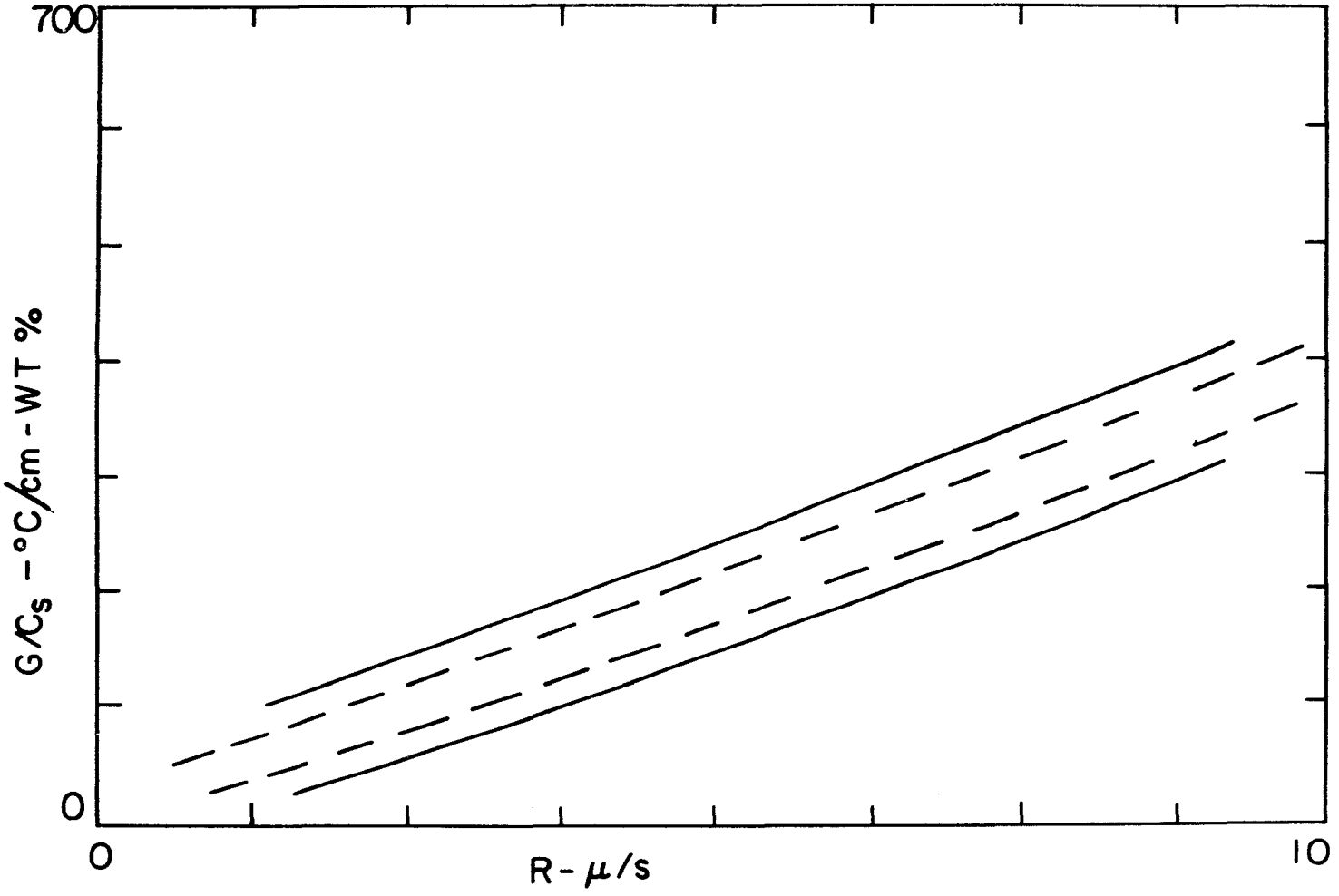

Fig. 15 -- Comparison of the predicted stable-unstable transition curves (solid lines) and the experimentally determined best fit (dotted lines). The upper pair of lines is for E positive

the theoretical predicted curves and the best fit lines through the observations. Although the transition lines are not straight because the interface temperature changes with C_s, the similarity to Fig. 12a is clear. The probability of obtaining this matrix by chance alone is 0.004; the C.I. is 99.2 pct. Hence one can be 99.2 pct sure of the statement, "the theoretical predictions do not correctly predict the experimental observations."

Some terms must be changed to obtain a good fit of the theoretical predictions of the data. Because so many parameters are functions of temperature and composition, there are a large number of possibilities. The solidus line is linear; the liquidus is quadratic, Eq. [102] contains four constants; D contains two; and the temperature and composition dependence of U adds five more constants for a total of 16. The determination of D was considered weak, and the initial matrix indicated clearly that UE had to be changed in order to improve the fit, so D_o, the pre-exponential factor, and U were chosen as the terms to adjust. U was adjusted by altering all 5 constants in U(C,T) coefficients simultaneously by the same factor.

First U was changed. Decreasing U rapidly improved the quality of the fit, as indicated by the increase in P_t and decrease in the C.I., shown in Table VII. Simultaneous adjustments in D_o and U resulted in still more improvement,

Table VII. The effect on the M/L matrix when U_{12} only is altered. $D_o = 0.6998 \times 10^{-3}$ cm^2 per s, $\bar{D} = 0.858 \times 10^{-5}$ cm^2 per s. The matrix form results from the combination of the columns headed E pos and E neg

$\bar{U}_{12}$	E Pos M/L	E Neg M/L	p_t	C.I. (pct)
-0.00142	5/1	1/8	0.004	99.1
-0.00112	4/2	2/7	0.062	87.6
-0.00074	4/2	5/4	0.344	31.2
-0.00067	3/2	5/3	0.363	27.3
-0.0006	3/2	5/3	0.363	27.3

shown in Table VIII.

Two questions naturally arise at this point. First, is the result significantly different than assuming U = 0, that is, can a reasonable fit be obtained when the electric field is ignored? Table IX gives the results of adjusting D_o to obtain a best fit in this case. The best fit has a C.I. of 55 pct.

Second, what values of the adjusted constants do produce good agreement with the observations? The values of D_o and U which result in a fit with the C.I. less than 30 pct are given in Table X. The fit which produced the highest probability and the lowest confidence interval is compared with the observations in Tables XI and XII.

Table VIII. The effect of adjustment of D_o when U_{12} is near the optimum

$\bar{U}_{12}$	D_o (10^3)	$\bar{D}$	E Pos M/L	E Neg M/L	p_t	C.I. (pct)
-0.00075	0.5869	0.720	6/1	11/0	0.000	100.0
-0.00075	0.66025	0.809	4/2	8/3	0.078	84.4
-0.00075	0.69693	0.854	4/2	5/4	0.344	31.2
-0.00075	0.6998	0.858	4/2	5/4	0.344	31.2
-0.00075	0.7100	0.870	3/2	5/4	0.500	0.
-0.00075	0.7200	0.883	3/2	5/5	0.623	---(-25) [a]
-0.00075	0.7300	0.895	3/2	5/5	0.623	---(-25)
-0.00075	0.7400	0.907	3/2	4/6	0.377	24.6
-0.00075	0.7500	0.920	3/2	4/6	0.377	24.6
-0.00075	0.7600	0.932	2/2	3/7	0.236	52.7
-0.00075	0.7703	0.944	2/2	1/7	0.048	90.3
-0.00075	0.8070	0.989	2/3	1/8	0.020	96.1
-0.00067	0.5869	0.720	5/1	11/0	0.000	100.0
-0.00067	0.6998	0.858	3/2	5/3	0.363	27.3
-0.00067	0.7278	0.892	3/2	5/4	0.500	0.
-0.00067	0.7336	0.899	3/2	5/5	0.623	---(-25)
-0.00067	0.7500	0.920	2/2	5/5	0.857	---(-71)
-0.00067	0.7600	0.932	2/2	4/6	0.518	---(- 4)
-0.00055	0.6998	0.585	3/2	5/3	0.363	27.3
-0.00055	0.7138	0.875	3/2	5/3	0.363	27.3
-0.00055	0.7336	0.899	2/2	5/4	0.687	---(-37)
-0.00055	0.7698	0.944	2/3	4/6	0.377	25.6

[a] While strictly speaking confidence intervals cannot be negative, the calculated values are included for comparison.

Table IX. The effect on the M/L matrix when U_{12} is zero. No good fit is obtainable

D_o	$\bar{D}$	E Pos	E Neg	P_t	C.I.
0.55984	0.68637	4/2	17/0	0.000	100.0
0.59483	0.72972	3/2	16/0	0.000	100.0
0.62982	0.77217	3/2	15/0	0.000	100.0
0.66481	0.81507	2/3	12/0	0.000	99.9
0.6998	0.85797	2/4	10/2	0.013	97.3
0.70680	0.86655	2/4	8/2	0.038	92.5
0.71380	0.87513	2/4	8/2	0.038	92.5
0.72079	0.88371	2/4	7/2	0.062	87.6
0.72779	0.89229	2/4	7/2	0.062	87.6
0.73479	0.90087	2/4	6/3	0.175	85.1
0.74179	0.90944	2/4	6/3	0.175	65.1
0.75578	0.92660	2/4	6/3	0.175	65.1
0.76978	0.94376	2/5	6/3	0.115	77.0
0.78378	0.96092	2/5	5/3	0.165	67.1
0.80477	0.98666	2/5	5/3	0.165	67.1
0.83976	1.0296	2/5	5/4	0.227	54.7
0.87475	1.0725	2/5	2/6	0.065	86.9
0.90974	1.1154	2/5	2/8	0.025	95.0
0.94473	1.1583	2/5	1/9	0.005	99.0

Table X. Summary of those fits with a confidence interval less than 30 pct

$\bar{U}$ (cm^2/v-s)	D_o (10^{-3}) cm^2 per s	D_o (10^{-5} cm^2 per s)	E Pos M/L	E Neg M/L	P_t	C.I. (pct)
-0.00067	0.6998	0.858	3/2	5/3	0.363	27.3
-0.00055	0.6998	0.858	3/2	5/3	0.363	27.3
-0.00075	0.7100	0.870	3/2	5/4	0.500	0.
-0.00075	0.7200	0.883	3/2	5/5	0.623	---(-25)
-0.00075	0.7300	0.895	3/2	5/5	0.623	---(-25)
-0.00075	0.7400	0.907	3/2	4/6	0.377	24.6
-0.00075	0.7500	0.920	3/2	4/6	0.377	24.6
-0.00067	0.6998	0.858	3/2	5/3	0.363	27.3
-0.00067	0.7278	0.892	3/2	5/4	0.500	0.
-0.00067	0.7336	0.899	3/2	5/5	0.623	---(-25)
-0.00067	0.7500	0.920	2/2	5/5	0.857	---(-71)
-0.00067	0.7600	0.930	2/2	4/6	0.518	---(- 4)
-0.00055	0.6998	0.850	3/2	5/3	0.363	27.3
-0.00055	0.7138	0.875	3/2	5/3	0.363	27.3
-0.00055	0.7336	0.899	2/2	5/4	0.687	---(-37)
-0.00055	0.7698	0.944	2/3	4/6	0.377	25.6
Accepted best fits						
-0.00075	0.725	0.889	3/2	5/5	0.623	---(-25)
-0.00067	0.7336	0.899	3/2	5/5	0.623	---(-25)
-0.00067	0.7500	0.920	2/2	5/5	0.857	---(-71)
-0.0006	0.7336	0.899	2/2	5/4	0.687	---(-37)

Table XI. Calculations on the Sn-Bi data with the electric field positive. The value of D_o and the average of U_{12} have been adjusted to obtain the best statistical fit of the data

Run #	Rate μ/s	C_s wt pct	T_i	m_ℓ	k_o	D
2#26	3.856	6.19	204.9	-1.579	.32	.84201E-05
2#52	3.679	4.37	212.8	-1.468	.30	.90602E-05
2#68	3.012	4.47	212.4	-1.473	.30	.90279E-05
3#03	3.386	3.82	215.2	-1.438	.30	.92611E-05
3#15	2.482	6.42	203.9	-1.594	.32	.83408E-05
3#28	1.993	5.26	208.9	-1.520	.31	.87449E-05
3#32	3.650	4.14	213.8	-1.455	.30	.91450E-05
3#35	3.722	3.28	217.6	-1.409	.30	.94589E-05
3#39	3.784	2.88	219.3	-1.388	.29	.96087E-05
3#56	2.011	2.13	222.6	-1.352	.29	.98876E-05
3#69	2.344	8.00	196.9	-1.707	.33	.78059E-05
4#08	3.748	2.95	219.0	-1.392	.29	.95790E-05
4#09	3.825	3.22	217.8	-1.406	.30	.94810E-05
4#10	3.829	4.08	214.1	-1.452	.30	.91660E-05

Averages: k_o = .303; m = -1.474; T_i = 212.8; E = .0691; $\bar{U}_{12}$ = .672; $\bar{D}$ = .907E-05. Total no. is 14, no. more: 2; no. less: 2.

U_{12}	E	Sign of E	G/C_S Obs.	G/C_S Crit.	Int. Obs.	Int. Exp.	Stability
.662	.072	POS	104.5	179.5	F	B	MORE
.678	.069	POS	147.9	158.0	B	B	ok
.678	.069	POS	144.9	133.8	F	F	ok
.680	.068	POS	169.4	143.5	F	F	ok
.659	.073	POS	100.8	125.1	B	B	ok
.672	.071	POS	123.0	99.4	B	F	LESS
.679	.069	POS	156.3	155.3	F	F	ok
.680	.067	POS	197.3	152.1	F	F	ok
.679	.067	POS	225.0	151.9	B	F	LESS
.675	.065	POS	303.8	87.8	F	F	ok
.631	.075	POS	80.8	129.2	F	B	MORE
.679	.067	POS	219.0	151.1	F	F	ok
.680	.067	POS	200.9	155.4	F	F	ok
.679	.069	POS	158.5	161.4	B	B	ok

Table XII. Calculations on the Sn-Bi data with the electric field negative. The value of D_o and $\bar{U}_{12}$ have again been adjusted to obtain the best statistical fit to the observations

Run #	Rate μ/s	C_s wt pct	T_i	m_ℓ	k_o	D
2#20	3.891	1.78	224.1	-1.335	.28	.10020E-04
2#24	1.531	3.40	217.1	-1.415	.30	.94147E-05
2#25	3.878	5.27	208.9	-1.521	.31	.87413E-05
2#26	7.713	1.87	223.7	-1.339	.28	.99859E-05
2#60	6.957	2.37	221.5	-1.364	.29	.97954E-05
2#61	4.485	5.87	206.2	-1.558	.31	.85294E-05
2#62	3.564	8.56	194.5	-1.750	.33	.76233E-05
2#69	2.996	5.13	209.5	-1.513	.31	.87890E-05
2#71	5.532	5.17	209.3	-1.515	.31	.87767E-05
2#72	8.267	2.20	222.3	-1.355	.29	.98612E-05
3#04	5.108	3.26	217.7	-1.408	.30	.94662E-05
3#05	8.347	1.37	225.9	-1.316	.28	.10177E-04
3#12	5.003	2.48	221.1	-1.369	.29	.97560E-05
3#14	3.328	2.69	220.2	-1.379	.29	.96775E-05
3#27	6.077	4.04	214.3	-1.450	.30	.91812E-05
3#30	8.165	3.52	216.5	-1.422	.30	.93707E-05
3#33	8.234	.93	227.9	-1.297	.27	.10347E-04
3#34	8.269	2.24	222.1	-1.357	.29	.98461E-05
3#42	5.991	2.81	219.6	-1.385	.29	.96328E-05
3#43	5.808	3.54	216.4	-1.423	.30	.93615E-05
3#45	5.712	2.76	219.9	-1.383	.29	.96514E-05
3#47	5.659	2.33	221.7	-1.362	.29	.98104E-05
3#48	5.525	2.49	221.0	-1.369	.29	.97504E-05
3#49	5.355	2.51	220.9	-1.370	.29	.97429E-05
3#50	5.254	3.26	217.7	-1.408	.30	.94662E-05
3#57	5.375	5.79	206.6	-1.553	.31	.85583E-05
3#58	3.522	10.90	184.3	-1.960	.35	.68801E-05
3#59	5.077	6.29	204.4	-1.585	.32	.83839E-05
3#60	4.929	6.84	202.0	-1.622	.32	.81972E-05
3#61	3.010	8.52	194.7	-1.747	.33	.76347E-05
3#62	3.193	5.84	206.4	-1.556	.31	.85415E-05

U_{12}	E	Sign of E	G/C_s Obs.	G/C_s Crit.	Int. Obs.	Int. Exp.	Stability
.673	.065	NEG	363.5	112.2	F	F	ok
.680	.067	NEG	190.3	33.9	F	F	ok
.672	.071	NEG	122.8	128.2	F	B	MORE
.673	.065	NEG	346.0	241.6	F	F	ok
.677	.066	NEG	272.4	218.6	F	F	ok
.660	.072	NEG	110.1	156.7	F	B	MORE
.619	.076	NEG	75.6	141.0	B	B	ok
.673	.070	NEG	126.0	93.3	F	F	ok
.673	.071	NEG	125.1	191.3	B	B	ok
.676	.065	NEG	294.1	262.2	F	F	ok
.680	.067	NEG	198.5	160.2	F	F	ok
.668	.064	NEG	472.3	262.5	F	F	ok
.677	.066	NEG	260.9	152.1	F	F	ok
.678	.066	NEG	240.5	95.2	F	F	ok
.679	.069	NEG	180.1	201.0	B	B	ok
.680	.068	NEG	183.8	271.1	B	B	ok
.663	.063	NEG	697.2	262.9	F	F	ok
.676	.065	NEG	288.8	262.6	F	F	ok
.679	.066	NEG	230.2	188.1	B	F	LESS
.680	.068	NEG	182.5	187.1	F	B	MORE
.679	.066	NEG	234.4	178.1	F	F	ok
.677	.066	NEG	277.1	174.0	F	F	ok
.678	.066	NEG	259.3	170.2	F	F	ok
.678	.066	NEG	257.3	164.4	F	F	ok
.680	.067	NEG	198.5	165.3	F	F	ok
.667	.072	NEG	111.7	191.4	B	B	ok
.555	.080	NEG	59.4	163.5	B	B	ok
.661	.072	NEG	102.8	184.5	B	B	ok
.653	.073	NEG	94.6	184.1	B	B	ok
.620	.076	NEG	75.9	115.0	B	B	ok
.666	.072	NEG	110.8	104.8	B	F	LESS

Table XII. (continued)

Run #	Rate μ/s	C_s wt pct	T_i	m_ℓ	k_o	D
3#70	2.599	5.87	206.3	-1.558	.31	.85328E-05
3#71	4.490	4.53	212.1	-1.477	.30	.90045E-05
3#72	8.384	2.65	220.4	-1.377	.29	.96943E-05
3#73	8.282	1.21	226.6	-1.309	.27	.10238E-04
3#74	8.158	2.11	222.7	-1.351	.29	.98932E-05
4#02	8.430	1.90	223.6	-1.341	.28	.99745E-05
4#03	8.496	1.50	225.4	-1.322	.28	.10127E-04
4#11	4.697	4.26	213.3	-1.462	.30	.91035E-05
4#14	4.518	4.31	213.1	-1.465	.30	.90836E-05
4#15	4.504	3.85	215.1	-1.439	.30	.92502E-05
4#16	4.488	6.28	204.5	-1.584	.32	.83890E-05
4#20	4.677	3.96	214.6	-1.445	.30	.92102E-05
4#21	4.623	4.37	212.8	-1.468	.30	.90602E-05
4#22	4.540	4.65	211.6	-1.484	.31	.89634E-05
4#23	4.496	4.43	212.5	-1.472	.30	.90386E-05
4#24	4.460	3.48	216.7	-1.420	.30	.93835E-05

Averages: k_o = 0.300; m_ℓ = -1.454; T_i = 214.7; E = 0.0684; U_{12} = 0.669; D = 0.923E-05. Total no. is 47; no. more: 5; no. less: 5.

Averages for both E positive and E negative: k_o = 0.301; m_ℓ = -1.459; T_i = 214.2; E - 0.685; U_{12} = 0.670; D = 0.920E-05. Total no. is 61.

U_{12}	E	Sign of E	G/C_S Obs.	G/C_S Crit.	Int. Obs.	Int. Exp.	Stability
.666	.072	NEG	110.3	81.2	F	F	ok
.677	.069	NEG	142.8	146.4	B	B	ok
.673	.066	NEG	244.6	269.8	B	B	ok
.667	.064	NEG	534.7	261.0	F	F	ok
.675	.065	NEG	305.9	258.0	B	F	LESS
.674	.065	NEG	340.5	266.0	F	F	ok
.670	.064	NEG	431.3	267.3	F	F	ok
.679	.069	NEG	152.1	152.1	F	B	MORE
.678	.069	NEG	150.1	145.9	B	F	LESS
.680	.068	NEG	168.1	142.3	B	F	LESS
.661	.072	NEG	103.0	160.3	B	B	ok
.680	.068	NEG	163.4	149.3	F	F	ok
.678	.069	NEG	147.9	150.2	F	B	MORE
.677	.070	NEG	139.3	149.0	B	B	ok
.678	.069	NEG	145.9	145.9	B	B	ok
.680	.068	NEG	185.7	138.5	F	F	ok

The average value of U_{12} which resulted in the best fit was -0.00067 cm^2 per v-s, while the average value determined from Verhoeven's data (67) was -0.001421 cm^2 per v-s. The average value of D which produced the best fit was 0.920 x 10^{-5} cm^2 per s, compared to the predicted value of 0.858 x 10^{-5} cm^2 per s. In order to account for the results without drastic alterations in UE some phenomenon which is a function of the sign of E must be found. As shown by Eq. [106], alterations in m_ℓ , D and G cannot produce a reasonable fit when they are taken independent of E. Under the same condition of independence, changing k_o will not work either.

It seems highly unlikely that an electric field would affect m_ℓ, k_o, or D. If there were some effect which lowered the temperature gradient by 25°C per cm with E positive, and raised the gradient by the same amount when E was negative, then the original predictions would be borne out. The Peltier Effect is such a phenomenon. Duckworth (25) gives a clear description of how current passing between two dissimilar phases evolves or absorbs heat at the interface. The definition of Pfann, Benson, and Wernick (49) will be used,

$$_sP_\ell = Q/It \qquad [107]$$

Here Q is the heat evolved or absorbed, I the current,

t the time, and $_{s}P_{\ell}$ the Peltier coefficient for current passing from the solid to the liquid. The sign of $_{s}P_{\ell}$ is defined such that when $_{s}P_{\ell}$ is positive and positive current is passing from the liquid to the solid, then heat is evolved at the interface.

Assume the current is such that heat is evolved. The effect on the temperature gradients should then be similar to the effect of latent heat evolution during solidification. From the definition, Eq. [107], the heat flux due to Peltier heat is

$$Q/At = {}_{s}P_{\ell} \cdot J \qquad [108]$$

where J is the current density. At the interface we can make a heat flux balance,

$$-k_e G_\ell - \lambda R - {}_{s}P_{\ell} J = -k_s G_s \qquad [109]$$

where λ is the latent heat per cm^2 and k_s, k_ℓ are the thermal conductivities in solid and liquid, respectively. Dividing by $k_s G_s$ and manipulating, the ratio

$$\frac{G_\ell}{G_s} = \frac{k_s}{k_e}\left[1 - \frac{\lambda R}{k_s G_s} - \frac{{}_{s}P_{\ell} J}{k_s G_s}\right] \qquad [110]$$

is obtained. When the latent or Peltier heats become significant, then the liquid gradient will decrease with

respect to the solid gradient.

From Smithells (59), k_s = 0.08 cgs, and λ is 104.1 cal per cm^3. For the case of G_ℓ = 648.°C per cm and R = 5 μm per s, the total heat flux from the liquid is 51.84 cal per cm^2-s while the contribution from latent heat is only 0.052 cal per cm^2-s, or about 0.1 pct. The Peltier coefficient, ${}_sP_\ell$ has been reported as 0.6 x 10^{-3} v (29) and was calculated from the data of Marwaha and Cusak (38) as 0.25 x 10^{-3} v. The latter is probably more accurate. The current density used in this work was nominally 1200 amp per cm^2, so the Peltier term contributes about 0.072 cal per cm^2-s to the heat flux, on the order of magnitude of the latent heat term. Furthermore, since in Sn the Peltier heat is evolved when E is negative, it would tend to lower the gradient then, which is opposite to the effect required for an explanation of the observed results. In order to effect a 5 pct change in the liquid gradient, assuming the solid gradient was constant, ${}_sP_\ell$ would have to be about 90. x 10^{-3} v, and to fit the observed results it would have to have the opposite sign. In support of the conclusion that Peltier heat is insignificant, it should be noted that no difference in the temperature gradient was found when the gradient was measured with various solidification rates and current directions, as mentioned in the chapter, Determination of Mixing Length.

A number of conclusions can be drawn at this point. Most important is that the electric field has only about one-half the effect that was expected of it. The average value of U had to be reduced by a factor of 2.2 in order to obtain the best fit. No rational justification can be made for this result. Since the values of U and resistivity were obtained from the same source (67), a systematic error of approximately 50 pct would be required in the measurement of differential electrotransport velocity to account for the present observations. This is clearly an unrealistic requirement, particularly in view of the agreement with other work on the same system (3). The diminished effect of electric field cannot be accounted for by Peltier heating, either.

Nor can the discrepancy be accounted for by the use of the Tiller theory of groove stability (61) in which it is assumed that the composition in the liquid at z = 0, the interfacial plane, is C_s/k_o at all points. Hence at this point the flux due to electrotransport is the same regardless of the nature of the material behind this plane. As long as this assumption is used, the theory does not alter the basic stability equation for a planar interface.

As a result, Eq. [27], derived from his theory, is simply an Eq. [14] in modified form.

If a systematic error was made in the interpretation

of the photographs, it would have been equally distributed between those runs with current up and current down, so the effect would tend to cancel, or appear as a change in the average value of D. Since one set of runs was more stable than expected, on the average, and the other was less stable, this source of error can be ruled out as a possible explanation for the observed results. It is possible that the field polarity could alter the morphology of a slightly unstable interface. However, a detailed examination of the photographs did not support this possibility.

It is also clear that the electrotransport effect cannot be ignored altogether. A concerted attempt to find a reasonable fit with U = 0, tabulated in Table IX, resulted in only one value of D_o which produced an M/L matrix with a confidence interval less than 65 pct, and that (55 pct) was well over more successful fits.

There is, apparently, little or no melting effect due to small perturbations on the surface of a flat interface. Such an effect would be observed as a parallel displacement downward of the transition lines. Increasing D_o would have a similar effect on the M/L matrix, but the actual change required for the best fit, 6.5 pct, is sufficiently small that it can be considered within the margin of error.

Three sources of experimental error in the Sn-Bi study

were the measurements of R, G, and C_s. The rate was measured twice for each run, once over a period of 10 to 20 min, and once over the remainder of the run. An analysis of variance performed on all runs, including long eutectic alloy runs, showed that the standard deviation was 0.044 μm per s. The standard deviation in the average of two measurements would then be 0.031, or about 0.6 pct at the average rate of 4.9 μm per s.

In the measurement of the temperature gradient, G, described in detail in the chapter, Determination of Mixing Length, it was assumed that all the errors were caused by random errors in measuring. The best estimate was 648 ± 4.°C per cm at the 66 pct confidence level. Because of the difficulty of making and maintaining small thermocouples, and because a thermocouple was lost at each quench, none were used for the major portion of the work. It was assumed that the temperature gradient was the same in all the remaining runs, and care was taken to keep the furnace conditions constant.

Three methods were tried for the determination of C_s. The first was the atomic absorption method. Of thirteen samples analyzed a total of five times each on three successive days, the standard deviation between measurements on the same solution was 0.18 wt pct Bi. This was considered too large, especially as replication over days

increased the error.

A microprobe was also tried. By setting the probe beam on a line scan mode and making a pass at right angles to the scan line along a longitudinal section, one could obtain a concentration profile across the quenched solid liquid interface and determine not only C_s but also C_ℓ and dD/dz at the interface as well. This technique was used with five runs with flat interfaces. In one case the liquid followed the expected exponential drop away from the interface, Fig. 16a. In the other cases the liquid profile followed the curves indicated by Figs. 16b and 16c. In all of the anomalous situations the scatter in the liquid, as determined from the continuous record, was quite large.

Some kind of surface reaction must have taken place between the time the samples were polished and the time they were analyzed, about three weeks. A bulk chemical analysis from the region indicated by the arrow in Fig. 16b revealed a composition well below that shown by the microprobe, an indication of the validity of this deduction. Other samples have been observed with clear signs of a recrystallization reaction; Fig. 17 shows one of these.

Spectrophotometric analysis of specimens dissolved in solution was finally selected for use in this work and has been described in the chapter **Experimental** Method. In a

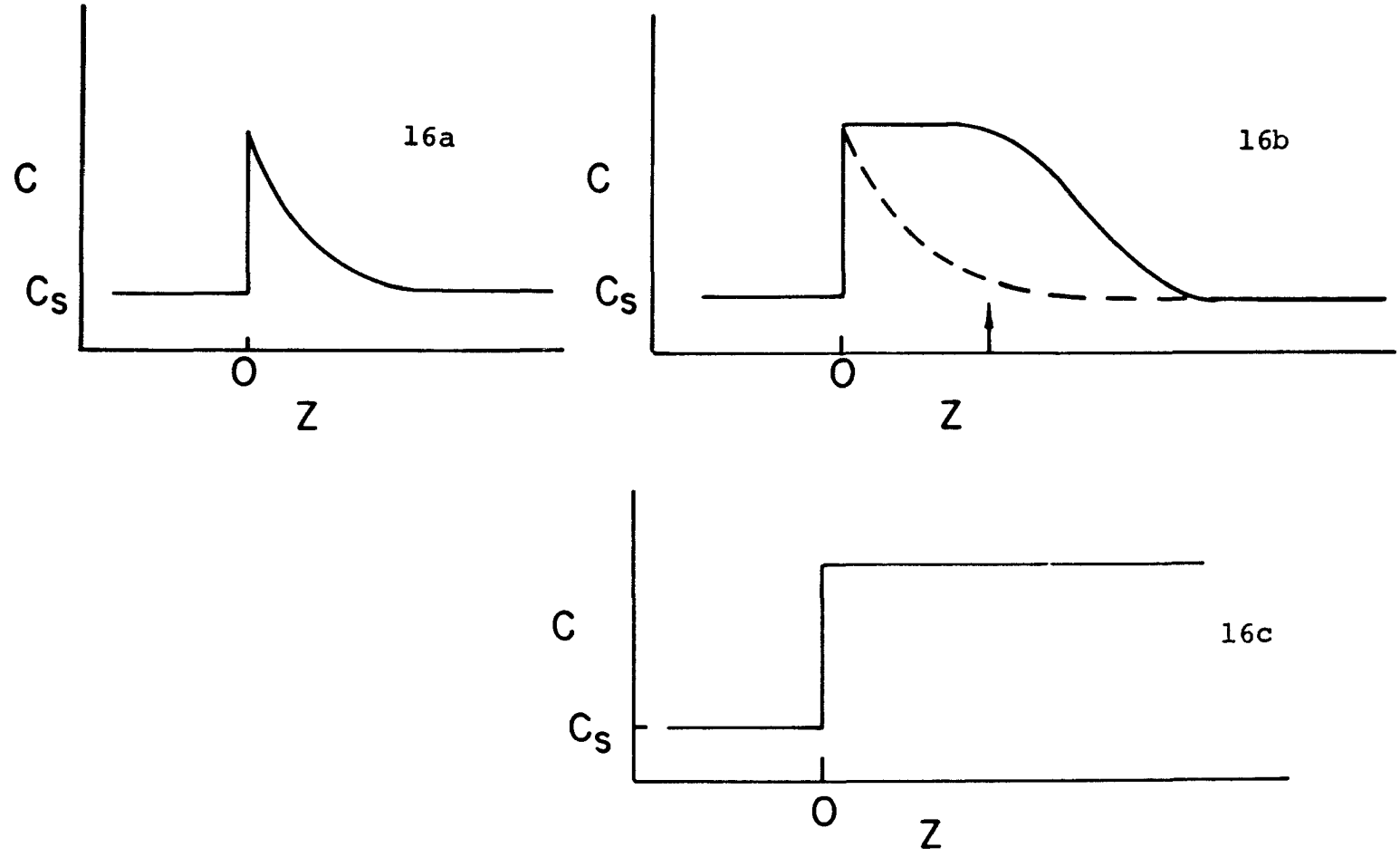

Fig. 16 -- Three solute profiles measured by microprobe. That shown in Fig. 16a was expected in all cases. A section for bulk analysis was removed from the region indicated by the arrow in Fig. 16b

particular test of this method, eight sections were cut from a single cast alloy of 7 wt pct Bi in weights about five times greater than sections from solidification runs. Four spectrophotometric measurements were made on each solution. The error between measurements on one solution was 0.012 wt pct Bi; the standard deviation between sections was 0.42 wt pct Bi, although the alloy had been cast with care to retain uniformity.

From each experimental run two sections were cut from immediately behind the interface. In order to use chemical analysis of these sections it was necessary to assume that quasi-steady state had been achieved well before the quench point and that the composition of the solid did not vary significantly over the region between the interface and the 4 mm from which the sections were taken.

The length of the initial transient can be estimated from the "characteristic distance" given by Tiller et al. (62), D/k_oR, which is valid for unmixed liquids and gives estimates close to those from the more exact solution due to Smith, Tiller, and Rutter (58). For the worst possible case, $D = 1. \times 10^{-5}$ cm^2 per s, $R = 2.$ μm per s, $k_o = 0.3$, the solid composition will be within 2 pct of steady state within $4D/k_oR$, or about 0.6 cm. When the liquid is stirred quasi-steady state is approached sooner. The runs were made for 2.5 cm before quenching, so even in the worst

possible case the analyzed sections were taken about 1.5 cm away from the initial transient.

For normal solidification of stirred alloys, the solid composition can be given by Eq. [84] derived by Pfann (48). One tenth of the total alloy was solid at the quench point. Again taking a poor case, if $k_e = 0.3$, then C_s/C_o can be expected to change by 2.5 pct between 0.09 and 0.1 of the total distance solidified. For $k_e = 0.6$ which is a more suitable estimate here the difference is much less. Neither of these assumptions, then, presents a serious likelihood of error, for this work.

To determine the average error and to test experimentally whether the two sections were equal, an analysis of variance was made on the sections of each run. Virtually no difference was found in the average difference between the first and second sections, while the standard deviation within each run was 0.72 wt pct.

The probable source of most of the error was in the preparation before weighing the milled sections. The actual weight was obtained quite precisely, but there was no good way to clean the millings of organic contaminants. Wiping the rod of alloy with alcohol before cutting was tried, but nothing was gained, and the samples had to be aired for some time to allow remnants of the alcohol to evaporate. The presence of organic materials on the millings would

reduce the reported concentration, and any iron or other metal from the cutting operation would tend to raise the concentration.

The standard deviation within each run of 0.72 wt pct is about 17 pct at the over-all average concentration. With two sections analyzed the error in C_s is reduced to 12 pct.

Of these three errors, in R, G, and C_s, that in C_s is most serious. While all the properties of the system used in Eq. [14] are functions of C_s, a 12 pct variation in C_s results in a much smaller variation in the right side of Eq. [14], on the order of 2 or 3 pct. The major variation due to error in C_s is thus in G/C_s.

Since the effect of electrotransport is unaccountably low the measurement of E should be examined with care. The current through the sample was measured to within ± 0.1 pct, as described previously. The quartz tubes were selected from 2 mm I.D. stock and sized to fit the copper insert and a small collar which supported an "O"-ring seal. While wide variations were found in the stock tube the sized tube was within ± 0.15 mm of nominal. The tubes were actually sized only at the bottom where the copper insert went in. They were quite uniform over a 10 cm length, however, and little error could be expected on that point. In order to account for the observed results, the tubes

would have to be near 3 mm I.D., clearly an impossibility.

As with all studies of single phase interface stability, the question of what is and is not a flat interface is not amenable to straightforward methodology. As suggested by Figs. [18-20] the first stage in the change from flat to a non-flat interface is the appearance of a groove in a photograph of a transverse section of quenched interface. Experimentally the number of such grooves appears to be a continuum corresponding to the changes from a flat interface to a completely dendritic structure. In general, as the G/C_s ratio decreases with constant R, the interface structure goes through a series of stages, the exact number and distinctiveness depending on the observer. At high G/C_s there is a flat interface in which the solid is clearly separated from the liquid. As G/C_s drops, small grooves of quenched liquid appear trailing back from the interface. As G/C_s drops further, more grooves appear and become wider and deeper with less space between them. Cole (12) presents excellent photographic examples taken from decanted samples of the earlier stages of breakdown.

Many of the early workers, Refs. (63, 75, and 14) for example, described a poxed or cellular interface as flat, and a heavily cellular interface as "broken." For this criterion of stability a lower critical G/R is obtained for a given C_o, and hence the slope of the G/R vs C_o

Fig. 17 -- Recrystallization near a quenched interface. The unstable interface was solidifying toward the right. 470X

Fig. 18 -- A quenched interface classified as flat. C_S = 5.87 wt pct, R = 4.485 μm per s, E negative. 100X

Fig. 19 -- A quenched interface classified as broken. C_S = 4.65 wt pct, R = 4.540 μm per s, E negative. 117X

Fig. 20 -- A quenched interface containing two crystals with different interface morphologies; classified as broken. C_S = 8.56 wt pct, R = 3.564 μm per s, E negative. 100X

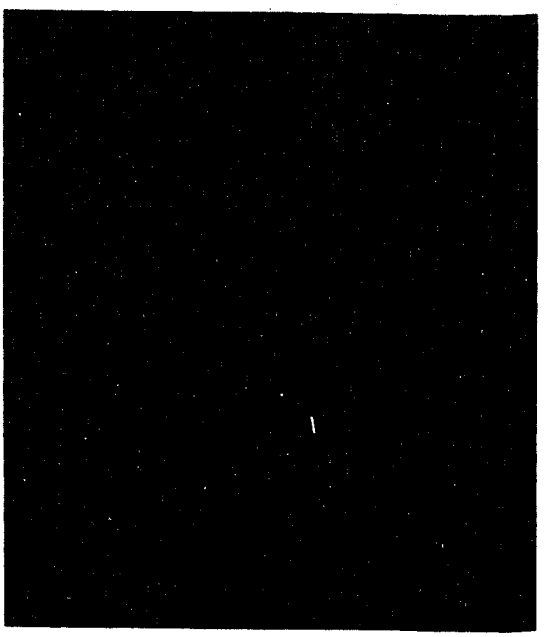

Fig. 17

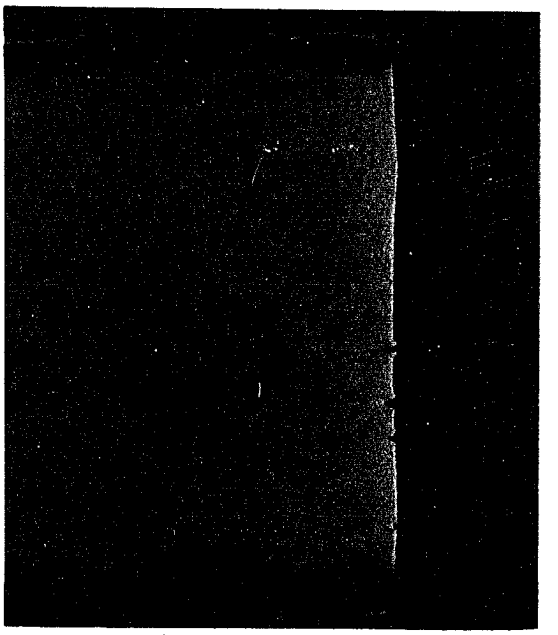

Fig. 18

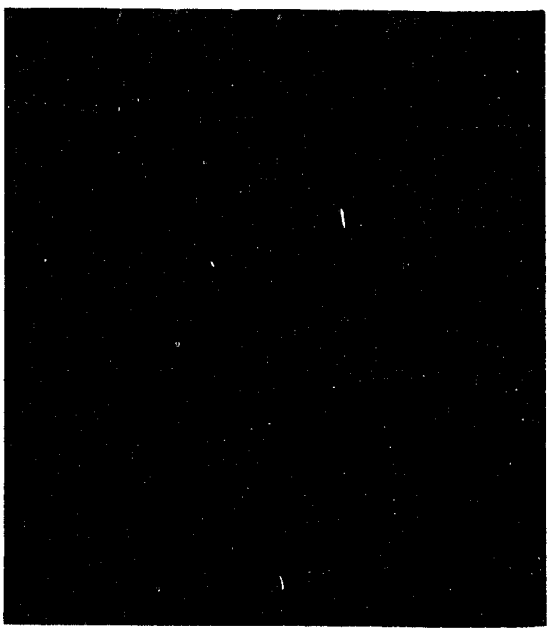

Fig. 19

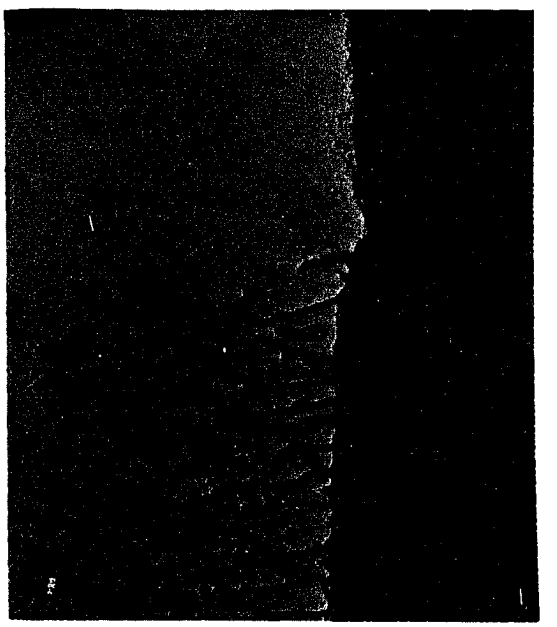

Fig. 20

curve is lower than it should be.

For this work, an interface with one or two grooves present, along grain boundaries, was taken as flat. Grooves present with no apparent grain boundaries were considered evidence of instability. Before the calculations were well under way, all the photographs were examined at one time and a decision was made about each one. All interfaces were specified either flat or broken. Thereafter the photographs were avoided and no decisions were changed. Figures 18 through 20 indicate something of the subtleties of the decisions required. It is apparent from Fig. 20 that crystallographic orientation can be significant. This source of variation was not controlled in this work, although some of the possible orientations should have grown out during solidification over 2.5 cm, reducing the randomness of the orientation.

There is ample room for error in the judgement of interface morphology. One can be too strict, ignoring Tiller's theory of grain boundary grooves, or one can be too lax and specify poxed structures as flat. Worst, one can reorder judgements on the basis of theoretical predictions. Every effort was made to avoid the third error. If there was a systematic error in choice of criteria, that is, being too strict or too lax, the effect would have been to raise or lower, respectively, both of the

observed transition lines together. In actual fact the observations supported transition lines which were shifted in both directions, one lowered, one raised, by an equal amount from the theoretical expectations. Hence, it appears likely that a reasonably accurate decision was made about each interface morphology.

RESULTS AND DISCUSSION - EUTECTIC SOLIDIFICATION

To compare the experiments with theory it was necessary to have values for U, E, D, C_E, and δ. In addition C_α and C_β were necessary to select the range of permitted experimental variables. Golotyuk, Kuz'menko, and Kharkov (27) determined U as -4.5×10^{-4} cm^2 per v-s for Sn-Pb at the eutectic composition and 350°C, which was used despite the approximate relation to the compositions and temperatures in this work. Specific resistivity at the eutectic composition and melting point was obtained from the detailed data of Adams and Leach (1). As discussed in Appendix A, $D = 0.67 \times 10^{-5}$ cm^2 per s is the value at the eutectic composition and temperature. However, $D = 1. \times 10^{-5}$ cm^2 per s was used, as an approximation to the average value over the temperature and composition range in front of the interface. The eutectic composition and the limits of the eutectic range were obtained from the phase diagram (28).

No determination of the mixing length was made. Considering that strong mechanical stirring in larger tubes resulted in a mixing length of 0.0064 cm (68) and that the maximum effect of the difference in direction of the electric field is felt when $\delta = 0.04$ cm in Sn-Bi alloys, $\delta = 0.0275$ cm appeared reasonable. This value was used for

both electric field directions.

As the eutectic work proceeded, however, it became increasingly clear that something was not working out. Only those portions of runs which contained no dendrites were considered. The first long run fitted the theoretical prediction reasonably well. For the second run, agreement with theory was less successful. The third run fitted the theory better when the opposite sign was used for electric field! The fourth run, essentially a repeat of the last, produced a similar result.

It was observed that the composition at the very bottom of the sample, which had been frozen quickly after outgassing and did not experience the electric field, was analyzed at much higher concentrations than could reasonably be expected. In a 40.0 wt pct alloy the concentration at the bottom was 68.4 wt pct. An indication of the build-up due to thermotransport has been made in the chapter, Eutectic Equations. The steady-state profile of Pb concentration can be expected in approximately 5 days, whereas here the outgassing time after the last mixing was one-half hour. Apparently the concentration at the bottom end of the tube builds up quite rapidly, even though steady state conditions are not reached for some time.

Two runs were made to determine the concentration profile in the liquid. The first was set up in the normal

way, but the furnace drive mechanism was not turned on and the electric field was run for 5.5 hr such that Pb was forced toward the bottom, which would enhance stability. The second run used neither drive nor electric field. The furnace was set at 725°C, the outgassing temperature, and left on for 18 hr. In the first case an approximately exponential concentration curve with a mixing length of about 2 cm was found. In the second case steady state was possibly not achieved, judging from the shape of the profile. The composition profile did not drop to the "bulk" liquid value until 5 cm of the interface.

These two results indicated that the assumption of uniform composition in the bulk liquid was seriously in question. Furthermore, by implication the use of the Burton, Prim, Schlicter model is not possible in the presence of large differential body forces, at least in the small tubes used here.

The experimental results were then compared with the theory with encouraging results by making adjustments in δ as deemed necessary. For those runs with C_B greater than C_E and the flux of Pb upward (E negative), δ between 0.005 and 0.01 cm worked fairly well. For those runs with C_B less than C_E and flux of Pb down (E positive), $\delta = 1$ cm provided a good approximation.

A comparison between the shapes of the actual and

theoretical profiles provided further information. Consider a run made with the flux of Pb upward, R = 3.94 μm per s, and initial concentration by mass balance of 39.55 wt pct. The entire run had an eutectic structure. As shown in Fig. 21, the initial predicted composition was somewhat above that observed. As solidification progressed, the observed concentration dropped more slowly than the theoretical curve and became greater than the latter before half of the alloy was solid. Qualitatively this is what one would expect if there were a solute gradient in the liquid, with more Pb at the top toward which the field was forcing it. The freezing solid should have lower composition at the start. As solidification progresses, the bulk composition should not drop as fast as the theory would predict, and so the change in the solid composition would not be as great as that predicted for the first half of a run.

Secondly, consider the case of a run with the Pb flux downward, at a freezing rate of 3.68 μm per s. The initial composition by mass balance was 37.13 wt pct. The structure was eutectic until near the end of the run, at about 0.6 of the total length solidified. Some agreement with theory was obtained for $\delta = 1$. At these rates larger values of δ have extremely little effect (73). The more correct value of $\delta = 2.$ cm was not used because the computer cannot handle

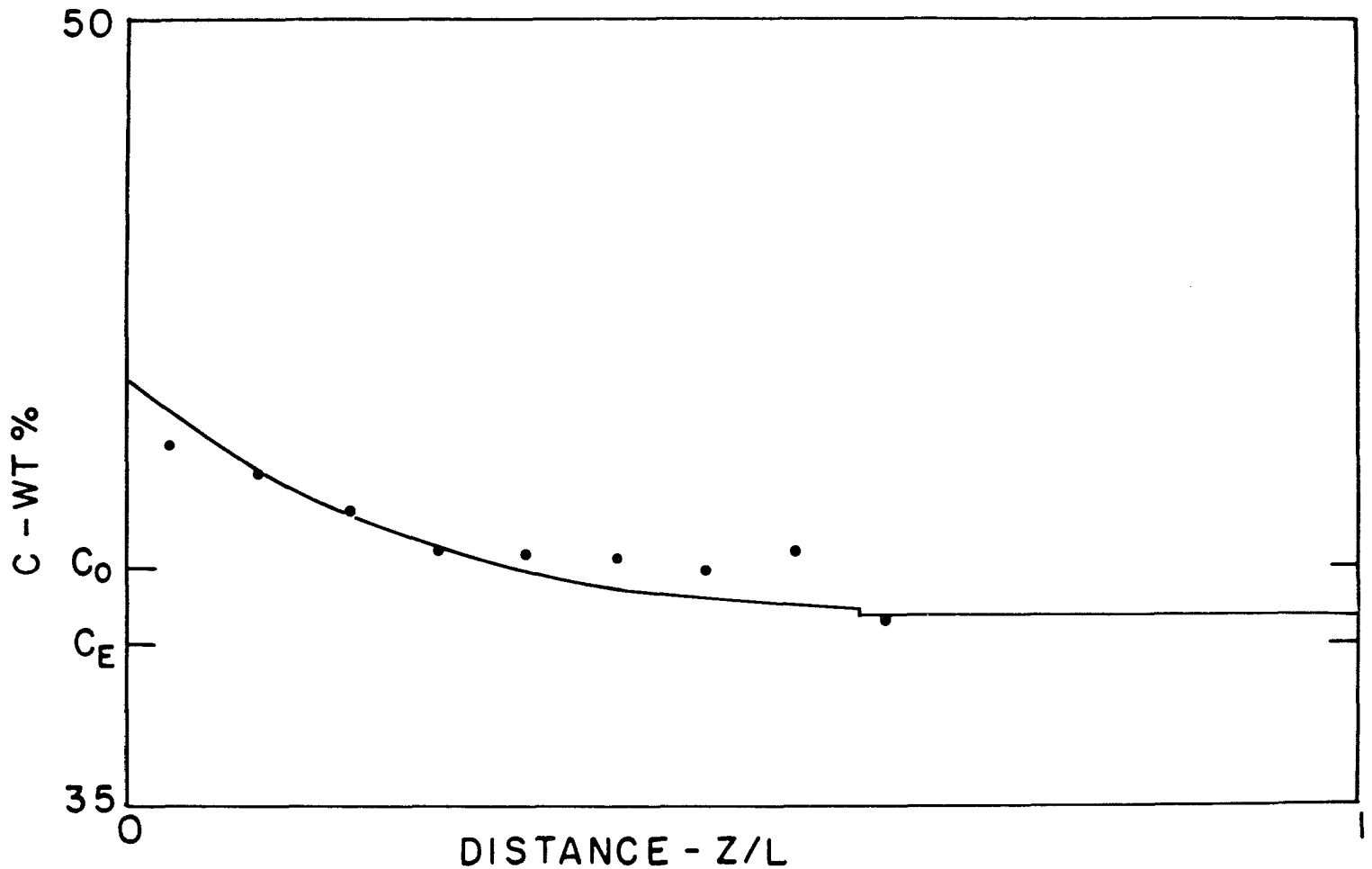

Fig. 21 -- Comparison of observed and predicted composition profiles in a directionally solidified eutectic alloy. The small break at z/L = 0.6 is the quench point. C_o = 39.55 wt pct, R = 3.94 μm per s, δ = 0.005 cm, E = -0.07 v per cm

exponents of the magnitude that would result. Figure 22 compares the theoretical curve with experiment for this case. The predicted curve was lower than observed all the way along the length until the quench at which point the bulk composition was nearly the same as the observed value.

Somewhat better agreement was obtained if the value of E was raised to 0.09 v per cm. Even higher values of E might have proved better, but the drop in C_B became much worse. Again, the result can be understood in terms of the effect of a concentration gradient in the "bulk" liquid with the greatest Pb concentration at the bottom.

One very surprising result was found when the equation was used to predict composition in regions where the interface structure included dendrites: the agreement was about as good as in the regions where the interface structure was completely eutectic, even though the equations were not expected to be valid when dendrites were present. For example, one run was made at 3.54 μm per s, mass balance composition 44.32 wt pct. With the Pb flux upward, a δ of 0.008 fitted quite well, even though most of the solidified section possessed a dendritic interface. As shown in Fig. 23, the initial solid composition was somewhat below that predicted, and as solidification proceeded the actual composition increased relative to the theoretical line and became higher than predicted. Qualitatively this is what

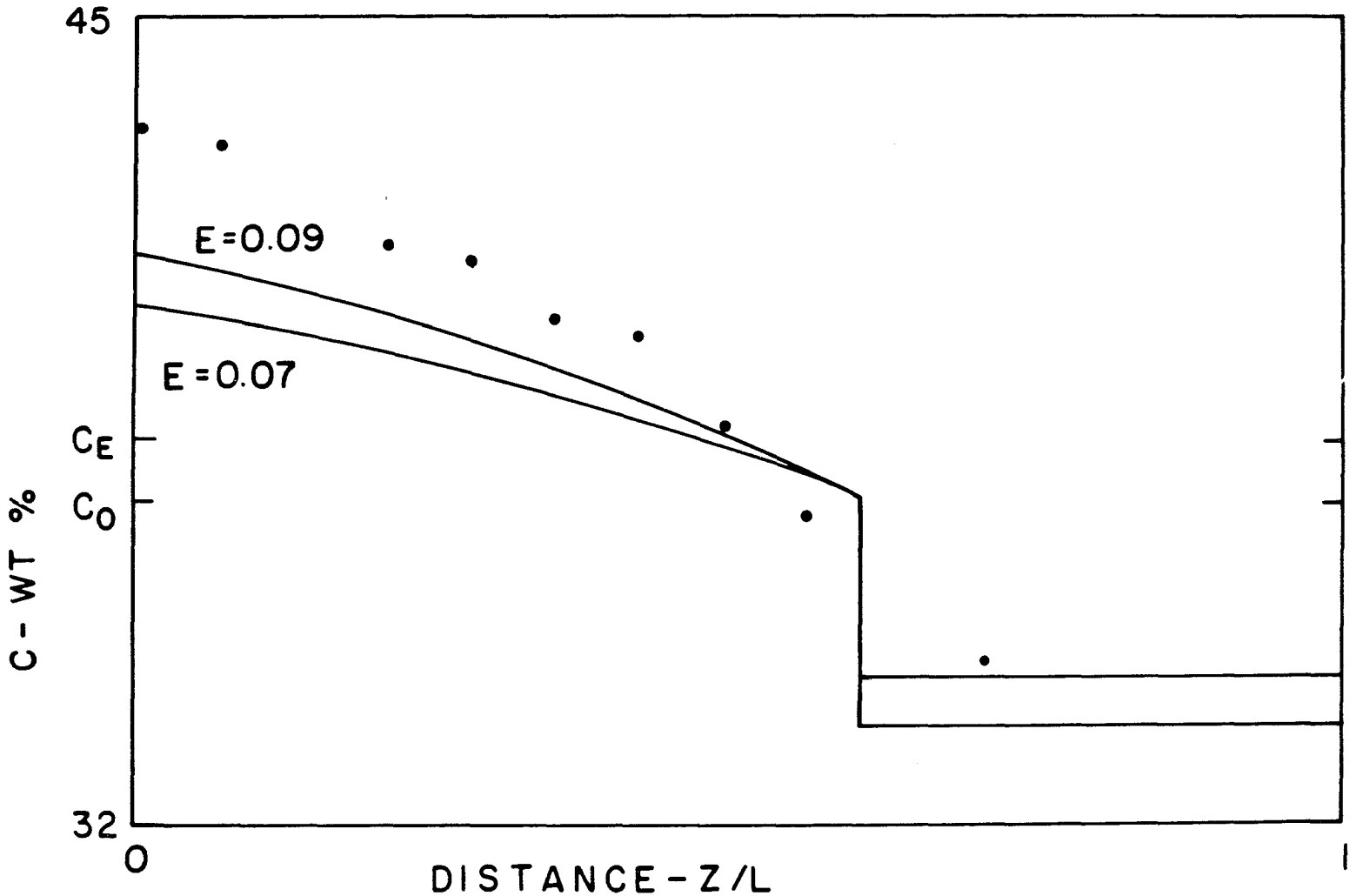

Fig. 22 -- Comparison of observed and predicted composition profiles for a directionally solidified eutectic. E = +0.07 and +0.09 v per cm, C_o = 37.13 wt pct, R = 3.68 μm per s, δ = 1. cm

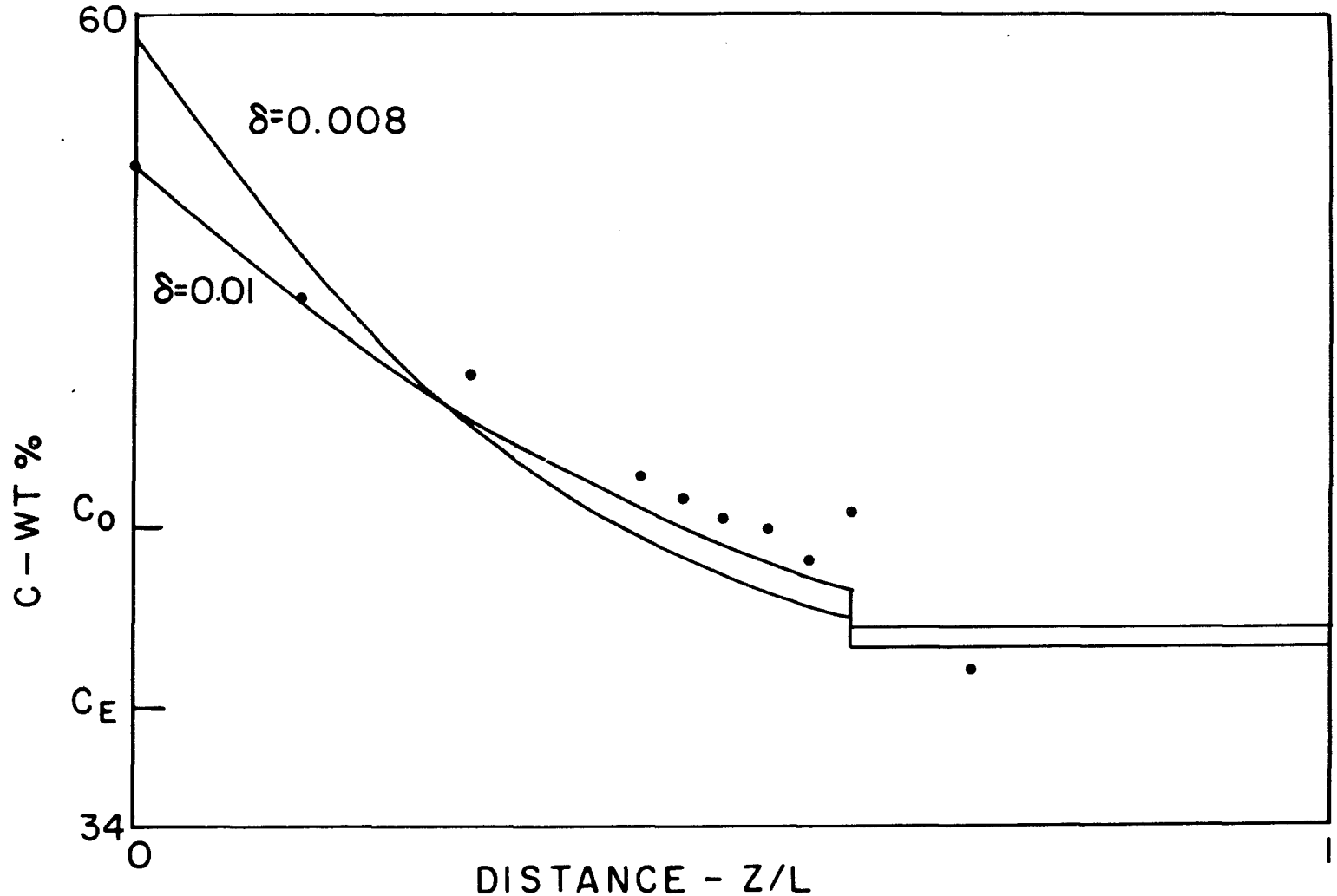

Fig. 23 -- Comparison of theoretical profile with that from a dendritically solidified sample. C_O = 44.32, R = 3.54 μm per s, δ = 0.008 and 0.01 cm

one would expect if the interface had been eutectic. It would appear that the presence of dendrites at the interface does not alter the average solid composition at a given cross-section. Perhaps the electric field has more effect on the composition of the freezing solid than the presence or absence of dendrites.

It has been observed in other work (68) that dendrites inhibit macrosegregation caused by mechanical stirring devices, which is to say they inhibit mechanical mixing in the vicinity of the interface. In the present case, however, the temperature gradient was quite high, which tended to make the dendrites short. Furthermore, mixing here was caused by body forces, probably density instability, and such mixing was much more likely to occur in deep recesses and corners than by mechanical mixing, since it could occur whenever the Rayleigh number in a bounded region exceeded a critical value (9). In addition, density instability due to composition differences is much more likely to occur than that due to temperature differences (64). The sum of this argument is that dendrites are not expected to inhibit mixing in the present case as much as they would inhibit mechanical mixing, so quite possibly they have less effect on the solid composition than might be expected.

It appears likely that the extent of mixing is

controlled far more by density inversions than by the electric field. The effect of thermotransport during solidification with no stirring was observed to be much larger than had been anticipated. In fact, using the equations derived in this thesis for eutectic solidification, and substituting D'G for UE, Verhoeven, Warner, and Gibson (73) were able to show that thermotransport in unmixed systems could be significantly greater than anticipated. Finally, it is probable that the solute profile in the liquid is not uniform. This last conclusion can be interpreted in the following manner. The Burton et al. (7) model specifies complete mixing at $z > \delta$ and no mixing at $0<z<\delta$, while we know there is a continuum in the contribution of convection to mass transport of solute. In fact, there has to be some concentration gradient for convection to transport mass from one location to another at all. I suggest that while convection may be the dominant form of mass transport in the bulk liquid, with small tubes in the presence of strong differential body forces mass transport due to the latter can be significant. Perhaps in the bulk liquid region using an effective D to include the combined effects of mixing and electrotransport might result in a better model.

There were more sources of error in this work than in the Sn-Bi study. The concentration at each analyzed point

was required, instead of that at only one point. No detailed analysis of a master alloy was made which would allow an analysis of variance computation of the chemical analyses. Since the major error appears to be in the steps preparing the sample for analysis, and these steps are the same for both types of samples, the sources of analytical error are about the same. Because of the difference in typical compositions, the samples contained approximately four times as much lead as the former contained Bi. An equal weight of contaminant, then, would have only one fourth the effect. The error would then be on the order of ± 0.2 wt pct.

The errors in measurement of R and G are the same as before. There might be a systematic error in G because of differences between conductivity of the Sn-2 wt pct Bi alloy used to determine G and the Sn-Pb alloys used here, and because of differences in the melting points.

The position of the analyzed sections along the entire sample was determined by measuring the distance covered by the tool bit on the lathe gauge in such a manner that errors were cumulative. Great care was taken to measure these distances, and individual errors were probably on the order of 0.5 pct.

A greater error, probably, involved the determination of the actual initial composition by mass balance. Since

only the 1 mm section in each centimeter was submitted for analysis, it was necessary to approximate the composition for the remaining sections. The large boule at the top contained approximately four tenths of the total weight of the sample and so gave a large emphasis to that composition. To aid in accurately determining the boule composition, the weight of the corresponding section was increased significantly.

A number of approximations required for mathematical analysis also contributed to potential error in fitting theory to fact. It was necessary to assume D, U, and E constant over the liquid for the whole region in which the electric field has a significant effect. In the case of the Burton model that means out to δ from the interface. Where δ is 1 cm, this assumption is patently false. It was also assumed for this work that the above terms were the same for all the runs, at every composition. The assumption of uniform liquid composition has already been discussed.

When the work with eutectic growth was begun, the report of Mollard and Flemings (40) and Cline and Livingston (11) were the only previous experimental efforts on eutectic growth by directional solidification of off-eutectic alloys. Their work supported the idea that the eutectic-dendrite transition was reversible, and they saw little reason to

question the concept. The later studies on different systems (34, 16) did not hint that the case might be otherwise. Very recently, however, Verhoeven and Gibson (69) have completed work which proves that there is in fact a hystersis in the eutectic-dendrite transition. It appears that, while dendrites disappear according to some function of G, R, and C_o, the dendrites appear on an eutectic interface by means of a nucleation mechanism. It would seem, too, that the method of starting the solidification run is critical to whether or not dendrites are formed when near to the critical conditions. The addition of an electric field only complicates the matter. Between unknowingly using incorrect values for δ and stumbling onto a hystereses problem, correct predictions from theory concerning whether a run should be with or without dendrites were never possible. Even without the nucleation problem, dendrites often behaved in strange patterns. In one run, for instance, dendrites appeared near the middle of a run in significant numbers, diminished by the next transverse section 0.5 cm away, remained for 0.5 cm, disappeared, then returned in mass 1. cm later.

These results should not suggest that the work on eutectic alloys ought to be passed over because of the theoretical and practical problems. Quite the contrary, the potential of <u>in situ</u> directional solidification of

composites from near-eutectic alloys is even now being realized by industry. It is my feeling, however, that not enough is known about eutectic solidification without electric fields to add, yet, that variable. In particular, the relationship of R, G, and C_o to the eutectic-dendrite transition needs to be developed much more than at present.

SUMMARY AND CONCLUSION

The original purposes of this work were to search for the presence of a "melt back" effect, to determine how much the temperature gradient was increased by an electric field, to consider Peltier heat effects and to test for changes in the kinetics of solidification. No melting effect could be found, nor was there any indication of changes in the kinetics. Peltier heat is on the order of latent heat, which was negligible in this work. A temperature gradient of greater than 1000°C was observed at current densities of 1900 amp per cm^2. While the measured gradient was only 650°C per cm at the current density used, 1286 amp per cm^2, this was well over the highest reported gradient obtained with a resistance furnace using low melting point alloys (40). Computer simulation of the heat flow in the system indicated that a thermocouple of 6 pct area or less should not adversly affect temperature measurements.

Because of the non-parametric nature of the final data, a modification of the sign test was used to provide statistical estimates of the quality of theoretical predictions. The initially predicted fit could be rejected at the 99.2 pct confidence level. Statistically the electrotransport effect could not be dispensed with altogether, either. The electrotransport of solute at the

interface is about one-half as intense as predicted, a result which cannot be accounted for by any of the above effects, nor by a consideration of the Tiller theory of groove stability (61). A surface reaction effect was found with Sn-Bi samples, which seriously impeded analysis with an electron microprobe.

The theoretical equations derived for eutectic solidification were able to predict the composition profile for the directionally solidified eutectic alloys reasonably well, considering the approximations made in the analysis. Apparently mixing is due more to density inversions in the liquid than to the presence of the electric field. The major approximation in the analysis appeared to be the validity of the Burton model of mixing (7). In small tubes with differential body forces this model is felt to be in serious error. One very surprising result was that the equations were able to predict the profile when dendrites were present at the interface as well as when they were not, even though the equations were not expected to apply in the former case. This would suggest that dendrites do not alter the liquid profile as much as might be expected, even in the presence of significant mixing promoted by density inversions.

SUGGESTIONS FOR FURTHER RESEARCH

The Tiller et al. theory (62) of interface stability has been tested a number of times, and supported within experimental error (18). But the fundamental question of methodology in the selection of interface morphology raises a good many reservations about that work. In connection with this, only one study (42) has made a serious attempt to compare Tiller's theory with the Mullins and Sekerka theory (43, 56). There are four areas in which the two theories predict differences, of which the most interesting is for conditions with very high R/C_o. At very high rates, Sekerka predicts a flat interface due to capillarity, while the older theory requires astronomical gradients to maintain stability. The experimental difficulties would be significant. A difference in the predicted critical gradient of at least a factor of two should be used. At very high rates the dendrite spacing might be so fine that the distinction from single phase solid could be hard to make. Large gradients are difficult to maintain at high freezing rates, and how one could quench an interface structure when the solidification rate was over a centimeter per second raises subtle questions.

Although it may seem mundane, the review of diffusion data shows that this parameter is very poorly known in

these frequently studied systems. In addition to the measurements of U and resistivity when electric fields are used, accurate information on all the parameters is necessary to make detailed tests of solidification theory.

Figure 20 indicates crystallographic orientation may be significant. This has not been studied in great detail yet and probably should be. It will not be easy. Some means of seeding the sample will be necessary, or else a large number of semi-randomly oriented trials must be made. A scanning electron microscope with selected area channelling would certainly help, particularly if eutectic alloys were considered.

The original theory of eutectic growth (33) assumed the absence of mixing in the liquid, so the solid composition was always equal to the original, C_o. Measurements of the solid composition over the length of a directionally solidified eutectic offer a number of experimental advantages over single point measurements as a means of testing theoretical predictions. It would be interesting to test closely, for example, the theory of Verhoeven and Homer (72) for mixing in eutectic solidification and in this way test the validity of the assumption of constant D in the stagnant layer. If possible, it would be equally valuable to work out a more correct theory for eutectic

growth, using variable D, UE (or D'G), making appropriate allowances for a non-uniform solute profile.

REFERENCES

1. Adams, P. D. and Leach, J. S., Ll., "Resistivity of Liquid Lead-Tin Alloys," Phys. Rev. 156: 178-183 (1967) Numerical data provided by the authors

2. Angus, John; Ragone, David V.; and Hucke, Edward E., "The Effect of an Electric Field on the Segregation of Solute Atoms at a Freezing Interface," Met. Soc. Conf., 8: 833-840 (1961)

3. Belashchenko, D. K., "Mechanism of Electrotransfer in Liquid Binary Metallic Alloys," Izv. Vyssh. Ucheb. Zaved., Chern. Met., No. 9, 5-12 (1961)

4. Bird, R. Byron; Steward, Warren E.; and Lightfoot, Edwin N., Transport Phenomena, John Wiley & Sons, Inc., New York, 1960. Pp. 495 ff

5. Brody, Harold D. and Flemings, Merton C., "Solute Redistribution in Dendritic Solidification," Trans. TMS-AIME, 236: 615-624 (1966)

6. Buell, C. H. and Shuck, F. O., "Diffusion in the Liquid Bi-Bn System," Met. Trans., i: 1875-1880 (1970)

7. Burton, J. A.; Prim, R. C; and Slichter, W. P., "The Distribution of Solute in Crystals Grown from the Melt. Part I. Theoretical," J. Chem. Phys., 21: 1987-1991 (1953)

8. Cahn, John W., "Theory of Crystal Growth and Interface Motion in Crystalline Materials," Acta Met., 8: 554-562 (1960)

9. Chandrasekher, S., Hydrodynamic and Hydromagnetic Stability, Oxford Univ. Press, Oxford, England, 1961, p. 10

10. Chiang, S. H. and Shuck, F. O., "A Review of Experimental Results of Diffusion in Liquid-Metal Systems," USAEC Report. IS-3118 (Ames Laboratory, Ames, Iowa) (1972)

11. Cline, H. E. and Livingston, J. D., "High Speed Directional Solidification of Sn-Pb Eutectic Alloys," Trans. TMS-AIME 245: 1987-1992 (1969)

12. Cole, G. S., "The Structure of Ingot Castings," Can. Met. Quart., 8: 189-218 (1969)

13. Cole, G. S. and Winegard, W. C., "Thermal Convection During Horizontal Solidification of Pure Metals and Alloys," J. Inst. Metals, 93: 153-158 (1964-1965)

14. Cole, G. S. and Winegard, W. C., "The Transition from Plane to Cellular Interface in Solidification of Tin-Lead-Antimony Alloys," J. Inst. Metals, 92: 322-326 (1963-1964)

15. Darken, L. S., "Diffusion, Mobility and Their Interrelation through Free Energy in Binary Metallic Systems," Trans. TMS-AIME, 175: 184-218 (1948)

16. David, Stan A., Solidification of Niobium-Niobium Carbide (Nb-Nb,C) Eutectic and Off-Eutectic Composites By Zone Melting Techniques, Ph.D. Dissertation, Univ. of Pittsburgh. 1972

17. Davidson, A. C., The Constitution of the Alloys of Tin with Bismuth, Tech. Pub. Int. Tin Research Development Council Ser. A, No. 77 (1938)

18. Davies, G. J., "Correlation of Parameters Controlling Interface Stability," Iron and Steel Institute Publication P110, The Solidification of Metals, Pp. 66-69. Discussion Pp. 125-129 (1968)

19. Davies, O. L., Statistical Methods in Research and Production, Oliver and Boyd, London, 1961, Pp. 208-272

20. Davis, K. G., "Diffusion Constants in Liquid Lead-Tin Alloys," Can. Met. Quart., 5: 245-263 (1966)

21. Davis, K. G., "Distribution Coefficients in Dilute Binary and Ternary Alloys," Met. Trans., 2: 3315-3323 (1971)

22. Davis, K. G. and Fryzuk, P., "Determination of the Distribution Coefficient and Diffusion Constants in Dilute Alloys of Thallium in Tin," Trans. TMS-AIME, 239: 1105-1106 (1967)

23. Davis, K. G. and Fryzuk, P., "The Stability of a Planar Solid-Liquid Interface for Alloys of Indium in Tin," J. Cryst. Growth, 8: 57-60 (1961)

24. Davis, K. G. and Hogan, L. M., "The Dendrite-Eutectic Transition in Tin-Lead Alloys Solidified with Low Temperature Gradients," J. Aust. Inst. Metals, 15: 29-33 (1970)

25. Duckworth, Henry E., Electricity and Magnetism, Holt, Rinehart and Winston, New York, 1960, Pp. 181 ff.

26. Endo, H., Technol. Rep. Tohoku Imp. Univ., 14: 489-495 (1925)

27. Golotyuk, F. P.; Kuz'menko, P. P.; and Kharkov, E. I., "The Concentration Dependence of Atomic Mobility in the Sn-Pb and Sn-Zn Liquid Systems," (trans. title) Ukr. Fiz. Zh., 10: 1371-1373 (1965) (Language Service Bureau translation, #10904c)

28. Hansen, M. and Anderko, K., Constitution of Binary Alloys, 2nd ed., McGraw-Hill Book Co., Inc. New York, 1958, Pp. 336-339; 1106-1109

29. Harrison, T. R. and Foote, Paul D., "A Precise Method of Measuring Small EMF's and the Change in Thermo-electric Power of Tin at the Melting Point," J. Opt. Soc. Am., 7: 389-398 (1923)

30. Hultgren, Ralph; Orr, Raymond L.; Anderson, Philip D.; and Kelley, Kenneth D., Selected Values of Thermodynamic Properties of Metals and Alloys, John Wiley & Sons, Inc., New York, 1963, Pp. 549-552

31. Hunt, M. D.; Spittle, J. A.; and Smith, R. W., "Constitutional Supercooling in Tin-Base Alloys," J. Inst. Metals, 95: 123-124 (1967)

32. Jackson, K. A. and Chalmers, Bruce, "Kinetics of Solidification," Can. J. Phys., 34: 473-490 (1965)

33. Jackson, K. A. and Hunt, J. D., "Lamellar and Rod Eutectic Growth," Trans. TMS-AIME, 236: 1129-1142 (1966)

34. Jordan, R. M. and Hunt, J. D., "The Growth of Lamellar Eutectic Structures in the Pb-Sn and Al-$CuAl_2$ Systems," Met. Trans., 2: 3401-3410 (1971)

35. Kubaschewski, O. and Evans, E. L., Metallurgical Thermochemistry, Pergamon Press, New York, 1958

36. Lieu, F. Y., "Electrotransport of Bismuth in Liquid Tin," Acta Met., 15: 1405-1407 (1967)

37. Lomell, J. M. and Chalmers, B., "Isothermal Transfer from Solid to Liquid in Metallic Systems," Trans. TMS-AIME, 215: 499-508 (1955)

38. Marwaha, A. S. and Cusak, N. E., "The Absolute Thermoelectric Power of Liquid Metals," Phys. Letters, 22(5): 556 (1966)

39. Mollard, F. R. and Flemings, M. C., "Growth of Composites from the Melt. Part I," Trans. TMS-AIME, 239: 1526-1533 (1967)

40. Mollard, F. R. and Flemings, M. C., "Growth of Composites from the Melt. Part II," Trans. TMS-AIME, 239: 1534-1546 (1967)

41. Moore, A. and Elliot, R., "The Undercooling at the Solid/Liquid Interface of the Lead-Tin Eutectic," J. Inst. Metals, 95: 369-372 (1967)

42. Morris, L. R. and Winegard, W. C., "The Development of Cells During the Solidification of a Dilute Pb-Sb Alloy," J. Cryst. Growth, 5: 361-375 (1969)

43. Mullins, W. W. and Sekerka, R. F., "Stability of a Planar Interface During Solidification of a Dilute Binary Alloy," J. Appl. Phys., 35: 444-451 (1964)

44. Niwa, Kichizo; Shimoji, Mitsuo; Kado, Satoshi; Watanabe, Yoshihiko; and Yokokawa, Toshio, "Studies on Diffusion in Molten Metals," Trans. TMS-AIME, 209: 96-101 (1957)

45. Oelson, Willy and Golücke, Karl Friedrick, "Zur Thermodynamischen Analyze XI. Kalorimetric und Thermodynamik der Wismut-Zinn-Legierungen," Arch. Eisenhuttenw., 29: 689-698 (1958)

46. Onoprienko, G. I.; Kuz'menko, P. P.; and Kharkov, E. I., "Diffusion of Impurity Atoms in Liquid Metals," (trans. title) Ukr. Fiz. Zh., 12: 39-42 (1967) (in Ukr., with English summary)

47. Pelto, Pertti J., Anthropological Research: The Structure of Inquiry, Harper & Row, New York, 1970, Chapter 7

48. Pfann, W., "Principles of Zone Refining," Trans. TMS-AIME, 194: 747-753 (1952)

49. Pfann, W. G.; Benson, K. E.; and Wernick, J. H., "LVI. Some Aspects of Peltier Heating at Liquid Solid Interfaces in Germanium," J. Electron., 2: 577-608 (1957)

50. Pfann, W. G. and Wagner, R. S., "Principles of Field Freezing," Trans. TMS-AIME, 224: 1139-1146 (1962)

51. Plaskett, T. S. and Winegard, W. C., "Cellular Growth in Tin Alloys," Can. J. Phys., 37: 1555-1557 (1959)

52. Rigaud, M. and Tougas, R., "Determination of Activity Coefficients in Solid Solutions," Can. Met. Quart., 3: 269-277 (1964)

53. Roberts-Austin, W. C., "On the Diffusion of Metals," Phil. Trans. Roy. Soc. London, Ser. A, 187: 383-417 (1896)

54. Savintsev, P. A. and Rogov, U. I., "Opredilenie Koeffitsientov Diffuzii V Evtekticheskikh Rasplavakh Metodom Kontaktnago Plavleniya," Zavod. Lab., 35(2): 195-199 (1969) (in Russ.)

55. Savintev, P. A. and Rogov, V. I., "Partial Diffusion Coefficients," (trans. title) Fiz. Meta. Metaloved., 26(6): 119-1121 (1968) (in Russ.), and Phys. Metals Metallogr., 26(6): 166-168 (1968)

56. Sekerka, R. F., "A Stability Function for Explicit Evaluation of the Mullins-Sekerka Interface Stability Criterion," J. Appl. Phys., 36: 264-268 (1965)

57. Siegal, Sidney, Nonparametric Statistics for the Behavioral Sciences, McGraw-Hill, New York, 1956. See expecially Chapter 4

58. Smith, V. G.; Tiller, W. A.; and Rutter, J. W., "A Mathematical Analysis of Solute Redistribution During Solidification," Can. J. Phys., 33: 723-745 (1955)

59. Smithells, Colin J., Metals Reference Book, vols, I, II, Butterworths, Washington, D. C., 1962, Pp. 619, 695-699

60. Stover, R. D. and Shuck, F. O., "Diffusion in Liquid Bismuth-Tin Alloys," Trans. TMS-AIME, 242: 768-770 (1968)

61. Tiller, W. A., "Effect of Grain Boundaries on Solute Partitioning During Progressive Solidification," J. Appl. Phys., 33: 3106-3107 (1962)

62. Tiller, W. A.; Jackson, K. A.; Rutter, J. W.; and Chalmers, B., "The Redistribution of Solute Atoms During the Solidification of Metals," Acta Met., 1: 428-437 (1953)

63. Tiller, W. A. and Rutter, J. W., "The Effect of Growth Conditions Upon the Solidification of a Binary Alloy," Can. J. Phys., 34: 96-121 (1956)

64. Verhoeven, J. D., "Convection Effects in the Capillary Reservoir Technique for Measuring Liquid Metal Diffusion Coefficients," Trans. TMS-AIME, 242: 1937-1942 (1968)

65. Verhoeven, J. D., "The Effect of an Electric Field Upon Solute Redistribution During Solidification of Bi-Sn Alloys," Trans. TMS-AIME, 239: 694-702 (1967)

66. Verhoeven, J. D., "Electrotransport as a Means of Purifying Metals," J. Metals, 18(1): 26-31 (1966)

67. Verhoeven, John Daniel, Electrotransport in Some Liquid Metal Alloys, Ph.D. Dissertation, Univ. of Mich., Ann Arbor, 1963

68. Verhoeven, John, "Macrosegregation During Steady State Growth of a Dendrite Array from a Stirred Melt," Met. Trans., 2: 2673-2680 (1971)

69. Verhoeven, J. D. and Gibson, E. D., "Hysteresis in the Composite to Dendrite Transition of Off-Eutectic Sn-Pb Alloys," in press, Met. Trans.

70. Verhoeven, J. D. and Gibson, E. D., private communication, 1971

71. Verhoeven, J. D. and Gibson, E. D., "The Use of Controlled Solidification and Melting Experiments to Determine Liquidus and Solidus Boundaries," Met. Trans. 2: 3021-3026 (197) (Additional data supplied by the authors)

72. Verhoeven, J. D. and Homer, R. H., "The Growth of Off-Eutectic Composites from Stirred Melts," Met. Trans., 1: 3437-3441 (1970)

73. Verhoeven, J. D.; Warner, J. C.; and Gibson, E. D., "Effect of Thermotransport Upon Off-Eutectic Composite Growth in Sn-Pb Alloys," in press, Met. Trans.

74. Verschnyder, F. L. and Piearcey, B. J., "Single Crystal Alloy Extends Turbine Blade Service Life Four Times," J. Soc. Automot. Eng., 74(8): 36-43 (1966)

75. Walton, D; Tiller, W. A.; Rutter, J. W.; and Winegard, W. C., "Instability of a Smooth Solid-Liquid Interface During Solidification," Trans. TMS-AIME, 203: 1023-1026 (1955)

76. Weinberg, F., "Solute Distributions in Directionally Solidified Rods of Dilute Sn-Ag Alloys," Trans. TMS-AIME, 227: 231-238 (1963)

77. Weinberg, F., "The Thickness of the Residual Layer on a Decanted Interface of Tin," Trans. TMS-AIME, 224: 628-629 (1962)

78. Wilcox, W. R., "Validity of the Stagnant Film Approximation for Mass Transfer in Crystal Growth and Dissolution," Mat. Res. Bull., 4: 265-274 (1969)

79. Wine, R. Lowell, Statistics for Scientists and Engineers, Prentice-Hall, Inc., Englewood Cliffs, N.J., 1964, Pp. 269-271

ACKNOWLEDGEMENTS

Many people in the Ames Laboratory helped a great deal with this work. I would especially like to thank Robert Hofer and Mel Tschetter for doing the many chemical analyses required. In addition to milling the samples Dean Woods provided an education in proper machine shop practice and equipment design. Fellow researcher Ed Gibson was always available for discussions, and did most of the development work on the small thermocouples. The guiding presence of Dr. John Verhoeven is no doubt evident throughout this work, and to him I shall ever be indebted. With a wealth of ideas, potential projects, insights, incisive analysis, he taught by example what makes a good scientist. On his office wall is the motto, "When the evening of this life comes, you will be judged on love." He is one of the few people I know who acts as if he believed it.

For the past two years I have had the privilege of working with the Follow-Through Program at Iowa State, and I would like to express my gratitude to the people of that Program for the benefit of their acquaintance. I hope I have aided them and the Program one tenth as much as they have enriched my life. In particular, I wish to express my deepest appreciation to Dan Robinson and Willis Bright. Thanks to them it has been a long way between steps in the

river.

It is customary at this point to offer deep felt appreciation to one's wife, for sticking through thick and thin. In addition to thanks for editing this thesis, Barbara deserves all the appreciation she can get. Particularly in the last few months when things got thick indeed, she has shouldered far more than her share of the activities and decisions required to make a household function. Both she and Tasha, who only knows that a thesis is a large pile of paper for which Daddy must go to work, have immoderately suppressed their own hopes, desires and plans throughout this period, even when the path seemed longest, and the prospect of our entry into the real world seemed dimmest. For that, no written thanks can suffice.

APPENDIX A. EVALUATION OF THE DIFFUSION COEFFICIENTS

Traditionally diffusivity, D, has been measured by means of a capillary technique. A small capillary, sealed at one end, is filled with an alloy of one composition and immersed in a large constant temperature reservoir of a slightly different composition for a set time. Then the capillary is removed and analyzed. The average composition can be related to the rate of diffusion of one component into or out of the cell. The major experimental problems are density inversions due to temperature or composition and end effects at the tube mouth. Virtually all diffusivity information is determined by the capillary-reservoir method. Davies (18) considers the experimental difficulties in detail. In particular, he estimates that solidification shrinkage on cooling the capillary can introduce an error of up to 10 pct in diffusivity.

Frequently a radioactive tracer is used to obtain concentration profiles. Chiang and Shuck (10) in their selective review of diffusion data include a discussion of the relations among tracer diffusivity, D_i^*, intrinsic diffusivity, D_i, and mutual diffusivity, D_{ij}. For the case of infinite dilution of tracer in an alloy A-B, the main diffusivity, $D_{A^*A^*}$, can be given by

$$\lim_{C_{A^*} \to 0} \quad D_{A^*A^*} = \frac{J_{A^*}}{\nabla C_{A^*}} = D_{A^*}^{+} \qquad [A\text{-}1]$$

As defined by Darken (15) D_A^+ is the diffusion coefficient "determined by tracer technique in an alloy of the same composition." Darken (15) determined the relation

$$D_{AB} = (D_A^+ N_B + D_B^+ N_A)\left(1 + \frac{\partial \ln \gamma_i}{\partial N_i}\right) \qquad [A-2]$$

Buell and Shuck (6), using their own mutual diffusivity data and other work, showed that Eq. [A-2] fits quite well in the Sn-Bi system at 340°C.

A very early study of diffusion in the Sn-Pb system is that of Roberts-Austin (53) who obtained a value of 3.68 x 10^{-5} cm^2 per s at 555°C and commented that this result was "less trustworthy than the other data." Onoprienko, Kuz'menko, and Kharkov (46) measured D of Sn in Pb and Bi by radioactive tracer methods in the range of 300 to 900°C. One hesitates to put too much faith in their Arrhenius equations because the data form smooth curves rather than straight lines when plotted as log D against 1/T.

Niwa, Shimoji, Kado, Watanabe, and Yokokawa (44) measured the diffusion of Bi in Sn, Sn in Bi, and Sn in Pb, each over the ranges of 0 to 10 at. pct and 450 to 600°C at four temperatures. They also measured the diffusion coefficient as a function of composition for both Sn-Pb and Sn-Bi at 510°C. Their results are given in Tables A-I and A-II. In this work no mention was made of

Table A-I. Diffusion in the Sn-Pb system, from Niwa et al. (44)

T(°C)	C_{Pb} (at. pct)	D (10^{-5} cm^2 per s)
510[a]	90.	3.9
	80.	3.5
	70.	3.25
	60.	2.3
	50.	1.8
	40.	1.85
	30.	2.15
450	90.	2.16
510		3.9
550		4.3
600		5.5
$D = 1.2 \times 10^{-3} \exp(-5900/RT)$	90 at pct PB	450-600°C

[a]This data taken from a graph.

density instability. The diffusivity was shown to vary with composition in Sn-Pb, but was assumed constant between 0 and 10 at. pct Sn to obtain the data of the remaining work. It is worth noting that while D is quite dependent on C in the Sn-Pb system, it is apparently almost constant between 10 and 50 at. pct Bi in the Sn-Bi system.

Davis (20) specifically avoided density inversions. He measured diffusion of 100 ppm of ^{113}Sn in Pb by radioactive

Table A-II. Diffusion in the Sn-Bi system, from Niwa et al. (44)

T(°C)	C_{Bi} (at. pct)	D (10^{-5} cm^2 per s)
500[a]	10.	5.0
	20.	4.95
	30.	5.1
	40.	5.4-
	50.	5.5
	60.	5.7
	70.	5.9-
	80.	5.95
	90.	6.0
450	10.	3.6
500		4.6
550		5.8
600		6.6
450	90.	5.5
500		6.5
550		7.3
600		8.2

$D = 1.3 \times 10^{-3} \exp(-5000/RT)$ 10 at. pct Bi 450-600°C

$D = 5.2 \times 10^{-4} \exp(-3200/RT)$ 90 at. pct Bi 450-600°C

[a]This data taken from a graph.

tracer methods, and of 1 pct Pb in Sn by chemical means. The results are presented in Table A-III. He also did two experiments in which pure Pb diffused out of the capillary tube into a tin bath containing 100 ppm of ^{113}Sn at 345 and 395°C, from which he was able to obtain a plot of D as a function of N_{Pb}. The extrapolated D values for nearly pure tin at these temperatures are about 3.6 and 4.4 x 10^{-5} cm^2 per s, respectively, while at N_{Pb} = 0.2, D has dropped to 1.9 and 2.0 x 10^{-5} cm^2 per s. D drops slowly and evenly from there to 1.4 and 1.6 x 10^{-5} cm^2 per s at 80 at. pct Pb, then rises again to 1.87 and 2.37 x 10^{-5} cm^2 per s at 99 at. pct lead. Davis points out that the technique contains significant calculating errors below 20 and above 80 at. pct Pb. He shows that thermodynamically the interdiffusion curve fulfills expectations.

Comparing this work with others, Davis notes that his results agree with those of Niwa et al. (44) at 450 and 510°C but are much lower than Niwa at 600°C. He feels this is probably due to convective mixing at the higher temperatures. If so, then D should vary less with temperature than Ref. (44) would suggest and be higher at the low temperatures used in this thesis than equations from Ref. (44) would predict. Roberts-Austin's work (53) is lower than Davis' by about 40 pct.

Savintsev and Rogov (54, 55) reported two sets of data,

Table A-III. Diffusion in the Sn-Pb system, reported by Davis (20)

C (at. pct Pb)[a]	D (10^{-5} cm^2 per s)[a]
19	1.88
28	1.75
38	1.65
47	1.49
57	1.38
67	1.33
78	1.33

For 100 ppm ^{113}Sn in Pb, between 350 and 600°C:

$$\log_{10} D_o = -3.31 \pm 0.06$$

$$Q = 4040 \pm 198.$$

For 1 at. pct Pb in Sn, between 250 and 500°C:

$$\log_{10} D_o = -3.36 \pm 0.11$$

$$Q = 3034 \pm 299.$$

[a]Data taken from a graph, for 345°C.

each taken in about the same manner. They placed a rod of tin on top of a solid rod of bismuth, encased both in a glass tube, and heated the couple to some temperature below the melting point of the pure components. In the first paper (55) they simply report what are apparently over-all diffusion coefficients. In the second paper (54) they

report partial diffusion coefficients. In order to calculate partial diffusion coefficients it is necessary to have markers which are stationary with respect to the molar average velocity at points within the diffusing region of the couple. They claimed to obtain this for liquid diffusion by observing the solid-liquid interfaces of the pure Sn and Bi sections.

Lieu (36) obtained D of 1 at. pct Bi in Sn by measuring D_{eff} in a capillary as a function of current density and then extrapolating to zero current. He obtained D = 4.35 x 10^{-5} cm^2 per s at 430°C, some 20 pct larger than predicted in Ref. (44). This extrapolation was based on a curve through four points, of which the two lowest suggest that perhaps 4.4 might be more likely.

Stover and Shuck (60) also studied the variation of D with composition in the Sn-Bi system. At 350°C they measured D in four widely spaced compositions but found no simple relationship between D and C. They showed that when the density gradient due to composition differences was inverted the observed diffusion was about ten times larger than when it was composition density stabilized, at a tube diameter of 1, mm.

Buell and Shuck (6) carefully measured the diffusivity of Sn-Bi at 300, 340, and 400°C. Calculations from their data, unlike those of Stover and Shuck, produce a smooth,

uniform relation of D to C.

A general review of diffusion which covers most of the work discussed so far has been made by Chiang and Shuck (10) who suggest that modern diffusion data imply that the Arrhenius equation, $D = D_o \exp(-Q/RT)$, might not be valid for liquid metal systems. Whether the reason is a new phenomenon, as they suggest, or failure to suppress convection at high temperatures, the end result is that for extrapolation of D to low temperatures the equations predict a lower D than one would get through direct measurements.

The data reviewed to this point do not offer much confidence in extrapolated diffusion coefficients. For comparison, in a related solidification problem, Mollard and Flemings (40) used the same diffusion coefficient as Jackson and Hunt (33), who in turn arrived at a value of 0.67×10^{-5} cm^2 per s by extrapolating the single value of Lomell and Chalmers (37), by use of the activation energy of viscosity. Davis and Hogan (24) repeated the work of Mollard and Flemings at lower gradients. They extrapolated from Davis (20) to obtain $D = 0.7 \times 10^{-5}$ cm^2 per s at 183°C and eutectic composition.

Diffusion coefficients may also be obtained, in addition to the more common methods, from solidification experiments, usually in one of three ways: the steady-state breakdown method, the quenched liquid method, or the initial transient

method.

One may make a number of experiments by solidification of a dilute alloy in a positive temperature gradient to determine the conditions for interface breakdown as a function of G/R and C_o. If there is no mixing in the liquid build-up region, at steady state with a flat interface one obtains

$$G/R \geq \frac{m_\ell (1-k_o)}{Dk_o} C_o \qquad [A-3]$$

With m_ℓ and k_o known, D can be calculated from the slope of the straight line separating flat from non-flat interfaces on a G/R vs C_o plot. The problems of the steady-state method have received a detailed criticism elsewhere in this thesis. Probably the most serious problem is that of determining what is and is not a flat interface. Much of the early work contains descriptions of the general appearance of a pox structure, or the appearance of cells, and uses these to specify the change from flat to broken interfaces. Accompanying photographs suggest that these studies often erred in not placing a strict enough criterion on the appearance of a flat interface. It is quite possible that this error may have caused the value of D to be high.

A third problem peculiar to this steady-state method is that of mixing in the region of the solute build-up. The

early work used horizontal boats, which means there was always mixing in those systems.

A second means of obtaining D from solidification studies is to solidify a near-eutectic alloy with an eutectic front, then quench rapidly and measure the quenched liquid composition as a function of distance. The equation to be fitted was derived by Jackson and Hunt (33)

$$C = C_o + B_o \exp(-Rz/D) \quad ; \qquad [A-4]$$

$$B_o = C_E - C_o \text{ at low } R$$

A plot of ln $(C-C_o)$ against z gives a slope of -R/D.

Such a technique provides a good reference point because at the low rates used to prevent dendrite formation the interface composition is always C_E. However, a temperature gradient is required for stability, which means that D is not really constant with distance. The maximum height of the concentration curve, $(C_E - C_o)$, is related to G/R through the requirement for a plane interface, so some experimental optimum must be found. The eutectic temperature is usually well below the melting point of the pure component and so D is small. The length of the build-up layer is thus fairly short, reducing uncertainties about the proper temperature to use.

One can analyze the composition over the initial transient, usually with tracers, and fit the resultant

curve to the equation of Smith et al. (58). This third method assumes that k_o and m_ℓ are constant, while in many systems both are a function of composition. The Smith equation cannot be recast into some form of straight line, so fitting can be difficult.

Despite these problems, Davis (21) and Davis and Fryzuk (22) used this method to obtain values of k_o in systems where k_o is very low. This author is not aware of any solidification studies which have used this method to determine D. In both this and the eutectic solidification method large ratios of G/R are frequently used. Verhoeven, Warner, and Gibson (73) have shown that thermotransport effects at high G/R can be much more important than a first consideration might suggest. Equations describing the effect of thermotransport on a transient have not been derived.

Most of the early work used the steady-state, interface breakdown method. Tiller and Rutter (63), taking k_o and m_ℓ from the phase diagram, obtained $D = 7. \times 10^{-5}$ cm^2 per s for lead containing 0.03 wt pct Sn. Their criteria for breakdown was the appearance of a general pox structure. Walton et al. (75), obtained $D = 2. \times 10^{-5}$ cm^2 per s for very dilute lead in tin. They apparently used the appearance of cells as the criterion for breakdown. Cole and Winegard (14), using low concentrations of lead in tin and similar

values of m_ℓ and k_o, got D = 4.5 x 10^{-5} cm^2 per s. Their criterion for breakdown was the appearance of a poxed structure. Plaskett and Winegard (51) used dilute Bi and Sn and specified the appearance of pox to indicate the onset of supercooling. All of these studies used horizontal boats and a decanting technique to examine the solid-liquid interface. Since the solid always retains a liquid layer when it is removed from the liquid (77), one must assume that the wetted surface morphology maintains a direct relationship to the actual solid-liquid morphology.

Davies (18) did a statistical analysis of the work using the steady-state solidification techniques. Because of the very low concentrations of solute, the temperature can be taken as very near to the melting point of the pure solvent. Among others, he covered Refs. (63, 75, 14, and 51) and compared the D obtained from their data with that from direct methods, Refs. (20, 72, and 44). Direct measures produced lower values than the solidification method. The reason, he felt, could be that mixing was present in the solidification work because of the horizontal boats. Both Weinberg (76) and Cole and Winegard (13) showed that mixing was present and could well be significant.

Davies' estimates of the exponents b and c in the equation

$$C_o = aC^bR^c \qquad [A-5]$$

were obtained by a multiple regression analysis technique, but the source of his numerical data is not clear.[1] In his results he gives estimates of b and c, together with 95 pct confidence error estimates and he assigns a level of significance to each referenced work. After calculating b and c for each reported work, Davies computed D. That one gets any sort of agreement using these reports is encouraging, considering that he lists values of b such as 1.2474 ± 0.6308 as highly significant. The calculated values of D are given in Table A-IV.

Moore and Elliot (41) used the equations derived by Jackson and Hunt (33) applied to a thermal valve technique, in which a section of Pb-Sn eutectic alloy was placed in a temperature gradient such that the interface was between two thermocouples. By cycling the high temperature furnace in a known manner, the resultant thermal wave detected at the lower end enabled them to obtain a diffusion coefficient of $D = 2. \times 10^{-5}$ cm^2 per s, which they felt to be in excellent agreement with Davis (20).

Jordan and Hunt (34), using the quenched liquid method on eutectic growth took microprobe traces in the quenched liquid in front of the interface and obtained $D = 0.62 \times 10^{-5}$ cm^2 per s at the eutectic temperature and composition.

---

[1]See the discussion on methodology above, page (112).

Table A-IV. Diffusion coefficients in Sn-Pb and Sn-Bi alloys, as calculated by Davies (18) from the data of others, using the steady-state interface breakdown method (in decreasing order of significance)

Solvent	Solute	D (10^{-5} cm^2 per s)	Ref.
Sn	Pb	1.7	75
Pb	Sn	7.2	63
Sn	Pb	7.6	51
Sn	Bi	9.1	51
Sn	Pb	5.6	14

They assumed D was constant because they took a straight line best fit of the log ($C-C_E$) against z plot. They used a gradient of 260°C per cm and took microprobe data out to 0.5 mm from the interface, so there was a 13° change in temperature over that length. One of their log plots has only eight experimental points on it, which fit the line very well, while the corresponding C vs z plot has 26 points on it; the justification for dropping 18 points is not given.

In unpublished work Verhoeven and Gibson (70) performed similar work using a bismuth radioactive tracer in a dilute Bi in Sn alloy. They found that the length of the build-up region extended as much as 5 mm into the liquid, which

meant a significant change in temperature, at the gradients used. Unexpectedly, the log plot was virtually a straight line, with very high significance. At the interface the calculated diffusion coefficient was about as anticipated, but far into the liquid the slope of the straight line indicated a diffusivity much smaller than predicted from an Arrhenius equation. Clearly, not everything is known about this technique. At very low rates they also observed a build-up in the bulk liquid which could only be explained by thermotransport.

Diffusivity as determined by these solidification techniques has the advantage that the temperature at which the work is done obviates the need for questionable extrapolation. But the inherent disadvantages, such as loss of independent verification, occasionally questionable methodology, and certain subtle requirements of the experimental method, generally outweigh the advantages in the present case. I feel that in all but one possible case (34) the values of D calculated by solidification are of little value to this work and are no more accurate than extrapolation from higher temperatures of work done by "standard" techniques. The initial transient method has real possibilities, as shown by some excellent work in determining k_o (21), but it has not been used carefully yet to determine D.

Still to be answered is the question of what value of D will be used in the present work. The capillary diffusivity data were reduced to those studies which allow extrapolation to 183-232°C. There are only two (6, 44) for the diffusion of Bi in Sn-Bi alloys up to 10 at. pct Bi. Since the equations used in this part of the work apply at the solid-liquid interface, the temperature range is from about 190 to about 229°C. The extrapolations of Refs. (6) and (44) are given in Table A-V together with comparisons with other studies (36, 55, 60) at comparable temperatures. Buell and Shuck (6) usually predict higher diffusivity than everyone else, while Niwa et al. (44) predict lower values than everyone else. It would seem reasonable to make the same criticisms of Niwa et al. for their Sn-Bi work as for their Sn-Pb work (20). If so, then the 600°C data suffers from convection, and the variation of D with T is less than predicted. Thus D at the interface would be higher. Since Niwa gave no error estimates, the Arrhenius equation was recalculated from his reported data. The standard deviation in activation energy is about 10 pct and about 5 pct in log D_o. These comparisons show that D is not very well specified. In the absence of other evidence, then, the diffusion coefficient will be taken as $D = D_o \exp(\Delta H/RT)$ fitted to Niwa's lowest reported temperature, 450°C, and the point $D = 1.0 \times 10^{-5}$ cm^2 per s at 232°C.

Table A-V. Comparison of diffusion coefficients 10 at. pct Bi in Sn predicted by Buell and Shuck (6) and Niwa et al. (44) with each other between 200 and 232°C, and with observed values reported by others

T (°C)	D (10^{-5} cm^2 per s) Niwa (44)	Buell (6)	Others	Ref.
430	3.63	4.80	4.35 (1 at.pct)	36
400	3.09	4.31		
350	2.29	3.53	1.28	60
340	2.14	3.38		
200	0.637	1.50	1.9	53
232	0.892	1.88		
230	0.875	1.85		
225	0.832	1.79		
220	0.791	1.73		
215	0.751	1.67		
210	0.712	1.61		
205	0.671	1.55		
200	0.637	1.50		

For the Sn-Pb system, there are four Arrhenius equations to consider, at various compositions. Values of D between 183 and 510°C, as calculated from the equations, are given in Table A-VI. The measurements made at compositions near the extremes should be higher than for compositions near

Table A-VI. Calculated values of diffusion coefficients for the Sn-Pb system from three reports, including composition and temperature range at which measurements were made

	Niwa (44)	Onoprienko (46)	Davis (21)	Davis (21)
C (at.pct Pb)	90.	90 or 100	99.99	1.
T range (°C)	450-600	400-900	350-600	250-500
	Extrapolated Diffusion Coefficients (10^{-5} cm^2 per s)			
510	2.706	5.196	3.645	6.204
500	2.577	5.002	3.525	6.049
400	1.456	3.215	2.384	4.511
345	0.983	2.372	1.822	3.686
300	0.674	1.771	1.407	3.036
200	0.226	0.758	0.664	1.728
183	0.178	0.632	0.566	1.532

the center of the system. Davis' results (21) indicate that there should be only a small variation of D with composition between 20 and 80 at. pct.

Among the data on diffusivity developed from solidification work, those reviewed by Davies (18) all involve very dilute solutions. Because of the errors involved in those studies the reliability of the diffusion data is

questionable, at least for the present application. The results of Jordan and Hunt (34), however, apply directly to the study at hand. Because the length of the liquid layer was only 0.5 mm, the change in temperature of 13°C can be considered small enough to take D as constant. Calibration of the microprobe output was done well enough to obtain an interface composition right on C_E. If a statistical fit of <u>all</u> their data on the log $(C-C_o)$ curve yields the same D as that shown by the eight points they show on the figure, then we can put a good deal of faith in their result, $D = 0.62 \times 10^{-5}$ cm^2 per s. This conclusion lends more credence to the suggestions contained in Table A-VI, that the diffusivity of the eutectic alloy at 183°C is actually somewhat less than $1. \times 10^{-5}$ cm^2 per s.

In this thesis $D = 0.62 \times 10^{-5}$ cm^2 per s will be used for Sn-Pb eutectic at the eutectic temperature.

APPENDIX B. THE DETERMINATION OF THE LIQUIDUS SLOPE AND THE EQUILIBRIUM DISTRIBUTION COEFFICIENT

The tin-rich side of the Sn-Bi phase system has been studied a number of times (17, 26, 31, 45, 52, 65, 71) The items of interest are m_ℓ, the slope of the liquidus line, and k_o, taken as $\left.\frac{C_s}{C_\ell}\right|_T$ at equilibrium. In most work the liquidus and solidus temperatures were measured at specific compositions, so one cannot obtain k_o directly, but must calculate composition as a function of temperature for both curves. Because it was known that both lines are nearly straight when concentration is given in weight percent, all data were converted to those units.

The work of Davidson (17) is accepted by Hansen and Anderko (28) is generally the standard of comparison. Table B-I gives Davidson's data determined by using thermal analysis of cooling and heating curves plus metallography. His solidus data does not extrapolate to 232°C, but is slightly below a parallel line which does.

Endo (26) determined the liquidus by cooling curves and the solidus by electrical resistivity on heating. His data result in approximately the same liquidus as Ref. (17) but his solidus curve is slightly higher and extrapolates nearer to the melting point.

Oelson and Golücke (45) also determined liquidus and

Table B-I. Liquidus and solidus data of Davidson (17) for Sn with Bi additions

Wt Pct Bi	Liquidus	Solidus
2	229.5	220.5
4	227.0	211.5
6	225.0	202.0
8	222.0	193.5
10	219.0	185.5
12	216.5	177.0
14	213.0	169.0
16	210.0	167.5
18	207.5	152.5
20	204.5	144.0

solidus curves on this system in the process of testing a calorimetric system. Their data agree closely with Davidson's.

The above results were obtained by standard methods. Verhoeven and Gibson (71), making careful use of solidification techniques, were able to determine solidus and liquidus curves by a rather different approach. They solidified an alloy in a temperature gradient such that the solid-liquid interface was always flat and simultaneously measured the temperature of the interface, to obtain the solidus temper-

ature at the composition of the alloy. Melting with the same care gave the liquidus temperature. Their results are given in Table B-II. Because of the method used there is reason to believe their solidus curve is more accurate than those determined by other methods. Their liquidus curve agrees well with Davidson's, but the solidus is slightly above his, is parallel to it, and extrapolates very nearly to the melting point.

Three papers have measured k_o directly. Rigaud and Tougas (52) used a normal solidification technique at low freezing rates but did not have planar interfaces, so they were restricted to the normal freezing equation given by Pfann (48). Hunt, Spittle, and Smith (31) used the same technique in an effort to determine the extent of solute interaction in dilute ternary alloys. In the process they found k_o for Bi in Sn to be 0.25 for concentrations between 0.8 and 2.4 wt pct Bi. They used horizontal boats with a freezing rate of 1.1×10^{-4} cm per s and did not determine the flatness of the interface. Verhoeven (65) also used normal solidification but made sure the freezing interface was flat, and in addition, varied the rate slightly to be certain it could be extrapolated to zero.

The available data for both liquidus and solidus curves over a range of temperatures (17, 26, 45, 71) were used to calculate the polynomial of best fit for the data.

Table B-II. Data of Verhoeven and Gibson (71), determined by controlled solidification techniques

Wt Pct Bi	Solidus T		Liquidus T	
	Reported data	Original data	Reported data	Original data
1.5 [1.47][a]	225.6 ±0.1[b]	225.475 225.525 225.825 225.400 225.350	229.7	229.725
1.5	225.3 ±0.1	225.463 225.003 225.348	230.5	230.5
1.5	225.5 ±0.2	225.887 225.555 225.46 225.22 225.61	230.1	230.125
2.0	223.2	223.2		
2.0	222.7	222.7		
2.0	222.9 ±0.2	222.7 223.1		
3.0	218.6	218.55	228.2 ±0.2	227.92 228.15 228.49
3.0 [3.02]	218.7 ±0.6	217.47 219.12 218.62 219.09 219.41	227.9 ± 0.2	227.68 228.11
7.5	198.8	198.80		
7.5	199.8	199.76		

[a]Concentrations in brackets indicate results of chemical analysis. Others were weighed-in composition.

[b]Average deviations were reported.

The two criteria for a best fit were the sum of squares due to regression be a maximum, and that the coefficient of the highest order term be significantly different from zero at the 67 pct level. To facilitate later calculation of k_o, the fit was made with C as dependent variable and T as independent variable. In this type of polynomial fit one must assume that all of the error is in the observation of the dependent variable and that the independent variable is exact. Consequently, a fit of the data to a T(C) curve results in slightly different values for $T\big|_{C=0}$ and m_ℓ, m_s than a fit to a C(T) curve. In this case, however, the differences are not large. Figure B-1 includes a plot of all the data between 180°C and the melting point.

The region with which this work is concerned is from about 1 to 10 wt pct of the solidus curve, which is from about 228 to 185°C. Consider the liquidus curve first. Comparison of all the results shows that Endo's data are consistently higher than the others. Oelson and Golücke report no data above 213°C. Verhoeven and Gibson were only able to do their work out to 3.0 wt pct Bi on the liquidus and only reported data for two compositions on that line. For these reasons the data of Davidson are accepted for the liquidus. The liquidus curve in figure B-1 is the best fit of Davidson's data.

Determination of the solidus by cooling curve thermal

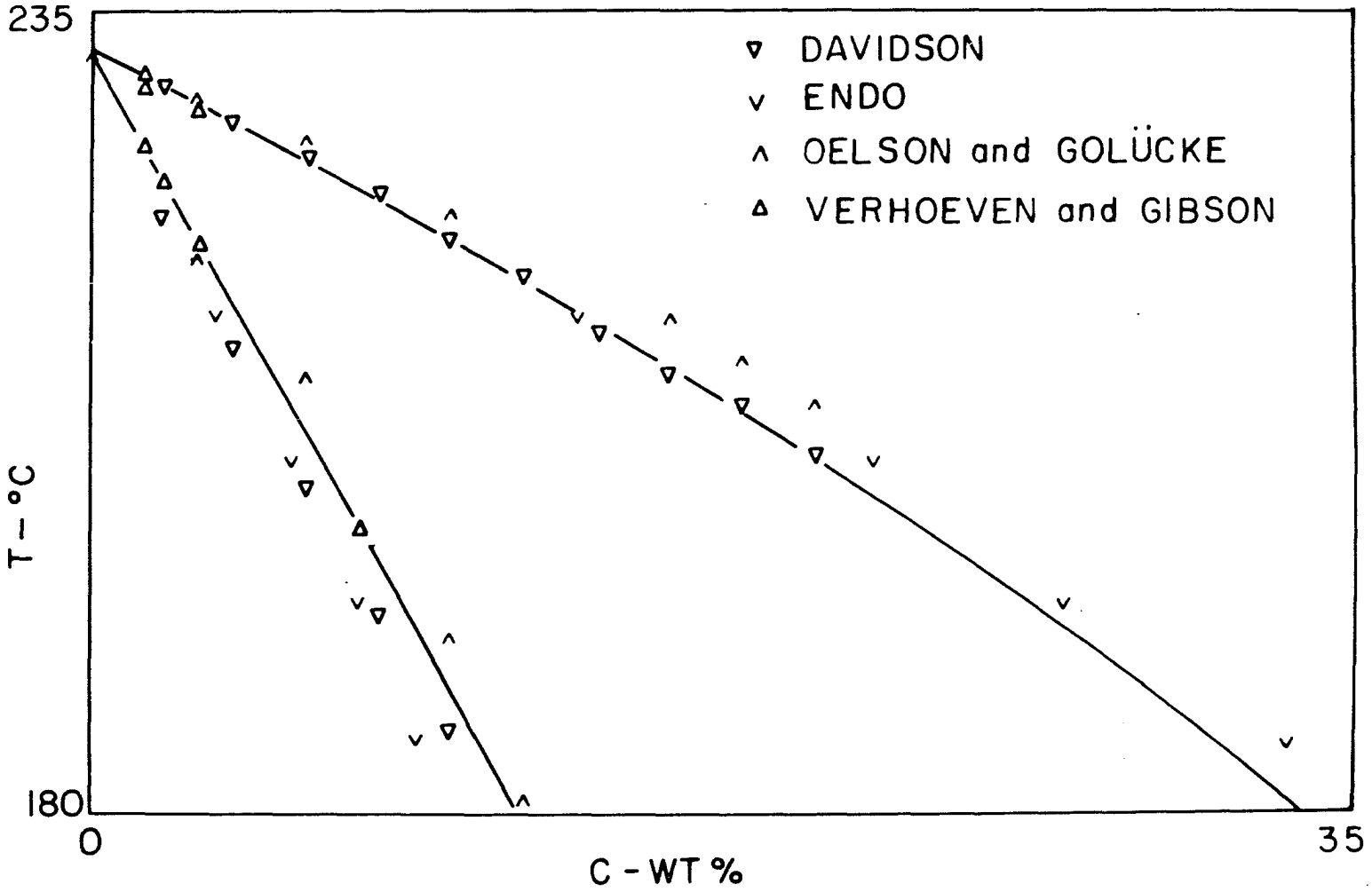

Fig. B-1 -- Comparison of observed results with that of Davidson (liquidus) and Verhoeven and Gibson (solidus) for alloys of Bi in Sn

analysis has always been a difficult proposition. In addition, half of Davidson's data is outside the range of interest, Oelson and Golücke's data are consistently below the others, while Endo's, obtained by resistivity measurements on heating, are always high. The method of Verhoeven and Gibson appears to have several advantages for determination of the solidus, as discussed in Ref. (71). Hence it is accepted for the solidus curve. Figure B-1 also includes the best fit line calculated from their solidus data.

Table B-III gives the values of k_o, m_ℓ, and m_s calculated from Davidson's liquidus and Verhoeven and Gibson's solidus. If the best fit of all the data together is used, k_o is slightly smaller. The curves chosen for the solidus and liquidus do not provide good values of k_o within about 4°C of the melting point, as may be seen from the calculation of k_o in Table B-III. The reason is that the least squares fit of the liquidus curve is displaced about 0.36°C above the solidus at the C = 0 intercept. A thermodynamic derivation valid at small dilutions is given in Appendix C. This derivation suggests that k_o should tend to 0.27 at low dilutions and thus correlate well with the observations at higher concentrations. Above 227°C then, $k_o = 0.27$ will be used in preference to the statistical calculations.

Table B-III. Computed values of the liquidus and solidus concentrations, m_ℓ, m_s, and k_o, from the best fit of Davidson's liquidus data and Verhoeven and Gibson's solidus data

Temp (°C)	k_o	m_ℓ (°C per wt pct)	m_s (°C per wt pct)	Davidson (17)	Verhoeven and Gibson (71)
232.0	0.100	-1.256	-4.368	0.213	-0.021
231.9	0.006	-1.257	-4.368	0.293	0.002
230.0	0.243	-1.275	-4.368	1.793	0.437
228.0	0.267	-1.295	-4.368	3.350	0.894
226.0	0.227	-1.316	-4.368	4.882	1.352
224.0	0.283	-1.337	-4.368	6.390	1.810
220.0	0.292	-1.381	-4.368	9.335	2.726
216.0	0.299	-1.428	-4.368	12.184	3.642
212.0	0.305	-1.479	-4.368	14.937	4.557
208.0	0.311	-1.533	-4.368	17.594	5.473
204.0	0.317	-1.592	-4.368	20.155	6.389
200.0	0.323	-1.655	-4.368	22.620	7.304
196.0	0.329	-1.723	-4.368	24.990	8.220
192.0	0.335	-1.797	-4.368	27.263	9.136
188.0	0.341	-1.878	-4.368	29.441	10.051
184.0	0.348	-1.967	-4.368	31.522	10.967
180.0	0.355	-2.064	-4.368	33.508	11.883

APPENDIX C. THERMODYNAMIC DETERMINATION OF k_o

At low compositions where errors in statistical fitting of liquidus and solids data become larger, one can estimate k_o by resort to thermodynamics. This also gives a good check on the calculated values of k_o, as the observed and thermodynamically calculated value should agree reasonably well.

Following the approach of Davis (21), let us examine an ideal solution, where component 1 is the major constituent and component 2 is the minor one. The ratio of solid to liquid composition of the major component can be written as

$$\frac{N_{1,s}}{N_{1,\ell}} = \frac{1-N_{2,s}}{1-N_{2,\ell}} \qquad [C-1]$$

We know that

$$\bar{G}_{1,\ell} - {}^{\circ}G_{1,\ell} = RT\ln N_{1,\ell} \qquad [C-2]$$

where ${}^{\circ}G_{1,\ell}$ is the standard state of pure liquid 1 at the temperature T. The free energy equation for the solid phase is similar,

$$\bar{G}_{1,s} - {}^{\circ}G_{1,s} = RT\ln N_{1,s} \qquad [C-3]$$

At equilibrium the partial molar free energies of the two phases must be equal, so we can write

$$\bar{G}_{1,\ell} = \bar{G}_{1,s} = RT\ln N_{1,\ell} + {}^{\circ}G_{1,\ell} = RT\ln N_{1,s} + {}^{\circ}G_{1,s} \qquad [C\text{-}4]$$

from which we get,

$$\frac{N_{1,s}}{N_{1,\ell}} = \exp\left(\frac{1}{RT}\left[{}^{\circ}G_{1,\ell} - {}^{\circ}G_{1,s}\right]\right) \qquad [C\text{-}5]$$

Now the difference in the standard states is just the free energy of melting at T, which for small deviations from the melting point of the pure component 1 can be given as

$$\Delta G = \Delta H^* - T\Delta S^* \qquad [C\text{-}6]$$

where the superscript * indicates the value at the melting point. Since $\Delta H^* - T^* \Delta S^* = 0$, Eq. [C-6] can be reduced to

$$\Delta G = \Delta H^* \left[1 - \frac{T}{T^*}\right]$$

Putting this into Eq. [C-5] with Eq. [C-1] we have

$$\frac{1-N_{2,s}}{1-N_{2,\ell}} = \exp\ \frac{\Delta H^*}{R}\left[\frac{1}{T} - \frac{1}{T^*}\right] \quad ; \quad \ln\frac{N_{2,s}}{N_{2,\ell}} = \frac{\Delta H^*}{R}\left[\frac{1}{T} - \frac{1}{T^*}\right] \qquad [C\text{-}7]$$

For $N_2 << 1$, this reduces to

$$N_{2,\ell} - N_{2,s} = \frac{\Delta H^*}{R}\left[\frac{1}{T} - \frac{1}{T^*}\right] \cdot \frac{1}{N_{2,\ell}} \qquad [C\text{-}8]$$

Davis left off here, but there is a relationship between $N_{2,\ell}$ and T, namely through m_ℓ , the liquidus slope, such that

$$m_\ell = \frac{dT}{dC} = \frac{T^*-T}{0-N_{2,\ell}} = -\frac{\Delta T}{N_{2,\ell}} \qquad [C-9]$$

near the melting point. As T approaches T*, $TT^* = T^{*2}$. Using this, and the relation of m_ℓ to replace $N_{2,\ell}$, we get an equation for k_o

$$k_o = 1 - \frac{\Delta H}{R}\frac{(-m_\ell)}{T^2} \qquad [C-10]$$

Equation [C-10] requires experimental information on m_ℓ and ΔH and is valid for ideal solutions at low concentrations. This analysis should apply quite well to the Sn-Bi system because it is close to ideal (38, 35).

The liquidus slope has been determined in the course of calculating k_o at higher concentrations. Since calculated values of m_ℓ were in terms of wt pct, they were converted to atom fraction by noting that at low dilution

$$\text{at. pct/wt pct} = M_1/M_2 \qquad [C-11]$$

where M is the molecular weight of the component. The value of ΔH was taken as 1690 cal per mole from Smithells (59). Estimates of k_o calculated from Eq. [C-10] are given in Table C-I. The liquidus data of Verhoeven and Gibson, while replicated well, is based on measurements at only two

Table C-I. Values of the liquidus slope of m_ℓ determined from observations on the Sn-Bi system and the equilibrium distribution coefficients k_o calculated from Eq. [C-10]

	Source				
	Davidson (17)	Endo (26)	Oelson (45)	Verhoeven (71)	All
From C = f(T)					
m_ℓ (°C per wt pct)	-1.256	-1.201	-1.264	-1.463	-1.226
m_ℓ (°C per at. pct)	-2.211	-2.115	-2.226	-2.576	-2.159
k_o	0.262	0.294	0.257	0.141	0.280
From T = f(C)					
m_ℓ (°C per wt pct)	-1.225	-1.197	-1.074	-1.347	-1.129
pct error (67% C.I.)	-6.8	-2.6	-15.8	-12.6	-4.0
m_ℓ (°C per at. pct)	-2.156	-2.108	-1.892	-2.371	-1.988
k_o	0.281	0.297	0.369	0.209	0.337

concentrations. For various reasons having to do with the statistical assumptions required, the equations obtained from the C = f(T) correlations produced better extrapolations than the T = f(C) correlations did. Partly for this reason there is a greater variation in the value of k_o calculated from the latter equations; they are included here to give an indication of the errors involved. Using the C = f(T) correlations only and giving equal weight to the result calculated from Davidson and all the work combined, a value of $k_o = 0.27$ was obtained.

It is evident that this sort of calculation is good mostly for confirmation of experimental data. A change in m_ℓ of about 4 pct results in a change in k_o of about 11 pct, at the values used, and $\frac{\partial k_o}{\partial m_\ell}$ gets larger as the second term approaches 1. We can draw some conclusions of value, however. The calculated value of k_o, 0.27, should be approached as the bismuth concentration approaches zero, so this value will be used at very low concentrations.

APPENDIX D. MATHEMATICAL SOLUTION OF THE FLUX EQUATION FOR EUTECTIC GROWTH

For an alloy solidifying with a planar eutectic front the differential equation for the concentration of the liquid in front of the interface is given by Eq. [28] The boundary conditions, assumptions and definitions of terms are also given there. To obtain a solution, we let $C = ZY$, and assume quasi-steady state. Then, from Eq. [28]

$$Y \frac{d^2Z}{dz^2} + Z \frac{d^2Y}{dy^2} + \frac{R-UE}{D} Y \frac{dZ}{dz} = 0 \qquad [D-1]$$

separating variables, we get

$$- \frac{1}{Y} \frac{d^2Y}{dy^2} = \frac{1}{Z} \frac{d^2Z}{dz^2} + \frac{\rho'}{Z} \frac{dZ}{dz} = \lambda^2 \qquad [D-2]$$

where λ is a constant, and ρ' is defined as $\rho' = (R-UE)/D$. Taking only the y portion of Eq. [D-2]

$$\frac{d^2Y}{dy^2} + \lambda^2 Y = 0$$

we get

$$m^2 + \lambda^2 = 0 \Rightarrow m = \pm \sqrt{-\lambda^2} \qquad [D-3]$$

λ is not less than 0.

If $\lambda^2 < 0$, then $m = \pm \lambda$

$$Y = Ae^{\lambda y} + Be^{-\lambda y} \qquad [D-4]$$

$$\frac{dY}{dy} = A\lambda e^{\lambda y} - B\lambda e^{-\lambda y} \qquad [D-5]$$

Applying Eq. [bc-2] (Eq. [30], we get

$$\frac{dY}{dy} = 0 \ , \ y = 0 \Rightarrow A\lambda - B\lambda = 0 \Rightarrow A = B \qquad [D-6]$$

$$= 0, \quad y = \frac{W}{2} \Rightarrow A\lambda e^{\frac{\lambda W}{2}} - B\lambda e^{\frac{\lambda W}{2}} = 0 \Rightarrow A = 0 \qquad [D-7]$$

If $\lambda^2 = 0 \quad Y = A + By$, then

$$\frac{dY}{dy} = B = 0, \quad y = 0 \Rightarrow B = 0 \qquad [D-8]$$

so λ^2 is not equal to 0 in general. It must be that $\lambda^2 > 0$. The solution to Y then, is

$$Y = B \cos(\lambda y) + C \sin(\lambda y) \qquad [D-9]$$

$$\frac{dY}{dy} = -B\lambda \sin(\lambda y) + C\lambda \cos(\lambda y) \qquad [D-10]$$

Adding Eq. [bc-2] (Eq. [30]), we get

$$y = 0, \ Y' = C\lambda = 0 \Rightarrow C = 0 \qquad [D-11]$$

$$y = \frac{W}{2} \; ; \; -B\lambda \sin\left(\lambda\frac{W}{2}\right) = 0 \Rightarrow \lambda = \frac{2n\pi}{W} \qquad [D\text{-}12]$$

so that

$$Y = B \cos\left(\frac{2n\pi}{W} y\right) \qquad [D\text{-}13]$$

From the Z portion of Eq. [D-2], we have

$$\frac{d^2Z}{dz^2} + \rho' \frac{dZ}{dZ} - Z\lambda^2 = 0 \qquad [D\text{-}14]$$

and

$$m^2 + \rho' m - \lambda^2 = 0 \quad ; \quad m = -\frac{\rho'}{2} \pm \sqrt{\frac{\rho'^2}{4} + \lambda^2} \qquad [D\text{-}15]$$

For simplicity, let

$$\gamma_n = \sqrt{\frac{\rho'^2}{4} + \lambda^2} = \sqrt{\frac{\rho'^2}{4} + \frac{4n^2\pi^2}{W^2}} \qquad [D\text{-}16]$$

So that

$$Z = e^{\frac{-\rho' Z}{2}} \left[Ce^{\gamma n Z} + De^{-\gamma n Z} \right] \qquad [D\text{-}17]$$

At $n = 0$, $\lambda^2 = 0$, so $\gamma_n = \rho'/2$, then

$$Z = e^{\frac{-\rho' Z}{2}} \left[Ce^{\frac{\rho' Z}{2}} + De^{\frac{-\rho' Z}{2}} \right] = C_o + D_o e^{-\rho' Z} \qquad [D\text{-}18]$$

At $\lambda^2 > 0$, one has Eq. [D-17]. Putting the Z and Y portions together again, we have, for $\lambda = 0$

$$ZY = AC_o + AD_o e^{-\rho' Z} = A_o + D_o e^{-\rho' Z} \qquad [D\text{-}19]$$

Note that D_o is changed. For $\lambda^2 > 0$,

$$ZY = B_n \cos\left(\frac{2n\pi y}{W}\right) \left[C_n e^{\gamma_n Z} + D_n e^{-\gamma_n Z}\right] e^{\frac{-\rho' Z}{2}} \qquad [D\text{-}20]$$

Therefore

$$C = A_o + D_o e^{-\rho' Z} + \sum_1^\infty B_n e^{\frac{-\rho' Z}{2}} \cos\left(\frac{2n\pi}{W} y\right) \left[C_n e^{\gamma_n Z} + D_n e^{-\gamma_n Z}\right] \qquad [D\text{-}21]$$

With ρ' replaced by ρ, this is exactly the result of Jackson and Hunt (33). Now it remains to determine the constants A_o, B_n, C_n, D_o, and D_n. First we apply [bc-3] (Eq. [31])

$$Z = \delta \qquad C(\delta, y) = C_B \qquad [31]$$

$$C_B = A_o + D_o e^{-\rho' \delta} + \sum_1^\infty B_n e^{\frac{-\rho' \delta}{2}} \cos\left(\frac{2n\pi}{W} y\right) \left[C_n e^{\gamma_n \delta} + D_n e^{\gamma_n \delta}\right] \qquad [D\text{-}22]$$

Here, C_B is not a function of y, so the summation term must be zero

$$C_n e^{\gamma_n \delta} = -D_n e^{-\gamma_n \delta} \quad ; \quad C_n = -D_n e^{-2\gamma_n \delta} \qquad [D\text{-}23]$$

$$C_n e^{\gamma_n Z} + D_n e^{-\gamma_n Z} = -D_n e^{-2\gamma_n \delta + \gamma_n Z} + D_n e^{-\gamma_n Z} \qquad [D\text{-}24]$$

$$= D_n \left[e^{\gamma_n (Z-\delta)} - e^{-\gamma_n (Z-\delta)} \right] \qquad [D\text{-}25]$$

$$= D_n \sinh \gamma_n (Z - \delta) \quad ; \; n \geq 1 \qquad [D\text{-}26]$$

Note that D_n changes between Eq. [D-24] and [D-26]. Now $\sinh(-x) = -\sinh(x)$ so let $D_n = -D_n$ and hence the right side of Eq. [D-26] becomes

$$D_n \sinh \gamma_n (\delta - Z) \qquad [D\text{-}27]$$

as $\delta > z$ anyway. Since the summation term is zero,

$$C_B = A_o + D_o e^{-\rho' \delta} \quad ; \quad A_o = C_B - D_o e^{-\rho' \delta} \qquad [D\text{-}28]$$

Therefore

$$C(Z,y) = C_B + D_o \left[e^{-\rho' \delta} - e^{-\rho' \delta} \right] + \Sigma D_n e^{\frac{-\rho' \delta}{2}} \cos \left(\frac{2n\pi}{W} y \right) \sinh \gamma_n (\delta - Z) \qquad [D\text{-}29]$$

$$\left.\frac{\partial C}{\partial Z}\right|_{o,y} = -\delta' D_o - \sum_1^\infty D_n \cos\left(\frac{2n\pi}{W}y\right) \gamma_n \cosh \gamma_n(\delta - z)$$

$$- \frac{\delta'}{2} \sum_1^\infty D_n \cos\left(\frac{2n\pi}{W}y\right) \sinh\gamma_n(\delta - Z)\, e^{\frac{-\delta' Z}{2}} \qquad [D\text{-}30]$$

$$\left.\frac{\partial C}{\partial Z}\right|_{o,y} = -\delta' D_o - \Sigma D_n \cos\left(\frac{2n\pi}{W}y\right) \left[\gamma \cosh\gamma_n + \frac{\delta'}{2} \sinh\gamma_n\delta\right] \qquad [D\text{-}31]$$

To get a solution for D_n, we multiply through by $\cos 2m\pi y/w$, and apply the principle $\int_o^\pi \cos mx \cos nx dx = 0$, $m \neq n$; $= \pi/2$, $m = n$.

$$\left.\frac{C}{Z}\right|_{o,y} \cos\left(\frac{2m\pi y}{W}\right) = -\delta' D_o \cos\left(\frac{2m\pi y}{W}\right) - \sum_1^\infty D_n \cos\left(\frac{2m\pi y}{W}\right) \qquad [D\text{-}32]$$

$$\cos\left(\frac{2m\pi y}{W}\right) [\quad]$$

where the brackets enclose the same terms as in Eq. [D-31]. If $m = n \geq 1$

$$\frac{W}{2\pi} \int_o^{W/2} \cos\left(\frac{2\pi m y}{W}\right) \cos\left(\frac{2\pi n y}{W}\right) \left(\frac{2\pi dy}{W}\right) = \frac{W}{4} \qquad [D\text{-}33]$$

otherwise the integral is zero. Adding $\rho' D_o$ to both sides of Eq. [D-23] and integrating

$$\int_o^{W/2} \left.\frac{\partial C}{\partial z}\right|_{o,y} + \rho' D_o \cos\left(\frac{2m\pi y}{W}\right) dy = \int_o^{W/2} -D_n [\quad] \cdot \cos\left(\frac{2n\pi y}{W}\right) \cos\left(\frac{2m\pi y}{W}\right) dy \qquad [D-34]$$

$$= -D_n [\quad] \frac{W}{4} \quad ; \quad m = n$$

Thus,

$$D_n = \frac{-\frac{4}{W}\int \left[\left.\frac{\partial C}{\partial z}\right|_{o,y} + \rho' D_o\right] \cos\left(\frac{2n\pi y}{W}\right) dy}{[\gamma_n \cosh \gamma_n \delta + \frac{\rho'}{2} \sinh \gamma_n \delta]} \qquad [D-35]$$

$$D_n = \frac{-4}{W[\quad]} \left[\int_o^{W/2} \left.\frac{\partial C}{\partial z}\right|_{o,y} \cos\left(\frac{2n\pi y}{W}\right) dy + \int_o^{W/2} \rho' D_o \cos\left(\frac{2n\pi y}{W}\right) dy \right] \qquad [D-36]$$

Here, a and b are assumed constant from [bc-4] (Eq. [34]

$$D_n = \frac{-4}{W[\ ]}\left[a\int_o^{W_\alpha/2}\cos\left(\frac{2n\pi y}{W}\right)dy + b\int_o^{W/2}\cos\left(\frac{2n\pi y}{W}\right)dy + \frac{W}{2\pi}\int_o^{W/2}\rho' D_o \cos\left(\frac{2n\pi y}{W}\right)\frac{2}{W\pi}\,dy\right] \qquad [D\text{-}37]$$

$$= \frac{-4}{W[\ ]}\left[\frac{a}{2\pi}\sin\left(\frac{2n\pi y}{W}\right)\Bigg|_0^{W/2} + \frac{bW}{2\pi}\sin\left(\frac{2n\pi y}{W}\right)\Bigg|_{W\alpha/2}^{W/2} + 0\right] \qquad [D\text{-}38]$$

Letting $f_\alpha = W_\alpha/W$, the volume fraction of eutectic which is alpha phase, Eq. [D-38] is evaluated as

$$D_n = \frac{-2}{W[\ ]}\left[a \sin n\pi f_\alpha - b \sin n\pi f_\alpha\right] \qquad [D\text{-}39]$$

and hence finally to

$$D_n = \frac{-2}{W[\ ]}(a-b)\sin n\pi f_\alpha \qquad [D\text{-}40]$$

For m = 0

$$\int_o^{W/2}\left.\frac{\partial C}{\partial z}\right|_{o,y}\cos\left(\frac{2m\pi y}{W}\right)dy = \int_o^{W/2}\delta' D_o \cos\left(\frac{2m\pi y}{W}\right)dy\ -\sum_1^{\infty}[\ ] \qquad [D\text{-}41]$$

$$\int_0^{W/2} \left.\frac{\partial C}{\partial z}\right|_{o,y} dy = -\rho' \frac{D_o W}{2} \qquad [D-42]$$

The summation term contributes nothing because n is never 0 in it.

$$\int_0^{W/2} \left.\frac{\partial C}{\partial z}\right|_{o,y} dy = \int_0^{W_\alpha/2} a\,dy + \int_{W_\alpha/2}^{W/2} b\,dy \qquad [D-43]$$

$$= aW_\alpha/2 + b\left(\frac{W}{2} - \frac{W_\alpha}{2}\right)$$

$$= \frac{W}{2}\left(af_\alpha + bf_\beta\right) = -\rho' D_o \frac{W}{2} \qquad [D-44]$$

so we get

$$D_o = -\frac{(af_\alpha + bf_\beta)}{\rho'} \qquad [D-45]$$

Combining all this we have

$$C(z,y) = C_B - \frac{[af_\alpha + bf_\beta]}{\rho'}\left[e^{-\rho' z} - e^{-\rho' \delta}\right] \qquad [D-46]$$

$$+ \sum_1^\infty D_n e^{-\rho' z/2} \cos\left(\frac{2n\pi y}{W}\right) \sinh\gamma_n(\delta - z)$$

where

$$D_n = \frac{-2(a-b)\ \sin n\pi f_\alpha}{[\gamma_n \cosh\gamma_n \delta + \frac{\delta'}{2} \sinh\gamma_n \delta]} \qquad [D-47]$$